USAGE OF REMOTE SENSING AND GEOGRAPHIC INFORMATION SCIENCES IN GOLD-SILVER EXPLORATION

PhD. THESIS

Clement KWANG

Eskisehir 2019

USAGE OF REMOTE SENSING AND GEOGRAPHIC INFORMATION SCIENCES IN GOLD-SILVER EXPLORATION

Clement KWANG

PhD. THESIS

Department of Remote Sensing and Geographic Information Systems
Supervisor: Assist. Prof. Dr. Hakan UYGUÇGİL

Eskisehir
Anadolu University
Graduate School of Sciences
March 2019

FINAL APPROVAL FOR THESIS

This thesis titled “Usage of Remote Sensing and Geographic Information Sciences in Gold-Silver Exploration” has been prepared and submitted by Clement KWANG in partial fulfillment of the requirements in “Anadolu University Directive on Graduate Education and Examination” for the Doctor of Philosophy (PhD) in Remote Sensing and Geographic Information Systems Department has been examined and approved on 18/03/2019.

Committee Members			**Signature**
Member (Supervisor)	:	Assist. Prof. Dr. Hakan UYGUÇGİL	....
Member	:	Prof. Dr. Alper ÇABUK	…………….
Member	:	Prof Dr. Recep BAKIŞ	…………….
Member	:	Assoc. Prof. Dr. Murat UYSAL	…………….
Member	:	Assist. Prof. Dr. Resul ÇÖMERT	…………….

Prof. Dr. Ersin YÜCEL

Director of Graduate School of Sciences

ABSTRACT

USAGE OF REMOTE SENSING AND GEOGRAPHIC INFORMATION SCIENCES IN GOLD-SILVER EXPLORATION

Clement KWANG

Department of Remote Sensing and Geographic Information Systems
Anadolu University,
Graduate School of Sciences, March 2019

Supervisor: Assist. Prof. Dr. Hakan UYGUÇGİL

The application of Remote Sensing techniques and Geographic Information Sciences have greatly improved the exploration of minerals. In this study, the argillic alteration associated with Gold-Silver mineralization were extracted with the proposed Illite index by considering the geology, and landcover of study area. The derived argillic alteration zones were then integrated with other geologic information such as lithology and faults to predict the potential gold locations. The illite index was proposed by examining the extracted image spectra and the USGS spectra of illite because of illite's close association with the gold-silver mineralization within the study. The illite index uses ASTER image and is a ratio of band 7 by band 6. The principal component analyses were also performed to validate and compare the hydrothermal alteration result obtained from the illite index. The weights of evidence and the fuzzy logic model were used to produce the gold potential map of the study area. The Ovacık Gold Mine was identified by both the weights of evidence and a fuzzy logic model. The mineral potential map and the proposed band ratio index would help in reducing the exploration work to the most probable mineralized zones.

Keywords: Argillic alteration, Epithermal Gold-Silver deposit, Weights of evidence, Illite index, Principal component analysis

ÖZET

ALTIN-GÜMÜŞ ARAMALARINDA UZAKTAN ALGILAMA VE COĞRAFİ BİLGİ SİSTEMLERİ KULLANIMI

Clement KWANG

Uzaktan Algılama ve Coğrafi Bilgi Sistemleri Anabilim Dalı
Anadolu Üniversitesi,
Fen Bilimleri Enstitüsü, Mart, 2019

Danışman: Dr. Öğr. Üyesi Hakan UYGUÇGİL

Uzaktan Algılama Teknikleri ve Coğrafi Bilgi Sistemlerinin uygulanması, minerallerin keşfedilmesini büyük ölçüde geliştirmiştir. Bu çalışmada; bant oranı dikkate alınarak jeoloji, değişmiş mineral ve çalışma alanının arazi örtüsünün spektral tepkisini alarak İzmir'de altın-gümüş maden sahaları için hidrotermal alterasyon mineralleri belirlemek için önerilmiştir. Elde edilen hidrotermal alterasyon bölgeleri daha sonra potansiyel altın lokasyonlarını tahmin etmek için litoloji ve faylar gibi diğer jeolojik bilgilerle birleştirilmiştir. Bu İllit endeksi, çıkarılan görüntü spektrumları ve İllit'in USGS spektrumları incelenerek geliştirilmiştir. İllit endeksi ASTER görüntüsü kullanır ve 7 bandının 6 bandına oranıdır. Temel bileşen analizleri, İllit endeksinden elde edilen hidrotermal alterasyon sonucunu doğrulamak ve karşılaştırmak için de gerçekleştirilmiştir. Çalışma alanının altın potansiyel haritasını üretmek için kanıt ağırlıkları ve bulanık mantık modeli kullanılmıştır. Ovacık Altın Madeni, yüksek oranda derecelendirilen potansiyel altın lokasyonlarını içerisinde tanımlanmış ve haritalanmıştır. Potansiyel altın modelleme ve İllit endeksi mineral keşif çalışmalarının fizibilite çalışmalarında hedef alanlarının daraltılması ile keşif çalışmalarına büyük katkı sağlayacaktır.

Anahtar Sözcükler: Arjilik alterasyon, Epitermal altın-gümüş cevherleşmesi, Kanıt ağırlıkları, İllit endeksi, Temel bileşen analizleri

ACKNOWLEDGMENT

My profound gratitude to my supervisor, Assistant Prof. Dr. Hakan UYGUÇGİL for his numerous supports, motivation, and encouragement. I am very lucky to have worked with him and his impacts on me is a lifetime experience. I would also like to express my gratitude to my thesis jury members most especially, Prof. Dr. Alper ÇABUK and Prof Dr. Recep BAKIŞ for their contributions to the successful completion of my Ph.D. thesis.

My appreciation to the Turkish Government for awarding me the scholarship opportunity to pursue my childhood dream of becoming a Ph.D. degree holder. I am grateful for the support and assistance offered.

To my friends both in Turkey and Ghana, I say big thanks to you all. Your advice and support gave me the strength for the successful completion of this program. Dr. Edward Matthew Jnr. Osei, I cannot forget your support and assistance, thank you, sir,

My final thanks go to my family who has always been the backbone of my success, I appreciate your support, care, and motivation. To mention a few of them, Mr. Stephen Okrah, Twene Eric, Alice Kwartemaa and Desmond Okrah Kwang.

Clement Kwang

18/03/2019

STATEMENT OF COMPLIANCE WITH ETHICAL PRINCIPLES AND RULES

I hereby truthfully declare that this thesis is an original work prepared by me; that I have behaved in accordance with the scientific ethical principles and rules throughout the stages of preparation, data collection, analysis, and presentation of my work; that I have cited the sources of all the data and information that could be obtained within the scope of this study, and included these sources in the references section; and that this study has been scanned for plagiarism with "scientific plagiarism detection program" used by Anadolu University, and that "it does not have any plagiarism" whatsoever. I also declare that, if a case contrary to my declaration is detected in my work at any time, I hereby express my consent to all the ethical and legal consequences that are involved.

....

Clement Kwang

TABLE OF CONTENT

Page

Page

Page

Page

Page

Page

LIST OF TABLES

Page

LIST OF FIGURES

Page

Page

Page

Page

LIST OF ABBREVIATIONS AND SYMBOLS

α	: Alpha
Ag	: Silver
AHP	: Analytic Hierarchy Process
ANP	: Analytic Network Process
ArcSDM	: Arc Spatial Data Modeler
ASTER	: Advanced Spaceborne Thermal Emission and Reflection Radiometer
Au	: Gold
C	: Contrast
DEM	: Digital Elevation Model
DN	: Digital Number
EM	: Electromagnetic Spectrum
ETM+	: Enhanced Thematic Mapper Plus
FLAASH	: Fast Line-of-sight Atmospheric Analysis of Spectral Hypercubes
GIS	: Geographical Information System
HDF	: Hierarchical Data Format
JHU	: Johns Hopkins University
JPL	: Jet Propulsion Laboratory
MCDA	: Multi-Criteria Decision Analysis
MNDWI	: Modified Normalized Water Difference Index
MSS	: Multispectral Scanner
NASA	: National Aeronautics and Space Administration
NDVI	: Normalized Difference Vegetation Index
NRSC	: United Kingdom National Remote Sensing Centre

OIF	: Optimum index factor
PC	: Principal Component
PCA	: Principal Component Analysis
RGB	: Red Green Blue
ROIs	: Regions of Interest
S (C)	: Standard deviation of Contrast
STUD (C)	: Studentized Contrast
SWIR	: Short-Wave Infrared
TIR	: Thermal Infrared
TOA	: Top-of-Atmosphere
USGS	: United States Geological Survey
UTM	: Universal Transverse Mercator
W-	: Negative Weight
W+	: Positive Weight
WGS	: World Geodetic System
WLC	: Weighted linear combination
VNIR	: Visible Infrared

1. INTRODUCTION

1.1. Background

Mapping and identification of similar features both on the earth and beneath the earth's surface based on their spectral similarities are becoming more accurate and easier with the new advancement in Remote Sensing technology and improved image processing algorithms. The role of Multispectral Remote Sensing in natural and earth sciences is crucial because of its multispectral and multi-temporal capabilities.

The remotely acquired image can serve as a source of base map for engineering and other civil works, updating existing maps and for producing a map of large coverage area at reduced cost and within a short period of time. For instance, in Geological applications, Multispectral Remote Sensing is used in mapping potential mineral alterations, rock units and interpreting structural and lithology of any particular geographical area. Multispectral data, especially Landsat and ASTER data have been utilized by many researchers in geological application ranging from mineral exploration to lithological mapping.

In December 1999, through the combined efforts of NASA and Ministry of Economy, Trade and Industry of Japan, the advanced spaceborne thermal emission and reflection radiometer (ASTER) was propelled into space. In total ASTER data possesses 14 spectral bands, three of the bands are visible near-infrared bands with 15m spatial resolution and radiometric resolution of 8bit, six bands are shortwave infrared bands with 30m spatial resolution and 8-bit radiometric resolution and five of them are thermal infrared bands with 90m spatial resolution and 16-bit data type. ASTER data's main advantage is its wide range of spectral band coverage which allows a lot of multiple band ratio and RGB combinations (Mohy et al., 2016). The SWIR bands of ASTER, for instance, are used to identify clay minerals and ferrous minerals because of their high absorption and high reflectance features within the SWIR bands (Mars and Rowan, 2010). The spatial resolution of ASTER may not be good as that of Sentinel 2A, but in terms of the spectral resolution, ASTER is far better than Sentinel 2A even though the SWIR part of ASTER is no more working. The Sentinel 2A does not operate in the thermal infrared portions and even within shortwave infrared portions, only three bands are available.

The wide spectral range of near-infrared and short-wave infrared bands of ASTER image facilitate its applications in geology and soil sciences. There are more options for performing band ratio in either the near infrared or short-wave infrared regions which is usually the key indicator for mineral alterations and lithological unit identification.

The use of Remote Sensing applications in earth sciences continues to advance and progress as new methods and algorithms for manipulating Remote Sensing data are developed by researchers daily. Band and ratio indexes and Red Green Blue (RGB) color combinations for detecting certain minerals and features in the remotely sensed image are being developed in recent times by various researchers. Mohy et al. (2016) and (Arindam and Kumar, 2016) developed new band ratio indexes for mapping lithology and some specific minerals within their researched study areas.

GIS apart its main functions as data inputting, data storage and retrieval, data manipulating and analyzing, and data outputting also supports decision-making activities (Malczewski, 1999; Sugumaran and DeGroote, 2011). In this case, GIS is considered "as a decision support system which involves the integration of spatial data in a problem-solving environment" (Cowen, 1988). GIS's ability to handle judgments, preferences, and opinions is of critical importance in the planning and decision process (Malczewski and Rinner, 2015). However, the conventional GIS without MCDA is not well-suited for performing the critical tasks of decision-making activities such as preferences, value judgments, and priorities. The main reason for integrating GIS and MCDA is to enhance the capabilities and abilities of GIS in decision making and planning (Sugumaran and DeGroote, 2011). Integrating MCDA into GIS can improve the limited capabilities of GIS in storing and analyzing data on the decision maker's preferences. MCDA guides the decision maker(s) in evaluating criteria (attributes and/or objectives) and outlining values that are crucial to the decision-making process. Integrating MCDA with GIS can offer the decision maker the opportunity to inculcate judgments with respect to evaluation criteria and/or decision alternatives into GIS-based decision making (Malczewski and Rinner, 2015). MCDA can also aid decision makers in understanding the results of GIS-based decision-making processes and use the results to develop a systematic and defensible policy recommendation (Nyerges and Jankowski, 2011).

GIS is one of the reliable sources of information for decision making as it has the set of tools for acquiring, manipulating and analyzing data. GIS provides the platform for coordinating and integrating data from different and diverse sources. This ability of GIS can boost the prediction accuracy of the mineral potential model. GIS can generate a set of alternative decisions through its spatial relationship methods such as proximity, overlay, connectivity, and contiguity (O'Sullivan and Unwin, 2010).

The process of creating a map that shows the level of mineralization in the area is mineral potential mapping (Skabar, 2003). The mineral potential map can be used as a tool for defining locations with a high potential to host mineral deposits (Ford and Hart, 2013). The mineral prospectivity mapping was first introduced in the late 80 by geoscientists as a statistical tool for integrating and interpreting geoscience datasets from multiple sources (Bonham-Carter et al., 1989). The main idea behind mineral prospectivity mapping is to determine the link between the existence or absence of potential mineralization and the evidential layers such as geology, geophysics (Granek, 2016). The evolution of GIS and Remote Sensing technology has enhanced mineral prospectivity mapping. The ability of GIS to integrate and analyze multiple datasets from Remote Sensing, geology, geochemical, geophysics, and other geoscience fields has enhanced the results of mineral potential prediction. GIS output maps can serve as a guide for discussing, analyzing and reviewing mineral potential model, which may help in updating of the model.

The two main approaches to mineral prospectivity modeling are the knowledge-driven and data-driven approaches (Hartley, 2014). In the data-driven mineral prospectivity mapping model, known mineral locations are used as training sites to determine the spatial relationship between the geoscience datasets and the known mineral locations. The data-driven mineral prospectivity model is a supervised classification and hence the accuracy of its prediction of potential mineral locations is affected by the number of the known minerals used as training sites (Bonham-Carter, 1994). The data-driven mineral prospectivity models work perfectly if the study area has many known deposits locations (Hartley, 2014). The biases from the judgment or preference of the decision maker are being avoided since the spatial relationships between data and evidential layers are obtained directly from the training data. The main problem with data-driven mineral prospectivity models is their inability to perfectly predict unknown mineral locations even though they do predict known mineral locations well (Coolbaugh et al., 2007). Examples of some of the models used in data-driven mineral prospectivity modeling are the weights of evidence, neural networks and logistic regression (Carranza, 2009).

The knowledge-driven mineral prospectivity models perform well in poorly explored zones than data-driven mineral prospectivity models (Carranza, 2008). The knowledge-driven methods are subjective to the preference of the expert or the decision maker. The relative importance of the evidential layers is determined based on the expert's knowledge in defining spatial relationships between evidential layers and mineral deposits (Hartley, 2014). The expert's understanding and knowledge of the spatial relationships between the evidential layers and mineral under investigation will play a vital role in weighing the evidential layers (Yousefi and Nykänen, 2016). Fuzzy logic, Boolean logic, AHP and binary index overlay are some examples of methods used in the knowledge-driven mineral prospectivity mapping (Hartley, 2014).

Many algorithms have been used in mineral prospectivity mapping and the most common ones are Weights of Evidence (Agterberg et al., 1990), logistic regression (Harris and Pan, 1999), fuzzy logic and neural networks (Porwal et al., 2003; Raines et al., 2010). The essence of mineral predictive mapping is to attain the essential information needed for strategic planning in mineral exploration and development (Carranza, 2009). The information obtained from mineral predictive mapping can make mineral exploration work more effective and efficient. Mineral predictive mapping also offers the opportunity to integrate different layers of spatial recognition criteria of prospectivity into a common environment such as Geographic Information Systems.

1.2. Problem Definition

Turkey is one of the few countries where epithermal Au-Ag deposits are being extracted in large quantities (Mining Turkey, 2011). The epithermal systems are predominant in northern and western parts of Turkey. All the different forms of epithermal systems are virtually available in Turkey, but its identification and mapping have in the past relied on the traditional geologic field. The usage of Remote Sensing and Geographic Sciences have not fully applied in the identification and mapping of the hydrothermal alteration associated with epithermal deposits. The application of Geographic Information System models such weights of evidence has not used in predicting the potential epithermal deposits. Many mineral exploration works have been undertaken in the İzmir province to discover new potential minerals.

1.3. Literature Review

Development of new band ratio for mapping mineralization and lithology has not been researched by many researchers and below are some of the few authors who have contributed to this field. Mapping the lithology or rock units within an area is one of the most important works undertaken by geologists. Remote sensing technique has proven to be more useful in lithological applications. Band combination, band ratio, and principal component analysis are normally used in discriminating the various rock units within any geographical location. Many researchers have exploited remote sensing methods in lithological and alteration mapping. An ASTER based ratio of 4/7, 4/10, 4/11 was developed by (Mohy et al., 2016), to discriminate the lithology of Fawakhir in the Central Eastern Desert of Egypt. In their proposed index, they maintained the band 4 of VNIR dataset as constant and varied spectral band 7 in the SWIR and spectral bands 10 and 11 of the TIR spectrum. Arindam and Kumar (2016) proposed 10/12 * 10/12 for mapping rocks containing quartz, 10/11 for rocks containing feldspar and 12/13*13/14 for discriminating rocks containing mafic. Arindam et al. (2015) proposed ASTER based index of (2 *2)/ (1 + 3) and 1/3 to delineate chromitite and meta-ultramafite respectively in Dharwar Craton, India. Guha et al established their band ratio indices by using the spectra of chromitite and meta-ultramafite derived in the laboratory and the shortwave infrared and the near infrared data of ASTER. Their proposed quartz index produced better results when compared with the quartz index developed by Ninomiya and the same result as the quartz index proposed by Rockwall and Hofstra. Rajendran et al. (2011) developed a new ASTER band ratios combination of ((1 + 3)/2, (3 + 5)/4, (5 + 7)/6) in the RGB color composite to successfully map potential iron minerals in Southern Peninsular of India. Their proposed band ratio mapped out iron ore deposit in their study area better than the existing band ratio. ASTER based index of ((2 + 4)/3, (5 + 7)/6, (7 + 9)/8) in RGB composite was proposed by (Amer et al., 2016). They indicated that results from their proposed index were able to be discriminate metagabbros, serpentinites, and metabasalts much better than the previous index. Aboelkhair et al. (2010) proposed an ASTER based index in the RGB combination of 12/ 13:11/12:14/13 to map out albite granitoids in the Central Eastern Desert of Egypt. Gad and Kusky (2007) developed ASTER index of band 4/band 7, band 4/band 6, band 4/band 10 in the RGB composite to map the rock type in Wadi Kid area, Sinai of Egypt. The mapped lithology included abilities, meta-psammites, volcanic, schist, and amphibolite. Kalinowski and Oliver (2004) compiled some mineral extraction enhancement ASTER index as showed in Table 1.1.

Table 1.1. *Mineral enhancement ASTER index (Kalinowski and Oliver, 2004)*

Mineral	ASTR based enhancement index
Ferric iron	band 2/ band 1
Carbonate	Band 13/band 14
Illite/Smectite/Sericite/Muscovite/	(5+7)6
Kaolinite	Band 7/ band 5
Silica	11/10, 11/12, 13/10
Amphibole	(6+9)/8 and 6/8
Dolomite	(6+8)/7
Chlorite/Amphibole /Epidote	(6+9)/ (7+8)
Silica	11/10, 11/12, 13/10
Phengite	Band 5/ band 6
Silicon (IV) oxide	13/12, 12/13
Siliceous rocks	(11×11)/ (10×12)

Abdeen et al. (2001) examined the spectral signature of rock types in Allaqi suture of Egypt and developed an ASTER based ratio of 4/1,3/1,12/14 in the RGB composite to discriminate serpentinites, granites, and marbles. Their new band ratio index used spectral bands of VNIR, SWIR, and TIR. From the literature review, most of the proposed band ratios were developed for mapping mineralization in a location and therefore using these proposed band ratios for mapping mineralization in different locations with different land cover type, geology, and spectral response might not provide the best prediction result.

Arafat et al. (2013) created an internet spectral database for Egypt by using the spectral signatures of different vegetation’s, soil and rock types that were compiled by Egyptian National Authority of Remote Sensing and Space Science.

The analysis of diagnostic spectral features exhibited by alteration minerals is the key principle remote sensing relies on detecting alteration associated with mineralization (Carranza and Hale, 2002). Carranza and Hale (2002) mapped the hydrothermal alteration areas of densely vegetated terrains of Baguio in the Philippines using principal component analysis and band ratio technique on Landsat TM images. They used the mineral images and the pixels of known alteration zones as training data in detecting other hydrothermal alteration zones within the district. Tommaso and Rubinstein (2007) mapped out the alteration zones associated with Cu–(Mo) porphyry deposits in Argentina by using ASTER data. They concluded that ASTER's VNIR and SWIR show better results in identifying and highlighting alteration zones associated with mineralization whiles thermal infrared data were also useful in identifying and mapping silica and K-feldspar mineral alteration. The Al– OH response in band 6 and Fe–OH response in band 7 were highlighted with a band ratio of 4/6, 4/7, 3/1 in the RGB color composite. Hewson et al. (2004), used band ratios of 5/6, 7/6, 7/5 in RGB color combination to highlight the advanced argillic alteration areas. Alteration zones associated Abu-Marawat gold mineralization in the Eastern Desert of Egypt was mapped out by Gabr et al. (2010) using ASTER based band ratio of 4/8, 4/2, and 8/9 in RGB composite.

1.4. Objectives

The aims of the study are as follows;

- To propose the optimal ASTER band ratio indexes for mapping hydrothermal alteration zones for gold mineralization in the study area.
- To map hydrothermal alteration zones associated gold mineralization using principal component (PCA) analysis.
- To integrate hydrothermal alteration zones with other geologic data such as faults and lithology to predict the occurrences of new gold deposits.

1.5. Hypothesis

In this study, it is hypothesized that the potential gold mineralization within the research area would best map out with proposed ASTER band index. Also, the proposed

ASTER band ratio would best predict potential gold mineralization in a different part of the world with the same spectral response characteristics, land cover type, and geology. It was therefore hypothesized that the best prediction of potential gold mineralization in any location depends on the type of band ratio used and other factors such as the land cover types and local geology of the study area.

1.6. Research Questions

The following research questions listed below were investigated and addressed by this study.

1. Which ASTER band ratio would best identify hydrothermal alterations for exploring potential gold mineralization in the study area?
2. Which hydrothermal alteration mapping methods would offer the optimal alteration results in the study area?
3. Do the integration weights of evidence and the fuzzy logic model yield the optimal gold-silver prediction results?

1.7. Novelty and Originality

The originality of this thesis is the integration of weight of evidence model and fuzzy logic model to predict the potential gold-silver locations in the study area. In other words, the prediction of the potential gold-silver locations was based on both the data and knowledge-driven approaches of mineral prospectivity mapping. The proposed ASTER band ratio index was chosen based on the type of hydrothermal alteration and geology of the study area. Although, ASTER band ratio indexes of 4/8, 4/2, 8/9 in the RGB composite by Salem et al. (2013) and 7/6×4/6 and (7 + 9/8) by Salem et al. (2016) have been proposed for mapping gold alterations zones in Southern and Central Egypt, difference in geology and the nature of terrain do not guarantee better results when mapping hydrothermal alteration associated with gold mineralization in different parts of the world with the same band ratio indexes. This calls for the need to propose a band ratio index for extracting hydrothermal alteration specific to a specific geographic location or locations with similar geologic and topographic characteristics.

1.8. Importance of the Study

The approach used in the study would improve the mapping of hydrothermal alteration zones associated with gold mineralization in İzmir and the identification of potential gold-silver mineralization in Turkey. The proposed approach would help in gold exploration works by reducing the broad scope of exploration in terms of the cost, time and budget. The application of Remote Sensing and Geographic Information Systems in mineral exploration models was demonstrated in this study.

1.9. Scope and Limitations of the Study

This study aims at proposing a band ratio index for highlighting and mapping alteration zones associated with epithermal low sulfidation gold deposits of Ovacık, İzmir. Another method for mapping hydrothermal alteration zones associated with gold deposits such as principal component analysis was explored in addition to the band ratio technique. The extracted argillic alteration zone was integrated with lithology and faults to predict the potential gold-silver based on the weight of evidence model and integrated weight of evidence and fuzzy logic model. The study focused on the low sulfidation epithermal deposits of Ovacık and its environs. The illite spectral signature was extracted from the satellite image and not from the field.

1.10. Organization of Thesis

This thesis comprises five chapters. The first chapter introduces this thesis by offering brief background knowledge, reviewing related literature, and statement of the problem. Chapter two reviews concept and theories for extracting hydrothermal alteration zones from satellite image for exploration purpose. The concept of the weights of evidence and fuzzy logic model was also explained in detail. In chapter three, the step by step procedures used in achieving the research's objectives are highlighted in detail. The displaying of the research's results and discussions are done in chapter four and finally, the conclusion and recommendations are given in chapter five.

1.11. Impact of the Study

This research contributes to the knowledge base by providing information on how to map out epithermal low sulfidation gold mineral using remote sensing techniques. Literature has been properly reviewed on how hydrothermal alterations associated with gold where been explored with remote sensing data and technique. The maps produced in this study can serve as guiding information when undertaking further exploration work in the study area.

1.12. General Methodology

Firstly, the ASTER image (L1T) of the research area was obtained and the necessary corrections were applied. Radiance calibration and atmospheric correction were performed on the visible infrared and short-wave infrared dataset after stacking them to obtain the surface reflectance of the data. The difference in spatial resolution of the VNIR dataset and SWIR dataset were solved by normalizing them into the same spatial resolution. Two approaches can be used to rationalize the various datasets into the same size in terms of spatial resolution. The first one is the resampling of the smaller resolution datasets down to the bigger resolution dataset and the second method is the interpolation of the bigger resolution datasets up to the smaller resolution dataset. Interpolating the bigger dataset up to the smaller resolution dataset was used because this would prevent data loss of the bigger resolution datasets.

Band ratio technique and principal component analysis were to extract the was used argillic alterations associated with gold-silver mineralization in the study. Band ratio techniques create a new image by performing arithmetic operations on the bands of the image with the aim of highlighting the feature in the image. Band ratio may cancel out or reduce the common features within the datasets and at the same time exaggerate or highlight the features which are different in the datasets. The ratio of different bands from the same Electromagnetic region is used in soils, and geologic studies to highlight or extract geologic features. The illite index was proposed by using the USGS spectral and the image spectral profiles of the illite mineral. The extracted image illite spectral profiles were produced by using the gold mineralized zones of the Ovacık Gold Mine as sampling points.

Other methods for highlighting and mapping hydrothermal alteration zones such as the principal component analysis were also used. The results from the principal component analysis were then compared with the result from the illite index for the validation purpose.

The integration of extracted argillic alteration zones with lithology and fault were done using Geographic Information systems. The weights of evidence method were combined with the fuzzy logic model to produce the mineral potential of the study area. The result was compared with the result from only the weights of evidence model.

2. THEORETICAL FOUNDATIONS

2.1. Remote Sensing for Mineral Mapping

Remote Sensing has been utilized in many areas such as geology, mining, natural sciences, and forestry because remotely sensed data provides detailed information about the object being studied. The information about the object can be examined in different bands for better understanding and prediction of the object. For mineral predictive mapping, remote sensing performs a significant role in terms of techniques and data.

Landsat and ASTER satellite provide high spatial resolution imagery and multiple spectral bands within the same electromagnetic spectrum for better extracting and examining of geologic features. The reflectance and emission of minerals and rocks can also be easily detected and captured at different wavelengths of the electromagnetic spectrum for better identification and examination of the object under study. According to Saadat and Ghoorchi (2009), for a better understanding of geological setting, the type of mineralization and the spatial relationship between different mineralization in an area, high-quality satellite imagery plays an important role (Saadat and Ghoorchi, 2009).

Remote Sensing technique employs the spectral anomalies of the mineralization in locating the mineral deposits (Rajesh, 2004) and therefore there is the need to fully understand the usage and principles of remote sensing in relation to mineralization. The distinct absorption feature of most minerals is within the visible infrared, the short-wave infrared and the thermal infrared portions and can assist in the identification and extraction of mineral deposits.

Although Geophysical and Geochemical methods are normally needed to confirm the existence of potential deposits, however, the general information about the potential deposits exploration can easily be inferred by examining and interpreting spectral anomalies associated with the mineral (Rajesh, 2004). Mineral exploration remote sensing relies on factors such as geology, rock wall alterations and other anomalies in locating potential deposits. Hydrothermal alteration associated with minerals, lineament, faults and other geologic features related to mineralization can be easily detected and examined under remotely sensed imagery. Alteration maps of minerals can be done easily and cheaply by using remote sensing imagery and in general, the use of remote sensing techniques has brought some improvement in exploration geology (Saadat and Ghoorchi, 2009).

2.2. Electromagnetic Spectrum (EM)

The electromagnetic spectrum (EM) comprises all the form of electromagnetic spectrum radiations range from the gamma radiation through to the radio waves (NASA, 2013). Radiation is a type of energy that spread out as it travels. The electromagnetic spectrum provides us with heat and light which support the life of human and plants on the earth. All electromagnetic radiations travel in a vacuum with the same velocity as the speed of light. The electromagnetic spectrum is divided into many portions in terms of frequencies and wavelengths of the radiations. The naming of the various portions of the electromagnetic spectrum depends on characteristic changes of the waves in terms of their emittance, transmittance, absorptive capabilities and also their applications (Encyclopædia Britannica, 2017). The range of radiations in the electromagnetic spectrum and their sources is illustrated in Figure 2.1.

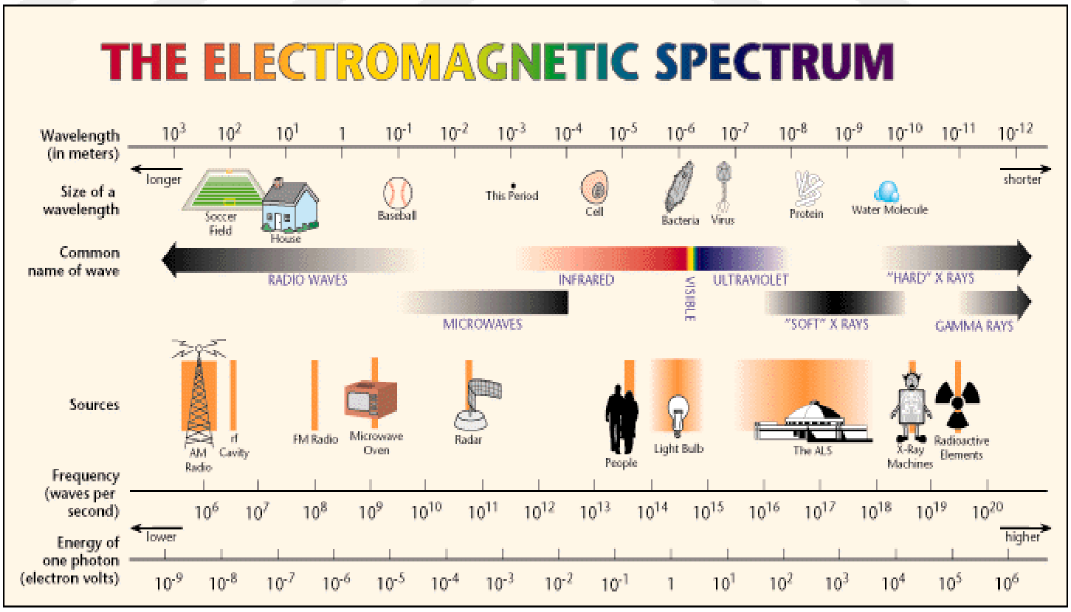

Figure 2.1. *Radiations in the electromagnetic spectrum (Humboldt State University, 2015)*

2.2.1. Visible-infrared (VNIR) remote sensing

The visible near infrared portion comprises the visible lights and the near-infrared regions. The visible portion is sensitive to the human eye while the near infrared part can only have detected by the sensor. The visible portion lies within 400nm to 700nm and the near infrared starts from 700nm to the 1400nm wavelength of the electromagnetic spectrum. The VNIR radiation is reflective in nature and is in color.

Both the crystal field and vibrational overtone absorptions can be detected with spectral characteristics within the VNIR spectral range depending on the composition and texture of the sensed materials (Traforti et al., 2017). Traforti and co. further, argue that are useful in mapping the spatial distribution and extent of fault core and damage zone domains for industrial and seismic hazard applications. The VNIR wavelength range of 800-1000nm exhibit absorption features of Iron oxide minerals (Cornell and Schwertmann, 2003). Gossans show some diagnostic spectral characteristics within the VNIR regions which help in their identification through remote sensing technique (Laakso et al., 2016).

2.2.2. Shortwave infrared (SWIR) remote sensing

The shortwave infrared remote sensing is a form of Remote Sensing technique that employs nonvisible light in the range of 1400 to 3000 nanometer (nm) in sensing objects. The SWIR is located between the infrared portion and thermal infrared region of the electromagnetic spectrum. The SWIR radiation is reflective in nature, but the imagery obtained from SWIR light is grey and not in color. SWIR Remote Sensing provides exceptional sensing capabilities which are often impossible when using other wavelength range (Baugh and Hamman, 2013). SWIR radiation can penetrate smoke and is less distracted by atmospheric aerosol. Many materials show diagnostic spectral features within the SWIR regions and are mostly used in detecting different rocks and mineralization types.

The high spatial resolution, the high sensitivity and the day and night working capabilities of SWIR radiation makes it applicable in many research areas such as mineral exploration, wildfire response, mining and geology, urban feature identification (Singh, 2015).

Electronic absorption and vibrational absorption are the two concepts that are applied in SWIR Remote Sensing in detecting materials. When SWIR light gets interaction with an object, one of these absorption phenomena takes place depending on the composition of the object. Absorption spectral diagnostic features within 1000 and 2500 nm of SWIR regions are mainly caused by Si-OH, Al-OH, CO_3, Mg-OH, Fe-OH, NH_4 and SO_4 compounds which are useful in identifying materials containing these compounds (Baugh and Hamman, 2013). The three atmospheric windows of SWIR radiation and the possible application areas are shown in Table 2.1.

Table 2.1. *Atmospheric window of SWIR light*

SWIR Atmospheric Windows	Application Area
Near 1250 nm	For vegetation studies and identification of material containing iron because of its iron absorption features
1500 and 1750 nm	For identification of artificial objects, petroleum, snow, and ice.
2000 and 2400 nm	For mineralization mapping

2.2.3. Thermal infrared (TIR) remote sensing

The thermal remote sensing focuses on capturing, analyzing and interpreting of data within the thermal infrared region of the electromagnetic spectrum (Prakash, 2000). In thermal remote sensing, emitted radiations from the object are measured rather than the reflected radiations from the object. The emitted radiations from the surface's object are stronger in the thermal infrared regions than in the reflective regions.

The thermal infrared can be located within 3 to 35 µm wavelength of the electromagnetic spectrum and thermal infrared radiations are in the form of heat which is invisible to the human eye and can only be detected by thermal sensors. All bodies having a temperature above the absolute zero produce some form of thermal infrared radiation and by analyzing and examining these emitted radiations, rock types and some minerals can be identified. Other application areas of thermal infrared remote sensing include coastal zones studies, forest fires identifications, detection of mine fires such as coal mining fires and environmental modeling.

The best atmospheric window for thermal infrared remote sensing lies between 8-14 µm wavelengths but there are other poor thermal infrared atmospheric windows, 3-5 µm, and 17-25 µm and analyzing data from these atmospheric windows are quick complex and complicated (Prakash, 2000).

The ratio of radiations emitted from an object to the radiations emitted from a blackbody (a perfect emitter) at the same wavelength and temperature is referred to as the emissivity of the object. In Geology and Geophysics, the composition of rocks and mineral are determined by the concept of emissivity. For example, in Figure 2.2 the emissivity of quartz, feldspars, and hornblende plotted against wavelength are shown.

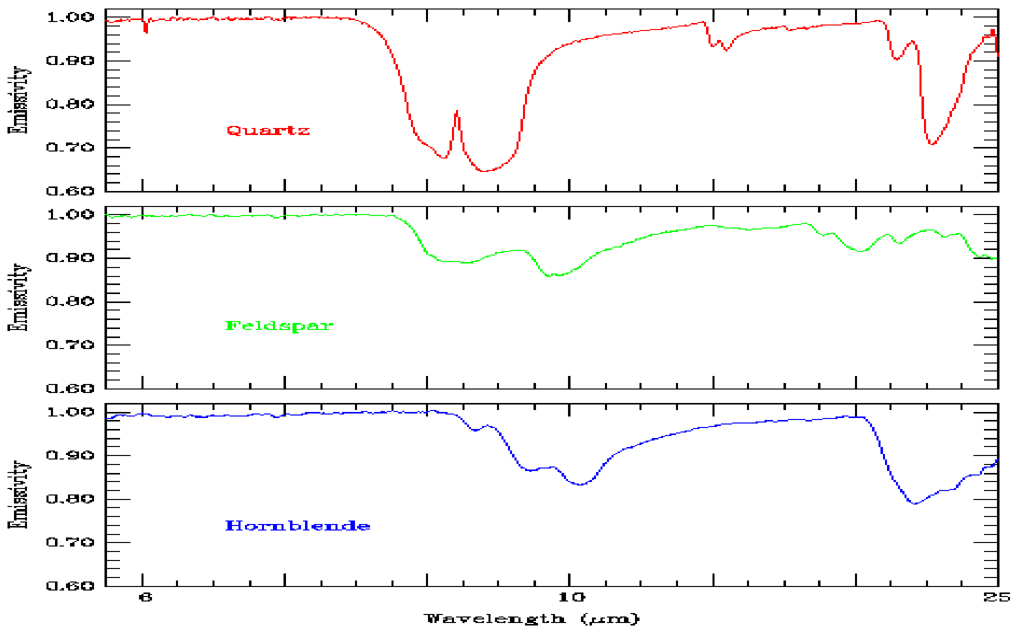

Figure 2.2. *Emissivity of Quartz, Feldspars, & Hornblende against wavelength (Humboldt State University, 2015)*

2.3. Electromagnetic Radiation Interaction with the Atmosphere

The first point of contact of the electromagnetic radiations from the sun is the atmosphere. Within the atmosphere, the atmospheric particles and the electromagnetic wave interact in the form of scattering, absorption, and transmission. The greater portion of the electromagnetic radiations is being absorbed by atmospheric particles in the upper atmosphere whiles atmospheric particles such as dust and water droplets reflect some portions of electromagnetic waves back into space. Between the wavelength of 13 and 17.5 µm, radiations of the sun are being absorbed by carbon dioxide, and near wavelengths of 1.1, 1.4, 1.9, 5.5, 7 and above 27 µm, the sun's radiations are also being absorbed by water vapor (USGS, 2016). Some portions of the shorter wavelength radiations are also scattered by atmospheric particles such as dust, smoke, and water droplets. Those portions of radiations that are not either affected by absorption or reflections find their ways to interact with materials on the earth's surface. Some portions of the atmosphere that allows transmission of electromagnetic radiations onto the earth's surface are called the atmospheric windows. The diagram in Figure 2.3 explains the concept of electromagnetic radiation interaction with the atmosphere.

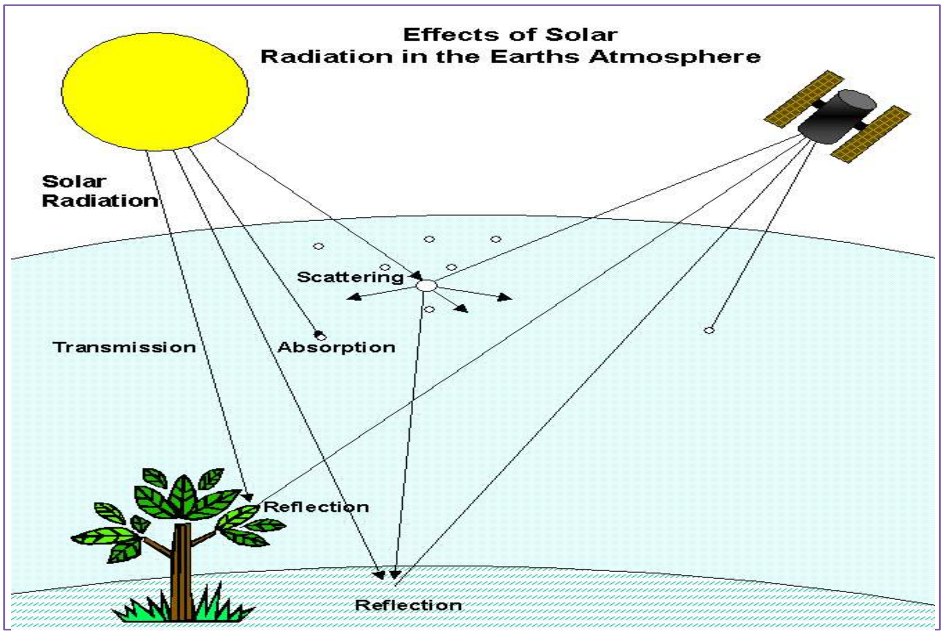

Figure 2.3. *Electromagnetic radiation interaction with the atmosphere (USGS, 2016)*

2.4. Electromagnetic Radiation Interaction with the Target

The sun's radiations interacting with earth's surface objects is one of remote sensing's major component. The object can only be studied in remote sensing through its interaction with the electromagnetic waves. The electromagnetic radiations transmitted through the atmosphere or scattered from atmospheric particles onto the earth's surface are called the incident radiations. The incident radiations upon reaching the earth can be transmitted, absorbed or reflected by features on the earth's surface. These three interactions of the incident radiation are demonstrated in Figure 2.4.

The magnitude of the energy being absorbed, reflected or transmitted through the object is dependent on composition and conditions of the interacting object and wavelength of the incident radiation (Department of Geology; Aligarh Muslim University, unknown).

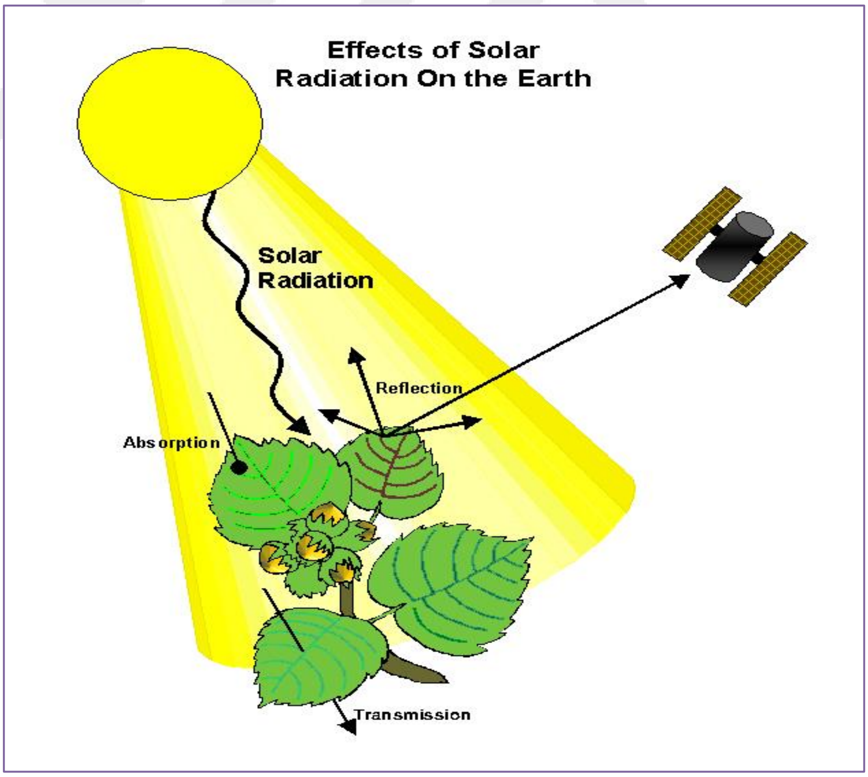

Figure 2.4. *Effects of solar radiation on the Earth (USGS, 2016)*

2.4.1. Absorption

When the incident radiations are stored within the earth's surface feature, the process of absorption takes place. Analyzing diagnostic spectral absorption helps in understanding the chemistry of minerals or rocks (Clark et al., 2007). Most minerals absorb radiations or photons in the visible-near infrared, shortwave infrared and thermal infrared portions of the electromagnetic spectrum. Absorption features in reflectance spectra are used in identifying mineralogy and chemical composition of different types of rocks

2.4.1.1. *Cause of absorption in minerals*

The main causes of absorption features in minerals are electronic transitions and vibrations. An electronic transition causes absorption in wavelengths up to about 1.0-micrometer wavelength while vibrations occur at the molecular level with absorption at around 0.7 micrometers through to the thermal infrared and beyond. Examples of materials that have important vibrational absorptions are water, hydroxyl, carbonates, phosphates, borates, arsenates, vanadates (Figure 2.5). Electronic transition exists in three forms and these are (a) *crystal field effect absorption* and is caused by Fe^{2+}, normally occur in transitional elements (b) *charge transfer absorption* and is called by Fe^{3+}, Fe_2O_3, FeOOH and (c) *conduction bands* and is called by S and HgS (Figure 2.6). Any material containing any of these absorptive elements will exhibit absorption features in the reflectance spectra.

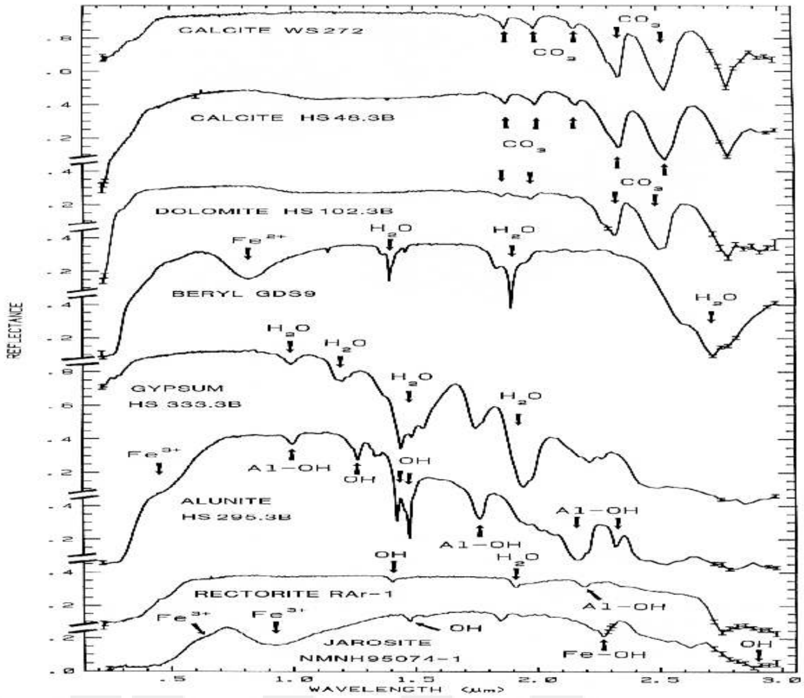

Figure 2.5. *Vibrational absorption band due to H_2O, Al, OH, Fe^{2+}(Clark, 1999)*

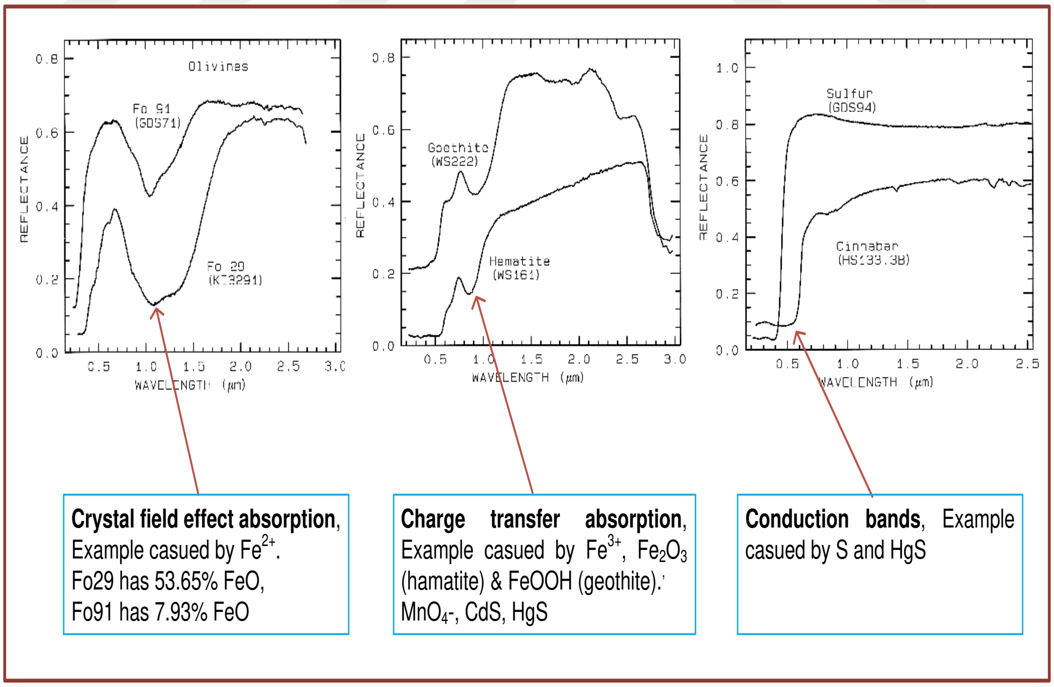

Figure 2.6. *Types of electronic transitional absorption (Clark, 1999)*

2.4.2. Reflection

The scattering of the incident radiations from the earth's surface features is the main pole of remote sensing as the sensors measure and capture these reflected radiations from the features for further examination and analysis. The amount of energy reflected by the object depends on the incident radiations and the composition of the object. Reflection from earth's surfaces can either be diffuse or specular. When the object surface is smooth, specular reflection and when there is a rough surface, diffuse reflection occurs. Most earth's features are neither too smooth nor too rough.

Radiance and reflectance are the two main word associated with reflection. Radiance is the amount of energy light or brightness measured by the sensor. Radiance may consist of the energy or radiations reflected from both the atmosphere and the earth's surface. The atmospheric effects on radiance are due to energy attenuation and the introduction of "path radiance" (Humboldt State University, 2015). Reflectance on the other hand is the energy reflected from the object and is expressed in percentage, thus; % Reflectance =100 x Reflected/Incoming (Humboldt State University, 2015). In remote sensing, the reflectance characteristics of surface features are key to identifying different objects. The concept of radiance and reflectance is illustrated in Figure 2.7.

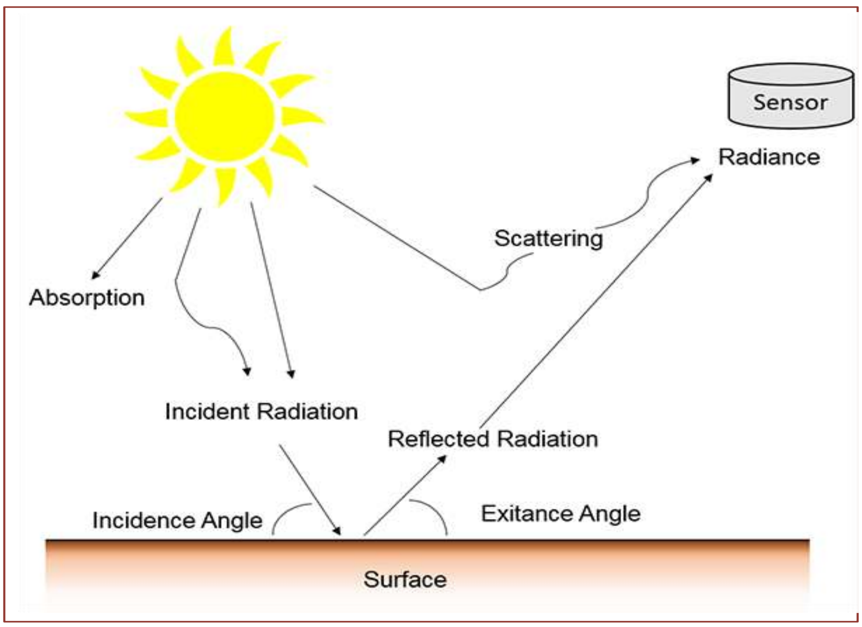

Figure 2.7. *Concept of radiance and reflectance (Humboldt State University, 2015)*

The reflectance of rocks is quite simple than soil and dependence on the mineral compositions, structure, and texture of the rocks. Lower reflecting minerals like goethite, show low to moderate reflectance at visible wavelengths while in near-infrared regions, they show high reflectance. High reflecting minerals, such as quartz and calcite, display virtually homogenously high reflectance throughout the near visible infrared and shortwave infrared wavelengths. Figure 2.8 shows the reflectance of some rocks in the visible-near infrared and shortwave infrared zones.

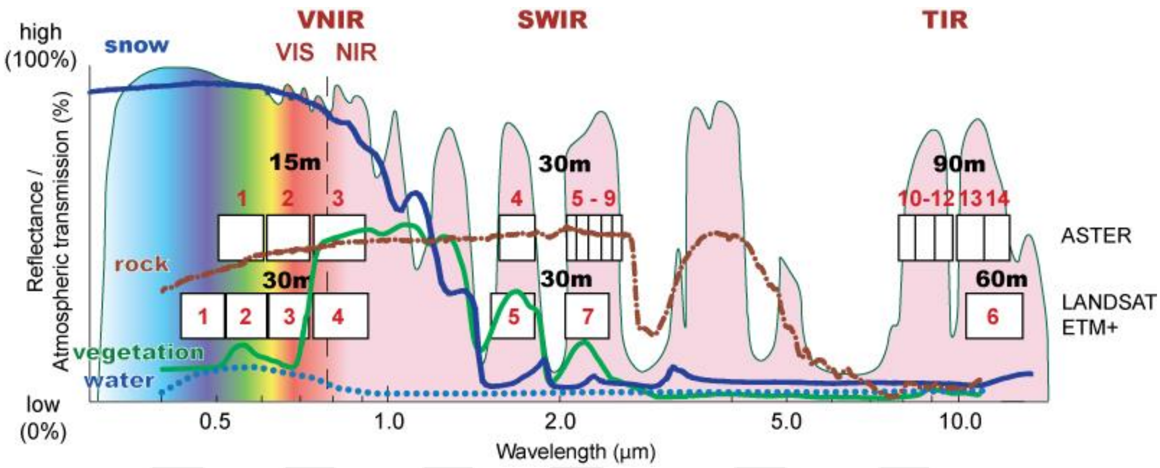

Figure 2.8. *Reflectance of rock in the VNIR and SWIR regions (European Space Agency,2014)*

2.5. Spectral Signature

The spectral reflectance properties of objects at varying wavelengths of the electromagnetic spectrum are the main factors used in Remote Sensing for discriminating different features on the earth. The physical, chemical and biological composition of objects make objects reflect, absorb and transmit different among the amount of the incident light at a different wavelength of the electromagnetic spectrum.

When the spectral reflectance is expressed as a function of wavelength, the spectral signature is then obtained. Each feature has a unique spectral signature and by examining and analyzing the spectral signature, features with the same spectral responses can be identified and grouped. On the spectral signature plot, there is high reflectance of the feature at some specific wavelengths and a low reflectance at some specific wavelengths as well and by analyzing the difference in reflectance, the feature under study can be easily identified.

The distinct spectral response of features or objects is the backbone of Remote Sensing analysis and therefore a critical examination of factors that influence the spectral response characteristic (thus within wavelengths we can find maximum and minimum reflectance) of the features under investigation are necessary for the correct interpretation and extraction features in Remote Sensing.

2.5.1. Minerals and rock's spectral signature

The key element used in identifying objects in remote sensing is the spectral signature or response of the objects. Examining the diagnostic spectral signature of rocks and minerals clarifies how to identify and map them when using Remote Sensing technique. Comparison of spectra from freshly cut rocks with the spectral outcrop rocks can provide detail information about the relationship between superficial alteration product and original rock which is useful in locating similar rocks (Rajesh, 2004). The most commonly used data for the identification of minerals of rocks on other planets and the earth's surface is the spectroscopic data (Guha and Vinod 2016). The concept behind the use of spectroscopic data for detecting minerals and rocks is based on the identification of absorption diagnostic features of the rocks and minerals (Guha and Vinod, 2016). Many authors in literature such as Hunt (1977) and Clark and Roush (1984) have done extensive works on minerals and rocks spectra.

Aggregation of minerals results in rock formation and mineral consists of one or more elements which are grouped together. The interaction between the chemical bonds of the crystalline lattice structure of rocks and minerals and incident electromagnetic radiation produces identifiable features in the reflectance spectrum of the object (NLN for Remote Sensing, 1999). These identified features in the reflectance spectrum of the rocks and minerals can serve as key information in identifying these rocks or minerals. The crystalline lattice structure of rocks and minerals make it impossible to be identified within a single wavelength as the various element components within the minerals that form the rock may exhibit different spectral response. The crystalline lattice structure of mineral allows for the existence of numerous absorption bands at varying wavelengths because of electronic transitions and ion vibrations within the mineral (Hunt, 1977). The spectral reflectance anomalies are within 1.1 and 2.5µm and in the near infrared zones are the results of vibrational transitions within the mineral (Rajesh, 2004).

Most rocks and minerals show diagnostic spectral response characteristics in the near infrared, short wave infrared and thermal infrared regions of the spectrum. The VNIR band of ASTER displays diagnostic absorption features of transition metals particularly rare-earth elements and iron minerals whiles Landsat TM 1 and 2 shows strong reflectance spectra of rocks containing iron oxides. The SWIR bands of ASTER show diagnostic absorption features of carbonate (2.3µm), hydrate and hydroxide mineral. Quartz has a diagnostic emissivity signature within the TIR bands of ASTER (Hewson et al., 2005).

Comparing the mineral spectral library with spectra derived from ASTER image can give a hint of the limitations and capabilities of using ASTER image in identifying a mineral or rock. Figure 2.7 and 2.8 shows the comparison of the mineral spectral library with the ASTER image derived spectra. The solid lines represent laboratory spectra of the minerals while dashed lines represent the ASTER equivalent resampled spectra.

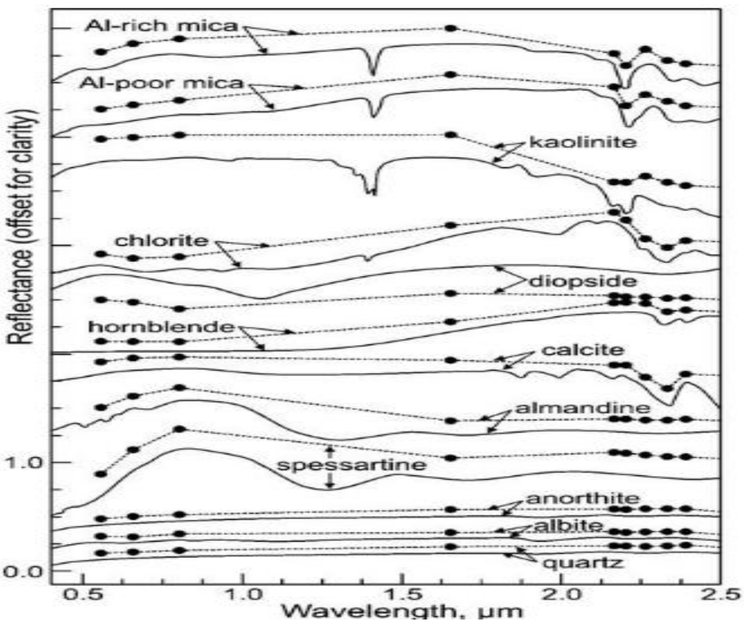

Figure 2.9. *Laboratory and ASTER-derived VNIR–SWIR mineral spectra library (Hewson et al., 2005)*

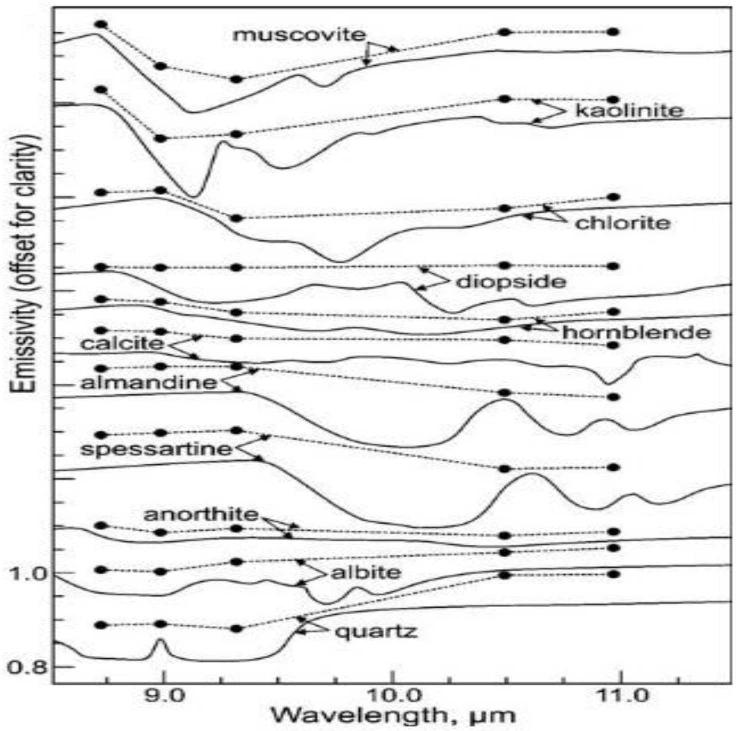

Figure 2.10. *Laboratory & ASTER-derived TIR mineral emissivity library (Hewson et al., 2005)*

2.5.2. ASTER spectral library

The successful application of ASTER data in mineralization and rock studies is mainly based on the availability of ASTER Spectral Library. The ASTER spectral library is a collection of spectra of materials from the Jet Propulsion Laboratory (JPL), Johns Hopkins University (JHU) and the United States Geological Survey (USGS) and it can be accessed at https://speclib.jpl.nasa.gov.

About 2300 materials' spectra were sampled within the wavelength range of 0.4 to 15.4 µm in a standard format with ancillary data. These materials include vegetation, soil, rocks, minerals, and other artificial objects. The first version of the ASTER spectral library was released in July 1998 and with the current version of 2.0 released on December 3rd, 2008. The ASTER spectral library can be obtained at no charge after completing the ordering form at https://speclib.jpl.nasa.gov/order and within 4-6 months the ASTER spectral library available on CD-ROM can be received.

The rock spectra are derived in the laboratory by examining spectra of the rock and its constituent minerals in VNIR and SWIR regions of the spectrum (Arindam and Kumar, 2015). The comparative analysis of rock spectra helps in identifying spectral diagnostic features of the rocks and minerals (Guha et al., 2012).

2.6. Hydrothermal Alteration of Minerals

The potential economic importance of hydrothermal alteration of rocks and their associated diagnostic spectral characteristics for remote identification of minerals has made the hydrothermal alteration analysis of minerals a major research area (Azizi et al., 2010). Hydrothermal alteration is the modification in mineralogy, texture, physics, and composition of rock because of its interaction with hot water fluids. Hydrothermal alteration results in a change of the primary minerals to more stable secondary minerals. Hydrothermal alteration occurs when hot water fluids travel through the rocks and alter rock composition by reducing or increasing or reallocating the mineral constituents (Lagat, 2009). Hydrothermal alteration usually differs from location to location and even among individual deposits (Shanks III and Pat, 2012).

The essences of identifying and examining hydrothermal alteration were identified by Shanks III and Pat as the following; (1) the systematic arrangement of hydrothermal alteration zones can give vital information in locating the mineral. (2) It can aid as a guide in identifying undiscovered deposits. (3) it can offer information on the originality of elements in the mineral.

2.6.1. Causes of hydrothermal alteration

The alteration of the mineralogy of the rock can be attributed to a lot of factors. The main causes of hydrothermal alteration are described below:

Permeability: Permeability of the rocks affects hydrothermal alteration by controlling the access of hot water fluids into the rock. Permeable rocks are more easily altered by hydrothermal fluids than the impermeable rocks. The permeability of the rock can also affect the level of precipitation of the secondary minerals of the rock (Lagat, 2009).

Temperature: The major important factor in hydrothermal alteration is temperature because higher temperatures are normally required for most of the chemical reactions between the thermal fluid and the rocks to take place and also minerals are more stable at higher temperatures (Lagat, 2009). Alteration mineral form is mainly determined by temperature and pressure. For instance, chlorite turns into biotite at a temperature above 250^o.

Pressure: Pressure is not the main contributor of alteration in mineral but plays some role in the hydrothermal alteration process by controlling the depth at which boiling occurs.

2.6.2. Type of hydrothermal alteration

There are many alteration types but only the most common ones are discussed in the thesis and these are; Phyllic alteration (quartz, sericite and pyrite), Argillic alteration (pyrophyllite, montmorillonite, kaolin and dickite), Potassic alteration (potash feldspar and biotite), Propylitic alteration (calcite, chlorite and epidote), Silicification (quartz and chert), Dolomitization, Greissenisation, Feldspathization, Fenitizaztion and Bleaching.

2.6.3. Geochemistry of hydrothermal gold deposits

The mineralization of gold is normally associated with clay minerals alteration, calcite alteration, and iron oxide alterations and can be located within quartz veins (Amer et al., 2016). Gold as a mineral could not be sensed by any remote sensing methods directly but its associated alteration zones can be rather sensed through remote sensing methods (Amer et al., 2016). The hydrothermal alteration of gold is mostly carried as Au-Cl and Au-S solutions, other solutions such as Au-As and Au-Sb are the possible medium through which gold can transport (Zhu et al., 2011). Gold precipitations are formed when there is a change in temperature, pressure, pH values, Cl^- concentration, and fugacity of H_2S in a hydrothermal system and normally occur at a temperature (above 400^0 C) (Zhu et al., 2011). According to Frimmel (2008), gold ore deposits are mainly formed through hydrothermal alteration (Frimmel, 2008). The alteration of gold deposition can be of two forms and these are Epithermal and Porphyry deposits. The formation of each type of deposition is shown in equation 2. 1 and 2.2.

Epithermal:

$$Au\,(H)_{2}- + 2H^{+} + e^{-} = Au_{(s)} + 2H_2S \qquad (2.1)$$

Porphyry:

$$Au_{(s)} + Cl^{-} + HCl_{(aq)} + \frac{1}{4}\,O_2\,(g) = AUCl_2^{-} + \frac{1}{2}\,H_2O_{(l)} \qquad (2.2)$$

2.6.4. Alteration as a tool in mineral exploration

A large volume of rocks and minerals are normally altered by hydrothermal alteration process and by correctly identifying and examining these alterations associated with mineral, the larger target of the ore body can easily identify. The hydrothermal alteration zone around an ore body can offer key information in locating ore body.

Hydrothermal alteration mapping can be done by using multispectral remote sensing technique. Hydrothermal alteration forms and its associated minerals have been mapped from remote sensing data such as Landsat, ASTER, worldview 3 by many authors in different locations (Amera, 2007; Clark, 1999). Creation of band ratios and color composite images from the VNIR, SWIR and TIR bands are some of the methods used in identifying hydrothermal alteration zones associated with ore body. The absorption features of minerals play an important role in identifying hydrothermal alteration.

2.7. Image Pre-processing Analysis

Pre-processing of the image are the various corrections performed on the satellite image before the actual extraction of data and other analysis takes place. Raw satellite image data contains some distortions, path radiance, and other errors. The purpose of pre-processing is the improvement or enhancement of the image for further processing (Sonka et al., 1993). For better output results, there is the need to apply pre-processing analysis to the imagery. The main operations performed in image pre-processing are radiometric and atmospheric correction, image registration and geometric correction. Each of these corrections helps in enhancing the quality of the raw satellite image data for further feature extraction.

2.7.1. Radiometric correction

The sun's azimuth and elevation and atmospheric conditions can make the sensors onboard aircraft or satellite detect and capture energy that is different from the earth's surface emissivity or reflectance. This situation normally distorts the interpretability and quality of the satellite data. Radiometric correction restores the distortion resulting from the sun's azimuth and elevation and atmospheric conditions. After radiometric and atmospheric corrections are being applied to the image, the true or actual reflectance of the earth's surface features can be obtained. The processes needed to obtain the ground reflectance are shown in Figure 2.14

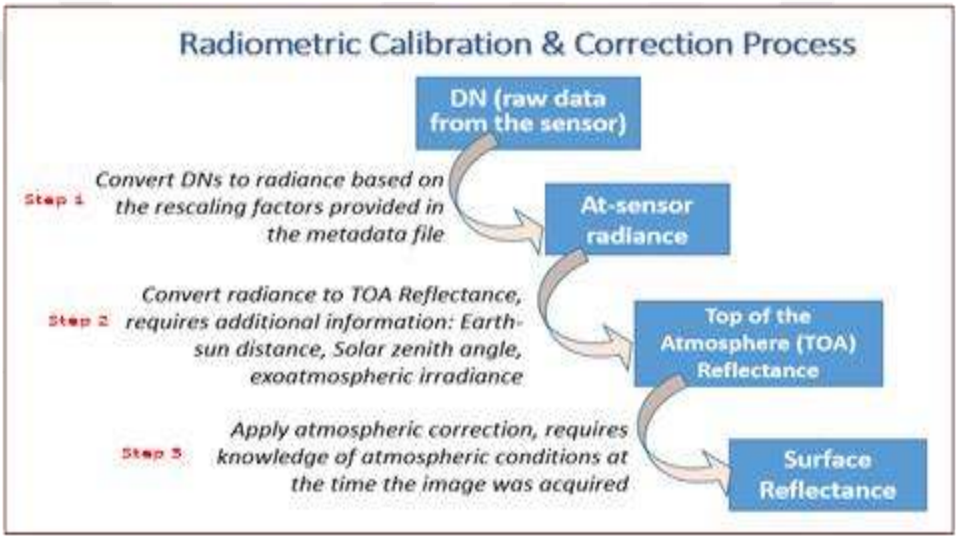

Figure 2.11. *Radiometric calibration and correction process (Humboldt State University, 2015)*

2.7.2. Radiometric calibration

The intensity or amplitude of the emitted or reflected radiations is recorded by the sensor onboard aircraft or satellite in a form of digital numbers (DN) (Humboldt State University, 2015). The radiometric resolution of the sensor determines the exact range of DN. This digital number needs to be changed into radiance, reflectance or emissivity. Green et al. (2000) stated the importance of converting DN to radiance or spectral unit as the following; (1) when the DN is converted into spectral units, a comparison can be made easily with other images of the same area. This is useful when performing change detection analysis. (2) the spectral library is made up of reflectance and not digital numbers. Although most image analysis is carried out using the digital number values without considering the feature's spectral reflectance, the problem with this approach is that only the intensity of the emitted or reflected energy is assessed not the spectral reflectance (Edwards, 2015).

2.7.2.1. *Converting Digital numbers to spectral radiance*

The radiance scaling factors accompanied with the image in metadata file is used when transforming digital numbers to radiance. Most of the image processing software packages have tool for converting the DN to radiance. The formula for converting DNS in Landsat 8 image to spectral radiance is given below;

$$\text{Radiance} = M_L * Q_{cal} + A_L \tag{2.3}$$

Where:
M_L = Radiance multiplicative scaling factor, A_L = Radiance additive scaling factor and Q_{cal} = L1 pixel value in a digital number

The formula for converting digital numbers in ASTER image to spectral radiance is given below;

$$L\lambda = (DN-1) \text{ x Unit conversion coefficient} \tag{2.4}$$

The gain can be obtained from the header file, GAINBand# = HGH or NOR in the metadata file. The gain or Unit conversion coefficients for each band of ASTER were also computed by (Abrams et al., 1999). For band 1, the gain value is 0.676, for band 2, 0.708, for band 3, 0.862, 0.2174 for band 4, 0.0696, 0.0625, 0.0597, 0.0417, 0.0318, 0.006822, 0.006780, 0.006590, 0.005693 and 0.005225 for bands 5, 6, 7, 8, 9, 10-14 respectively.

2.7.2.2. *Converting digital numbers to reflectance*

The radiance detected by the sensor above the atmosphere is called top-of-atmosphere radiance (TOA) and it can be obtained by converting the raw digital numbers (DN) in the images. Most of the image processing software packages have tool for converting the DN to TOA radiance. Figure 2.12 shows the steps for converting digital numbers to surface reflectance

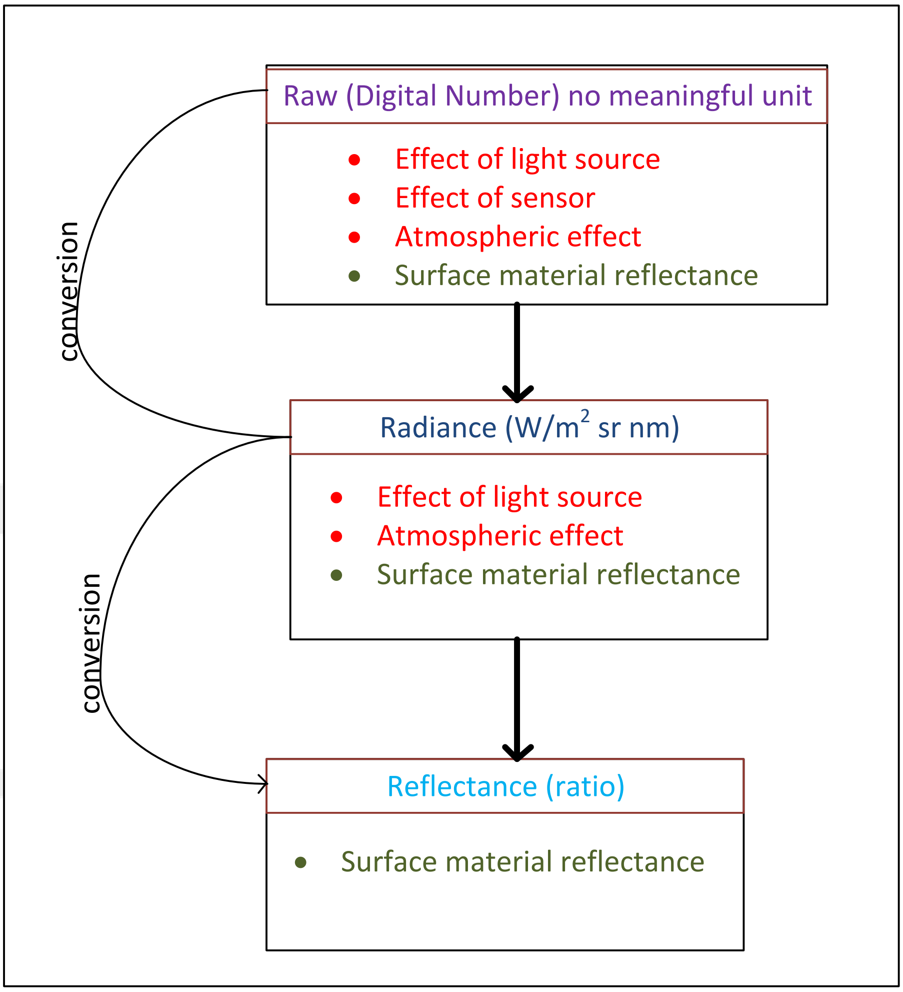

Figure 2.12. *Steps for converting DN to surface reflectance (Humboldt State University, 2015)*

2.7.3. Atmospheric correction

The process of removing or reducing the effect of atmospheric conditions on the image to obtain the surface feature's reflectance is called an atmospheric correction. In other words, atmospheric corrections are performed on the image to suppress atmospheric effects such as scattering and absorption on the electromagnetic radiation. Performing atmospheric correction is necessary when undertaking studies that involve data from multiple seasons and time.

2.7.3.1. *Types of atmospheric corrections*

The atmospheric correction converts radiances imagery to reflectance imagery (Gebreslasie et al., 2009). The two main types of atmospheric correction are empirical or absolute and relative atmospheric corrections (San and Suzen, 2010). In an absolute atmospheric correction is simply transforming the digital number into reflectance while relative atmospheric correction maintains the digital number without changing them into reflectance (Song et al., 2001).

Relative atmospheric correction uses only the statistics of the image in reducing the atmospheric effects and therefore prior information of features characteristic and the type of atmospheric model to be used are not necessary (San and Suzen, 2010). Some examples of the relative atmospheric correction methods is flat field, empirical line, and internal average relative reflection corrections.

Absolute or empirical atmospheric corrections are, however, applied to decrease scattering and absorption effects of the atmospheric particle (San and Suzen, 2010). The absolute or empirical atmospheric corrections methods utilize the atmospheric conditions and the difference in radiations in modeling the atmospheric effects on the image, thus reflectance is obtained by performing a ratio of the sensor radiance to irradiance (San and Suzen, 2010).

Examples of the absolute or empirical atmospheric corrections model are; the MODTRAN atmospheric model developed by Berk et al. (1998), for reducing clouds and thick aerosol effects, multiple scattering and strong molecular absorption. The Fast Line-of-sight Atmospheric Analysis of Spectral Hypercubes (FLAASH) is also one of the popular absolute atmospheric correction methods. FLAASH atmospheric correction technique is designed to remove or reduce the scattering and absorption effects of atmospheric molecular and particulates at the sensor to obtain the surface reflectance (San and Suzen, 2010). The FLAASH atmospheric correction is being employed in ENVI software package and the most often used for removing atmospheric effects.

Dark object subtraction is also an example of the absolute atmospheric correction and it is perhaps the simplest correction method. Dark object correction is normally recommended before performing image classification and change detection analysis. According to Song et al. (2001), the dark object correction method presumes the presence of no or small reflectance in the remotely sensed data and are usually associated with dark objects like sea water bodies. The lowest digital number is used in dark pixel correction by subtracting it from the other digital numbers in the entire image.

2.7.3.2. *Radiometric and atmospheric corrections essences*

The reasons why radiometric and atmospheric corrections are needed in image processing are highlighted by as the follow; (1) Radiometric and atmospheric corrections are applied in multi-temporal analysis (land use/land cover detection) to correct the effects of difference in sensor, atmospheric and illumination conditions of multiple images (Paolini et al., 2006). In multi-temporal analysis, the use of radiometric uncorrected images may result in pixel misclassification and wrong estimates of land cover areas because normally training data or spectral signatures derived from a particular image is used in classifying the land cover types of all the other images; (2) the comparison of spectral information of land cover types across multiple scenes can only be achieved after radiometric and atmospheric corrections have been applied; (3) the integration of different sensor data types and mosaicking are only possible after the application of radiometric and atmospheric corrections on the individual image types; (4) the image used in performing band ratio analysis should be radiometrically and atmospherically corrected to highlight the feature under-investigated.

2.8. Spectral Enhancement

Image enhancements, in general, are performed for better interpretation and understanding of remotely sensed data. Spectral enhancement improves the spectral characteristic of the multispectral image by creating a new dataset (Parece et al., 2015). Parecel et. al., (2015) elaborated on the essence of spectral enhancement as follows; (1) spectral enhancement makes the visual interpretation and classification of the image easier and simpler. (2) It helps in reducing redundant datasets from the multi-spectral image (principal component analysis). (3) Spectral enhancement can help in displaying hidden information within the image dataset.

Band ratio, Band combination, spectral indices, and Principal Components Analysis (PCA) are some of the most frequently used spectral enhancement techniques in image analysis.

2.8.1. Band ratio indices

The spectral reflectance of objects in different wavelength regions is the main principle behind the concept of image band ratio analysis. Minerals and rocks normally display different reflectance response at different spectral wavelength ranges and are most often identified and mapped with band ratio techniques (Chandrasekar et al., 2011). Iron oxide minerals, for instance, show high absorption feature in 800-1000 nm and high reflectance in other wavelength regions.

Combining band ratio image boosts the digital numbers or the reflectance of ratio band image by eliminating common features associated with bands involved in the band ratio operation (Jun et al., 2008). According to Juan et al., dividing the band with high reflection peak by the band with high absorption point can show or give more information about the material under study and at the same times reduces or eliminates other redundant information associated with the material.

The lost reflection intensity information of the surface features is the main setback of using band ratio analysis (Jun et al., 2008) and this defect can be corrected by combining one origin band with two ratio image to form one color image (Jun et al., 2008). The Laboratory–measured spectral profiles of materials are normally used to construct the band ratio indices for detecting the material but the main problem with the laboratory-measured spectra (ASTER library) is that the laboratory-measured spectra are at times different from the true spectra of the field material because of difference in conditions in the field and the laboratory (Gabr et al., 2010). This setback is most often overcome by comparing the laboratory measured spectra against the field-measured spectra of the same material at the same location.

2.8.1.1. *Importance of band ratio analysis*

Band ratio analysis is being utilized in many research areas such as mineral exploration and geologic structural studies and vegetation dynamics analysis. The band ratio analysis can be used for mapping the alteration zones associated with mineralization (Yajima, 2014). For instance, advanced argillic alteration zones can be highlighted and mapped with ASTER band ratio of 4/6, phyllic alteration zones are rather highlighted with ASTER band ratio of 5/6 and ASTER band ratio of 5/8 can also enhance the propylitic alteration zones.

Lineaments and geologic structures can be highlighted for easy visual extraction after band ratio analysis is being performed on the satellite image. Band ratio image can be used to detect or highlight the differences in similar land cover types that would have been very difficult to detect without performing the band ratio index on the raw image (Yang et al., 2008). Band ratio analysis can remove or reduce the effects of seasonal changes and slope shadows, and also can neutralize the sunlight angle or intensity difference within the image (Jensen, 1986), thereby providing only the spectral information without any topographic effects (Yang et al., 2008). Band ratio analysis can offer useful information that may not be present in any of the bands that were used to provide the band ratio image.

2.8.1.2. *Examples of band ratio index*

Band ratio indexes have been developed by researchers for easy identification and mapping of various objects of interest such as vegetation cover, water body, soil, minerals, and rocks. The common band ratio indexes are vegetation indexes such as Normalized Difference Vegetation Index (NDVI), clay ratio index, ferrous mineral ratio index, Iron oxide ratio index, soil index, and water index.

NDVI is a numerical scale that ranges from -1 to +1 and used to show the level of “greenness” of a land cover. Low NDVI values correspond to no vegetation areas and high NDVI values correspond to high vegetation cover. In 1973, the first application of NDVI was carried by Rouse and colleagues to monitor Great Plains vegetation systems by using MSS data from ERTS-1 (Rouse et al., 1973). After Rouse and colleagues, NDVI has been used by many researchers for different applications and it is considered as the most common ratio indices for vegetation.

NDVI was developed by using the visible red band and near-infrared (NIR) band of the spectrum because healthy vegetation cover exhibits a high reflectance in the near-infrared band and a high absorption peak in the visible red band. The formula for NDVI is shown in equation 2.5.

$$\mathrm{NDVI} = \frac{(\mathrm{NIR}-\mathrm{RED})}{(\mathrm{NIR}+\mathrm{RED})} \tag{2.5}$$

Clay Minerals Ratio is used to enhance hydrothermal alteration associated with clay and alunite minerals. For Landsat image, the clay mineral ratio is given in equation 2.6.

$$\text{Clay Mineral Ratio} = \frac{\text{SWIR 1}}{\text{SWIR 2}} \tag{2.6}$$

The wavelength range for SWIR1 ranges between 1.55 µm and 1.75 µm and for SWIR2, its wavelength range lies between 2.08 µm and 2.35 µm. SWIR1 corresponds to band 5 and SWIR2 corresponds to band 7 of both Landsat ETM+ and TM data. Whiles for ASTER image, the clay mineral ratio is given equation 2.7.

$$\text{Clay Mineral Ratio} = \frac{\text{SWIR 5}\times\text{SWIR 7}}{\text{SWIR 6}\times\text{SWIR 6}} \tag{2.7}$$

Ferrous Minerals Ratio highlights iron-bearing minerals. For Landsat data, it is given by dividing the SWIR band by NIR band as shown in equation 2.8.

$$\text{Ferrous Mineral Ratio} = \frac{\text{SWIR}}{\text{NIR}} \tag{2.8}$$

The wavelength range for SWIR is from 1.55-1.75 µm and 0.76-0.9 µm for NIR band. SWIR corresponds to band 5 and NIR corresponds to band 4 for both Landsat ETM+ and TM image.

For ASTER data Ferrous Minerals Ratio is expressed in equation 2.9.

$$\text{Ferrous Mineral Ratio} = \frac{\text{SWIR 5}}{\text{VNIR 3}} + \frac{\text{VNIR 1}}{\text{VNIR 2}} \tag{2.9}$$

2.8.2. Principal component analysis (PCA)

The principal component analysis is a statistical technique used to separate or enhance the difference within a correlated set of variables for easy exploration and visualization. Principal components analysis exhibits a strong pattern within the variables, or the dataset based on the concept of variance maximization. The original dataset is transformed into principal components or linear combinations which are independent and uncorrelated.

Principal component analysis has been utilized in many application areas such as image processing, classification, and recognition of objects. The principal component analysis is mostly applied in mapping alteration zones in metallogenic regions (Tangestani and Moore, 2014). Principal component analysis has the advantage of reducing or removing data redundancy in the multispectral image (Boloki and Poormirzaee, 2010), thereby decreasing the dimensionality of the image data.

The spectral response of earth's surface features (soil, rocks, minerals, vegetation, and water) are linked to the statistical variance within the multispectral image and the variance is also influenced by image's statistical dimensionality (Loughlin, 1991). According to Loughlin (1991), the bands of the multispectral image can be defined as variables and subjected to principal component analysis. By using the principal component analysis, the scene statistics (band statistical information) of the image can be transformed into linear combinations or principal components to offer vital information about spatial distribution and relative abundance of earth's surface features within the image. This is the main principle behind the use of principal component analysis in image processing and analysis.

In image processing and analysis, principal component analysis can be applied in three different forms and these are; standard principal component analysis, selective principal component analysis and developed selective principal component analysis (Crosta Techniques).

2.8.2.1. *Standard principal component analysis*

The standard principal component utilizes all the spectral bands of the image. The standard principal component analysis is the most widely used PCA type in enhancing hydrothermal alteration associated with mineralization.

Using the standard principal component analysis does not require prior knowledge of which bands could enhance the target feature. The first principal component image contains common information of all the inputted bands. The strong correlation between the bands as exhibited in the first principal component image is due to the presence of albedo or the scene brightness of the image (Tangestani and Moore, 2014) and is not usually suitable for distinguishing any target feature. The other principal component images rather give some spectral information and could be used to discriminate the target features. The main advantage of using the standard principal component analysis is that multiple combinations of principal component images are possible. Color composite images can be produced from the combination of principal components for visual identification of the target features.

2.8.2.2. *Selective principal component analysis*

The selective principal component analysis as the name suggests, only uses a spectral subset of the multispectral image as input for the analysis (Tangestani and Moore, 2014). The selective principal component analysis has the advantage of reducing data dimensionality and at the same time minimizing the loss of data information (Tangestani and Moore, 2014).

The input band for the selective principal component analysis is normally made up of two bands and these bands are selected based on the spectral response of the target feature. One of the bands must indicate high reflectance of the target feature whiles another band must also show strong absorption of the target feature. With only the two bands as an input for the selective principal analysis, the information common to the two bands will be in the first principal component image while the second principal component image will contain information distinctive to either one of the two bands (Tangestani and Moore, 2014).

2.8.2.3. *Developed Selective PCA (Crosta Technique)*

The Crosta Technique is a modified form of the standard principal component analysis which utilizes a group of four selected image bands (Loughlin, 1991). The Crosta Techniques was developed and applied by Crosta and McM.Moore in 1989 at the United Kingdom National Remote Sensing Centre (NRSC) (Loughlin, 1991). The Crosta Techniques examines the linear combinations of the PCA to determine which of the PCA images will best depict the theoretical spectral response of specific objects (Loughlin, 1991). The main advantage of the Crosta Technique is its ability to determine whether target feature type is enhanced in the previous PCA image as dark or bright pixels.

Loughlin (1991) used the Crosta Technique to map out hydroxyl and iron oxide-bearing minerals. Aydal et al. (2007) concluded from their study that, Crosta Technique can discriminate between different types of magmatite of different genesis and age despite its capability to detect hydroxyl and iron oxide alteration.

Selection of the bands of the multispectral image for the Crosta Technique analysis is based on several factors such as; type of feature under-investigation, the spectral response of the investigated feature and the geology of the areas. Before selecting the bands for the Crosta Technique, other image analysis such as band color combination and band ratio analysis should be performed to determine which band combinations or band ratio could best depict the feature under investigation so that those bands would be used in the Crosta Technique analysis. Another way of determining the bands to be used in the Crosta Technique can be based on the findings of previous researchers on the target feature(s).

2.8.3. Band color composite (RGB combination)

Color is an important component for visualization and remote sensing image processing is more or less assigning the same color to pixel locations of the same reflected or emitted values for easy identification and classification of the feature or object under investigation.

A multispectral image is made up of several bands which are stored in greyscale format but with the help of the computer, a color image can be produced from these grey scale bands through a process called band combination (Graham, 1999). Displaying any of three of the bands of the multispectral image in the three fundamental colors (Red, Green, and Blue) would result in the color composite image. Depending on the number of the bands of the image, several band combinations can be performed but the best combinations depend on event or feature under investigation (Riebeek, 2014).

When the red band of the image is placed onto the Red gun, the green band of the image is placed onto the Green gun and the blue band of the image is also placed onto the Blue gun, then the resulting image would be displayed in natural color. In other words, the natural or true-colored composite image consists of actual measurements of red, green, and blue light and the resulting image looks the same as how humans beings see features in the real world (Riebeek, 2014). For example, water bodies and vegetation cover in the natural color composite image would appear as blue and green respectively. Apart from the natural color combination, any other combinations are false color combinations.

Performing band combinations require adequate knowledge on each band and what type of information is accessible because different bands (or wavelengths) have a different contrast or level of brightness for each feature. Band combination can also be performed for the band ratio image. Normally, the band ratio image best depicting the feature is put into the Red channel, the next best band ratio image is put into the Green and the least band ratio image depicting the feature is put into the Blue channel to form the composite image.

First, the number of possible combinations of three bands can be determined by using the formula in equation 2.10.

$$\binom{n}{3} = \frac{n!}{(3! * (n-3)!)} \tag{2.10}$$

Where n is the total number of bands for the combinations. For 14 bands, there are $\binom{14}{3} = 364$ possible combinations. For 3 bands, there is 1 possible combination; for 4 bands, there are 4 possible combinations; for 5 bands, there are 10 possible combinations; for 6 bands there are 20 possible combinations; and for 7 bands, there are 35 possible combinations.

2.8.3.1. *Importance of band composite image*

Selecting band combinations can highlight features easily which could rather be difficult to detect in grey scale or single band image data. Band composite images are used for lithological mapping, mineral exploration mapping, and feature extractions such as vegetation cover, water bodies, and built-up areas. According to Simon et al. (2016), band combination technique is one of the most useful image processing methods for lithological discrimination.

2.8.3.2. *Optimum index factor (OIF)*

Forming color composite (RGB) to discriminate features in remotely sensed data is tiresome and time wasting because many bands combinations must be tried before obtaining the best results. The optimum index factor streamlines the selection process by quantitatively examining the scene statistics in order to avoid the numerous visual band combinations (Qaid and Basavarajappa, 2008). The optimum index factor was introduced by Chavez et al. (1982) and Chavez et al. (1984).

The optimum combination of bands out of all possible 3-band combinations is the one with the highest amount of 'information' (highest sum of standard deviations), with the least amount of duplication (lowest correlation among band pairs). Mathematically, OIF is expressed as in equation 2.11.

$$\mathrm{OIF} = \frac{\mathrm{Std}_i+\mathrm{Std}_j+\mathrm{Std}_k}{|\mathrm{Corr}_{i,j}|+|\mathrm{Corr}_{i,k}|+|\mathrm{Corr}_{j,k}|} \qquad (2.11)$$

Where; OIF is the optimum index factor, Std_i is the standard deviation of band i; Std_j is the standard deviation of band j; Std_k is the standard deviation of band k; Corr_{ij} is the correlation coefficient of band i and band j; Corr_{ik} is the correlation coefficient of band i and band k; Corr_{jk} is the correlation coefficient of band j and band k.

The optimum index factor technique has been employed in selecting band combinations for many geologic applications such as lithological and structural mapping. Qaid and Basavarajappa (2008) used the optimum index factor to rank all the possible band color combinations of ETM+ data for geological mapping of North East of Hajjah, Yemen. Patel and Kaushal (2011) applied the optimum index factor to extract features from satellite data with improved classification accuracy than using the principal component analysis.

2.8.4. Spectral angle mapper technique

The spectral angle mapper is a classification based on the determination of the spectral angle between the unknown spectrum and the reference spectrum in order to classify the pixels of the unknown material (Parashar, 2015). The spectral angle is measured in radians and treated as vectors in n-dimensional spectral space (Rowan and Mars, 2003).

The degree of the spectral angle determines the level of similarity between the unknown spectrum and reference spectrum, small angles correspond to high similarity whiles high angles exhibit low similarity. Pixels of the unknown material may not be classified if the spectral angle between them and reference spectra exceeds the defined maximum threshold spectral angle. The spectral angle mapper algorithm classifies the pixels of the unknown spectrum based on the number of the defined reference spectrum. The spectral angle mapper classification image allocates each pixel of the unknown spectrum to a class that denotes one of the materials form the selected reference spectrum (Harris Geospatial Solutions Inc., 2018). There may also be a class which contains the unclassified pixels of the unknown spectra once the spectral angle exceeds the defined threshold spectral angle.

The reference spectrum for the spectral angle mapping technique can be obtained from different sources but the most commonly used sources are from the spectral libraries (USGS spectral library), field measurement (ASCII files) and the image (Regions of interest, ROIs). For effective use of spectral angle mapper classification, the input image and the reference spectra must be in on one unit thus apparent reflectance. The difference in units between the input image and reference spectrum might result in misclassified of the pixels of the input image.

The principle of the spectral angle mapper is based on equation 2.12.

$$\alpha = \cos^{-1}\left[\frac{\sum_{i=1}^{nb} t_i r_i}{\left(\sum_{i=1}^{nb} t_i^2\right)^{1/2}\left(\sum_{i=1}^{nb} r_i^2\right)^{1/2}}\right] \quad (2.12)$$

Where; α is the spectral angle, nb is the number of bands, t_i is the test spectrum and r_i is the reference spectrum.

The spectral angle mapper technique can be illustrated visually by creating a 2D scatter plot of the unknown spectrum and the reference spectrum in a two-band image (Harris Geospatial Solutions Inc., 2018). This illustration is shown in Figure 2.13.

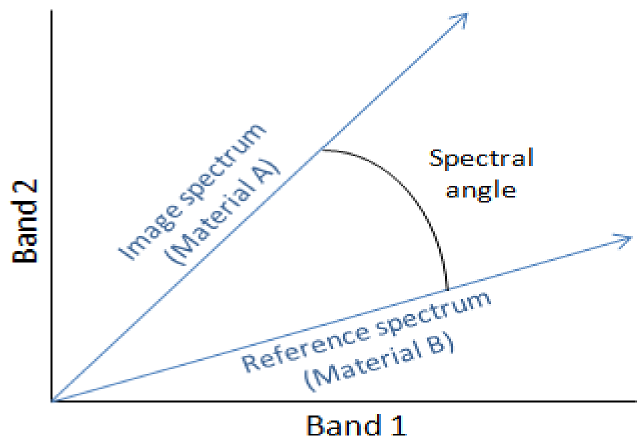

Figure 2.13. *Illustrating the spectral angle between two materials (Hamza, 2016)*

The main advantages of the spectral angle mapper are elaborated in the list below:

(1) The spectral angle mapper technique provides a quick method of classifying the similarity between different materials using unknown reference spectra.

(2) Solar illumination effects does not affected the classification by the spectral angle mapper technique because the measured spectral angle between the two spectra is independent of the vector length (Crosta et al., 1998).

(3) The spectral angle mapper can suppress the effects of shade (Carvalh and Meneses, 2000)

However, the main disadvantage of using the spectral angle mapper is the problem of the spectral mixture because one pixel may contain more than one material.

2.8.5. Spectral indices

Spectral indices technique is one of the methods for quantifying multispectral sensor response patterns (Yamaguchi and Naito, 2003) and the ideal of spectral indices was first introduced by kauth and Thomas (1976). They proposed Brightness, Greenness, Yellowness, and Nonsuch as the four spectral indices when using the four Landsat MSS bands. In 2003, another type of spectral indices was proposed by Yamaguchi and Naito (2003) as Brightness Index, Alunite Index, Kaolinite Index, Calcite Index and Montmorillonite Index for discrimination and mapping of surface rock types. They calculated these five spectral indices by a linear combination of reflectance values of the five SWIR bands.

The concept of spectral indices and PCA are similar because both methods are based on the orthogonal transformation of multispectral data (Yamaguchi and Naito, 2003). According to Yamaguchi and Naito (2003), the main difference between the spectral index and PCA is that in spectral indices, transform axes are used to represent specific spectral patterns of interest, while in PCA, the transform axes are mathematically defined to maximize the variance within the multispectral data.

2.9. Integrating Multi-Criteria Decision Analysis (MCDA) into GIS

GIS-based MCDA can seem as a process that transforms and integrate a spatial (geographic) data (input maps) and the decision maker’s (expert or agent) judgments into a decision (output) map (Malczewski and Rinner, 2015). In order words, the procedure consists of three main components (1) geographical data, (2) decision maker’s preferences, and (3) the integration of the spatial data and expert’s preferences according to a specified decision rule or combination (Malczewski, 1999; Jankowski et al., 2008). The most critical aspect of GIS-MCDA based procedure is the evaluation of the spatially defined decision alternatives based on the decision maker’s preferences and the criterion values (Malczewski and Rinner, 2015).

2.9.1. Approaches of GIS-MCDA integration

There are three main methods of integrating GIS into MCDA and these are conventional MCDA for spatial decision making, spatially explicit MCDA, and spatial multiobjective (multicriteria) optimization. Detail explanations of these methods are as follows;

2.9.1.1. *Conventional MCDA*

GIS-MCDA methods mainly make use of conventional MCDA approaches or decision rules in solving spatial problems such as site selection problem and land use/suitability analysis (Malczewski, 2006). The most common MCDA methods include the following: the weighted linear combination and related approaches (Carver, 1991), ideal/reference point methods (Tkach and Simonovic, 1997), the analytical hierarchy/network process (Zhu and Dale, 2001; Marinoni, 2004), and outranking methods (Carver, 1991; Joerin et al., 2001; Martin et al., 2003).

The conventional MCDA approaches have mainly been aspatial, thus they don't normally consider geographical or spatial properties of the data (Malczewski and Rinner, 2015). They assume spatial homogeneity of the decision maker's preferences on the data. The conventional methods only make use of existing MCDA methods to analyze spatial decision problems. The conventional MCDA approaches normally handle spatial variability of the decision maker's preferences by implicitly defining evaluation criteria on the principle of spatial relations such as adjacency, proximity, and contiguity (Van Herwijnen and Rietveld, 1999; Ligmann-Zielinska and Jankowski, 2008).

2.9.1.2. *Spatially explicit MCDA*

"A model is said to be spatially explicit when it differentiates behaviors and predictions according to spatial location"(Goodchild and Janelle, 2004), the spatially explicit MCDA approaches surpass the mere application of the MCDA methods to spatial decision problems. To determine spatial explicitly model, four tests were proposed by Goodchild (2001). The first test is the invariance test which considers a MCDA model spatially explicit if the outcomes (rankings or orderings of decision alternatives) of the decision are not invariant under relocation of the feasible alternatives. This means when the spatial pattern of feasible alternatives changes, their resulting rankings will also change. The seconded test is the representation test. This test requires that decision alternatives in a spatially explicit MCDA model be spatially or geographically defined. The alternatives are at least made up action (what to do?) and location (where to do it?). The location components of the alternative are defined with geographical coordinates. Formulation test is the third test used to determine the spatial explicit of the model. This test states that a spatially explicit MCDA model should contain spatial concepts such as location, distance, contiguity, connectivity, adjacency, or direction.

2.9.1.3. *Spatial multiobjective optimization*

This method tries to find the optimal solution for spatial decision problems. The decision alternatives used in the spatial optimization have geographic meaning and as results, the optimal solutions to the decision problems can be easily displayed on maps with their spatial structures such as distance, and boundary. The procedures for solving spatial multicriteria problems comprise of value scaling (or standardization), criterion weighting, and combination (decision) rule (Greene et al., 2011).

2.9.2. Components of GIS-MCDA

The GIS MCDA based model is made up of two main components and they include the GIS component and the MCDA component. Figure 2.14 give the hierarchical components of the GIS component of the GIS MCDA based model.

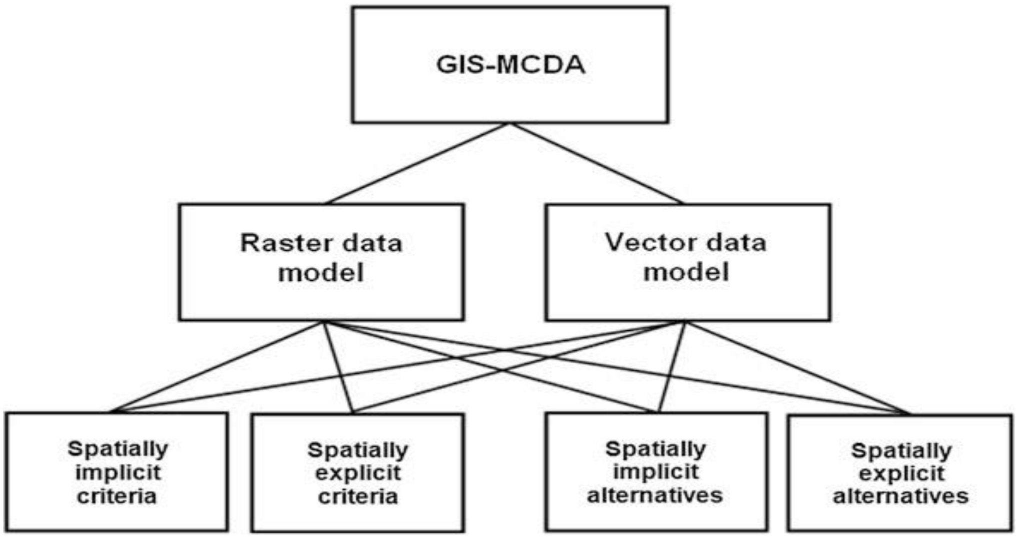

Figure 2.14. *Classification scheme for GIS components of GIS-MCDA (Malczewski and Rinner, 2015)*

GIS component of the GIS MCDA based model is made up of two main classification levels. The first classification level consists of the raster data model (Church et al., 2003), and vector data model (Rinner and Malczewski, 2002; Feick and Hall, 2004). These two data models are the main data types used in any GIS operations. It is worth note that some of the GIS-MCDA methods make use of both the raster and vector data models at the same time. Classifying GIS-MCDA as either vector or based model depends on the type of geographic data types used in the multicriteria combination rules (Malczewski, 2006).

The second level of classification of the GIS component is based on the nature of decision alternatives and evaluation criteria and grouped into spatially explicit and spatially implicitly categories (Malczewski, 2006).

The three approaches to GIS MCDA integration such as conventional MCDA, spatially explicit MCDA, and spatial multiobjective optimization are used to determine the spatial component of the GIS MCDA model (Malczewski and Rinner, 2015). Most often the conventional (aspatial) MCDA methods are used in handling the spatial component of the GISMCDA problems (Malczewski, 2002) .

The second component of the GIS-MCDA integration is MCDA Components. The MCDA component is made up the multiattribute decision analysis (GIS-MADA) and multi-objective decision analysis (GIS-MODA). The GIS-MADA and GIS-MODA of the MCDA component are further divided into individual and group decision making as indicated in Figure 2.15.

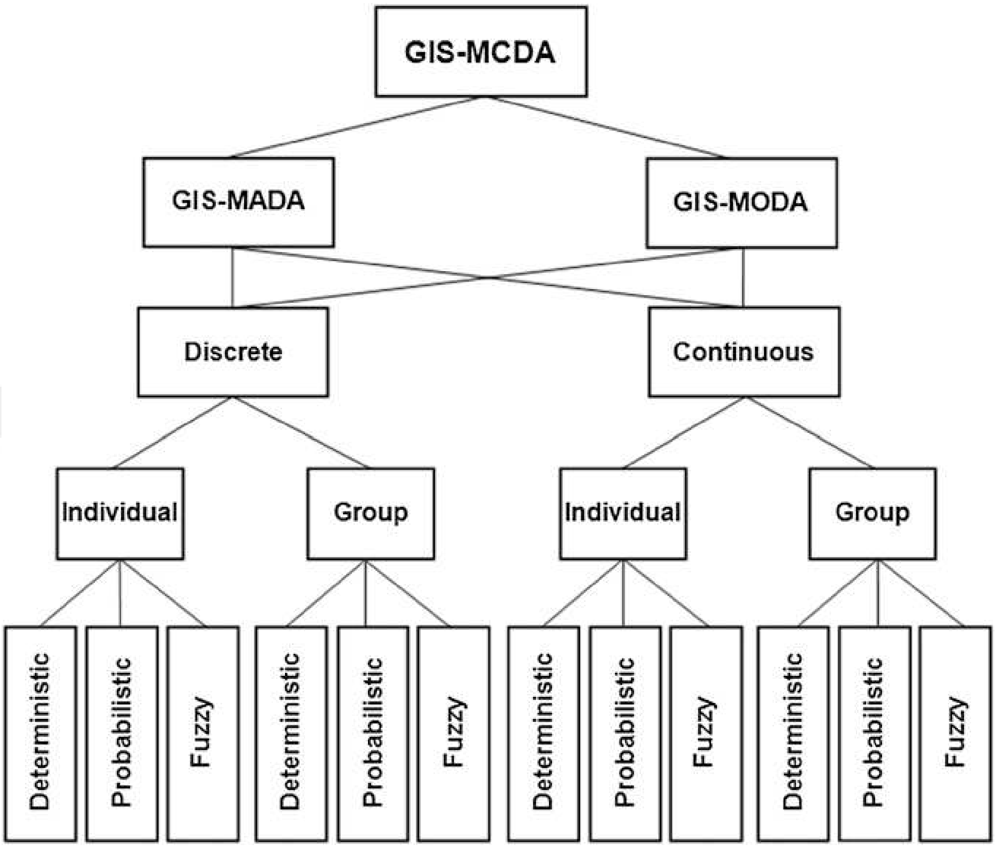

Figure 2.15. *Classification scheme for MCDA components of GIS-MCDA (Malczewski and Rinner, 2015)*

2.9.3. Method of GIS-MCDA integration

The most commonly applied methods of MADA methods are weighted linear combination, ideal point methods, the analytic hierarchy process/analytic network process, and outranking methods (Malczewski and Rinner, 2015).

2.9.3.1. *Weighted linear combination*

The most commonly used model of GIS-MADA approaches is the weighted linear combination (WLC) and its related models (Malczewski and Rinner, 2015). Weighted linear combination model is also called simple additive weighting (Malczewski, 2006). The WLC models assume the attributes are linear and are independence of each other.

The two main components of the weighted linear combination model are value functions, $V(a_{ik})$ and criterion weights (W_k).

The weighted linear combination model combines a set of criterion weights, w_1, $W_2,\ldots,W_n$, with the criterion (attribute) values, a_{i1}, a_{i2}, …, a_{in}, (i = 1, 2, …, m) to obtain the overall value of an alternative at a particular location. Mathematically the WLC model is expressed in equation 2.13 as follows:

$$\mathrm{V(A_i)} = \sum_{\mathrm{K}=1}^{\mathrm{n}} \mathrm{W_k}\, \mathrm{V(a_{ik})} \tag{2.13}$$

Where $V(A_i)$ is the overall value of the i^{th} alternative at location (X_i, Y_i); i is the X, Y locational information of ith alternative); $V(a_{ik})$ is the attribute value of the i^{th} alternative. The best alternative is with the highest overall value $V(A_i)$.

2.9.3.2. *Proximity-Adjusted weighted linear combination*

The proximity-adjusted weighted linear combination model takes into consideration of the spatial relationship between alternatives, or an alternative and some reference locations (Ligmann-Zielinska and Jankowski, 2012). Ligmann-Zielinska and Jankowski (2012) argued that the process of choosing a particular decision alternative should be based on the relative importance of criteria and the relative location of the alternative. The proximity-adjusted criterion weights can be used to operationalize the concept of spatial heterogeneity of preferences or decision alternatives.

The formula for proximity-adjusted weighted linear combination can be written as in equation 2.14.

$$V({A^p}_i) = \sum_{K=1}^{n} W_{ik}\, V(a_{ik}) \tag{2.14}$$

Where w_{ik} is proximity-adjusted weight assigned to the i^{th} alternative with respect to the k^{th} criterion and $V(A^p{}_i)$ being the overall value.

2.9.3.3. *Analytic hierarchy/network process (AHP)*

One of the most comprehensive techniques of multicriteria decision analysis is Saaty's analytic hierarchy process (AHP). The concept of AHP is based on decomposition, comparative judgment, and synthesis of priorities (Sadeghi-Niaraki and Kim, 2009). The hierarchical structure of AHP may consist of a goal, objectives, attributes, and alternatives. The decomposition principle makes sure the complex decision problem is being decomposed or breakdown into a hierarchy. The hierarchy should clarify the complexity and at the same time captures the vital elements of the decision problem. The comparative judgment principle deals assessment of decision elements through pairwise comparisons with respect to their parent in the next-higher level of the hierarchy. The synthesis principle deals with constructing an overall priority rating by taking into consideration each of the derived ratio scale priorities in the various levels of the hierarchy. The synthesis process of AHP defines the priority rating or overall evaluation score and is given in equation 2.15.

$$V(A_i) = \sum_{K=1}^{n} W_l \, W_{k(l)} V(a_{ik}) \tag{2.15}$$

Where the value function is $V(a_{ik})$, W_l and $W_k(l)$ are the weights associated with the lth objective and k^{th} attribute respectively.

GIS can be integrated with AHP in several many ways but generally, they fall under two main groups (Malczewski, 2006). The first group of GIS-AHP integration systems can estimate the weights associated with attribute/ criterion map layers based on the comparative judgment principle of AHP (Gemitzi et al., 2007; Karnatak et al., 2007) . The estimated weights of the criterion map layers may be combined with criterion map layers using one of combination rule such as weighted linear combination. The second category of GIS-AHP integration system are those systems whose AHP principles are based on decomposition, comparative judgment, and synthesis of priorities (Sadeghi-Niaraki and Kim, 2009).

If the hierarchy of AHP is made up only three levels thus the goal, attributes, and alternatives, then the AHP is comparable to the weighted linear combination method whose criterion weights are defined through the pairwise comparison technique. The main advantage of AHP over weighted linear combination model is that AHP helps the decision maker in capturing all the vital elements of a decision problem through the principle of decomposition. Also, the pairwise comparison method of AHP is more accepted for estimating criterion weights than weight estimation options used in other methods.

2.9.3.4. *Analytic network process (ANP)*

AHP method assumes independence of the elements of the hierarchical structure but this assumption rather does not hold to real-world spatial decision problems. Real-world spatial decision problems normally consist of interactive and dependence decision elements. Saaty (1996) proposed the analytic network process (ANP) to solve the issue of spatial interaction and dependency among elements of the decision problem. Analytic network process is the extended and generalized version of AHP method. Both the AHP and ANP are based on the concepts of decomposition, comparative judgment, and synthesis of priorities. The only difference between the AHP and ANP is how the decomposition of the decision problem is done. In the ANP method, the decomposition is structured in a form of the network rather than a hierarchy.

The main reason why AHP/ANP is commonly used is due to its ease-of-use and flexibility. Many authors had incorporated the pairwise comparison of AHP/ANP in several GIS-MCDA applications (Boroushaki and Malczewski, 2008; Eldrandaly, 2013). AHP/ANP method has been criticized despite its widespread usage by many authors such as (Goodwin and Wright, 1998; Barzilai 1998). some of the criticisms include the following: (1) 'rank reversal' problem (Belton and Gear, 1983), (2) Too many pairwise comparison if the elements of the decision problem are many and the ambiguity in the meaning of Saaty scale (1-to-9 scale) (Belton and Gear, 1983).

2.9.3.5. *Weights of evidence*

Weights of evidence approach are used to predict potential mineral deposit in areas with many known mineral locations (Carranza, 2004). Weights-of-evidence (WofE) is a statistical method based on the concept of a Bayesian conditional probability (Bonham-Carter, 1994). Weights of evidence give measures of confidence associated with its predicted mineral potential map (Hartley, 2014). Bonham-Carter et al. (1989) first introduced the concept of weights of evidence in mineral prospectivity mapping.

Weights of evidence modeling of mineral potential consists of three steps and these are (1) estimation of prior probability of known mineral occurrences or locations; (2) weighting of the evidential layers with respect to the known mineral occurrences; and (3) estimating posterior probabilities of known mineral occurrences by updating the prior probability with by weights of evidential layers (Carranza, 2004). The possibility of finding a mineral deposit within the study before using any of the spatial evidence is the prior probability. The prior probability that randomly selected pixels contains deposit can be expressed as the number of pixels that contains deposit divided by the total number of pixels within a study area. The posterior probability on the other hand is the likelihood that randomly selected pixels contain deposit, after considering the spatial evidence. The weights of evidence model use two measures W+ and W- to assigns weights to the evidential themes with respect to the deposit. The weights are sensitive to a number of pixels that contains deposit and the total number of pixels within a study area (Carranza, 2004).

The positive weight (W+) is determined from the training sites or deposits found within the spatial evidence while W- is estimated from the training sites or deposits found outside the spatial evidence. The two weights thus W+ and W- are combined to obtain the contrast which represents a measure of spatial association between the training sites and the spatial evidential themes. A large, positive contrast value shows an indication that the spatial evidential theme is strongly correlated with the training sites and the likelihood that the spatial evidential theme contains training sites is high. A negative contrast value indicates the opposite, and the likelihood that the spatial evidential theme contains training sites is low or unlikely.

The problem of conditional independence of the spatial evidence is one of the main criticisms for using weights-of-evidence method in mineral potential mapping (Agterberg and Cheng, 2002). The weights-of-evidence model assumes that to avoid posterior probability departure and unreliability of predictions, all the spatial evidence layers used in of the modeling must be conditional independence of mineralization (Agterberg and Cheng, 2002).

2.9.3.6. *Fuzzy logic*

Zadeh (1965) proposed the fuzzy logic based on the concept of fuzzy set theory. The fuzzy logic method is a knowledge-driven mineral prospectivity model and its function-member values are determined based on the expert's judgment in assigning weights to spatial evidence relating to the mineral under study (Quadros et al., 2006). Fuzzy logic provide the geologist with the opportunity to build mineral prospectivity model by choosing the spatial evidential layers that he believes are most vital for a specific type of mineralization based on his knowledge and experience (Zhang and Zhou, 2015). The Boolean set theory of the fuzzy logic is used to defines the membership as either 1 or 0 (true or false), whereas the degree of membership within a set is defined without a crisp boundary by fuzzy-set theory (Beuche et al., 2014). The fuzzy model based mineral prediction model consists of two procedures; fuzzification of data and combination of fuzzified data (Zhang and Zhou, 2015).

Fuzzification of the data can be achieved by determining the fuzzy function and this can be done in two ways (Zhang and Zhou, 2015). The fuzzy function can be either determined by calculating according to the membership function curve or by assigning values artificially to evidential layer based on the expert's geological knowledge (Zhang and Zhou, 2015). Variations of membership functions include Gaussian, triangular, trapezoidal and sigmoidal (Ali et al., 2015).

Combination of the fuzzified data can be done with one of the following basic fuzzy operators such as fuzzy AND, fuzzy OR, fuzzy algebraic product, fuzzy algebraic sum and fuzzy gamma (An et al., 1991). Fuzzy OR operator returns the maximum membership values of each evidential layer while fuzzy AND operator returns minimum membership values of each evidential layer. In fuzzy algebraic product fuzzy synthesis, synthesis result is obtained by multiplying membership values at each location of the evidential layer. The equation for fuzzy sets (A_{ij}) of the mineral prediction model consisting of a set of evidential layer, X_i (i = 1, 2, 3, . . ., n) and with r number of classes r_j (j = 1, 2, 3, . . ., r), can be expressed as in equation 2.16.

$$A_{ij} = \{(x_{ij},\mu A)/x_{ij} \in X_i\}, (0 \leq \mu A \leq 1) \qquad (2.16)$$

where μA is the membership value. When x_{ij} is favorable to mineralization, if membership value range falls within this $0.5 < \mu A < 1$, then x_{ij} is favorable to mineralization whiles membership range values between $0 < \mu A < 0.5$ indicate that xij is unfavorable to mineralization. If the membership value is 0.5, then it is not possible to determine whether x_{ij} is favorable or unfavorable to mineralization. A comprehensive fuzzy set of the model can be formed by combining the individual fuzzy set with any of the logic operators.

3. METHODOLOGY

3.1. Introduction

The sustainability of every mining operation depends on the availability of mineral reserves. The search for new potential mineral reserve is an integral part of mining and this has resulted in a search for methods and techniques that would facilitate the discovery of new deposits. In remote sensing application of mineral exploration, the most commonly used methods are band ratio technique and principal component analysis. In this methodology, a new band ratio index was introduced to map and identify epithermal gold-silver deposits in İzmir, Turkey. The new mineral index was developed by using the illite spectral signature extracted ASTER image and the USGS digital spectral of illite mineral. The procedures and the data used in developing the new mineral index are listed and explained in detail in subsequent sections. Three different forms of principal component analysis were performed to compare and validate the argillic alteration of epithermal gold mineralization generated from the proposed mineral index.

3.2. Geological Setting

3.2.1. Regional geology

The Ovacık Gold Mine lies in Western Turkey where magmatic rocks are the main dominant rock type. These magmatic rocks occurred from the late Oligocene to the early Miocene era and resulted in the filling of the Kozak pluton with Kozak granodiorite (Yılmaz, 2002). Two main magmatic intrusions have occurred in this region, Western Turkey. The first intrusion which was described as the Tibetan type by Yılmaz et al. (2001) was made up of calc-alkaline, and partially shoshonitic rocks (Yılmaz et al., 2013). The second magmatic intrusion phase comprises periodically established alkaline basalts and was deposited from the latest Miocene-Pliocene to the recent period (Seyitoğlu, 1997).

A lot of extensional activities have happened in this region especially in Neogene era the noticeable one was the northwest-southeast trending which later resulted in the north-northeast-south-southwest trending and northeast-southwest trending grabens

(Yilmaz, 2002) and these trending occurred in the Early Miocene times (Akay and Erdoğan, 2004). The next obvious extensional event after the first one was the north-south trending and it happened in the early Pliocene to Quaternary periods.

The main lithologic types within the region are of Paleozoic, Mesozoic, tertiary granitoids, Miocene volcanic and volcaniclastic sediments and Plio-quaternary sediments as indicated in Figure 3.1. The oldest lithologic unit in the region is the Paleozoic metamorphic rocks and it comprises of chlorite, low-grade muscovite, Late Cretaceous ophiolites and quartz schists (Yılmaz et al., 2013) whiles the youngest is Plio-quaternary sediments.

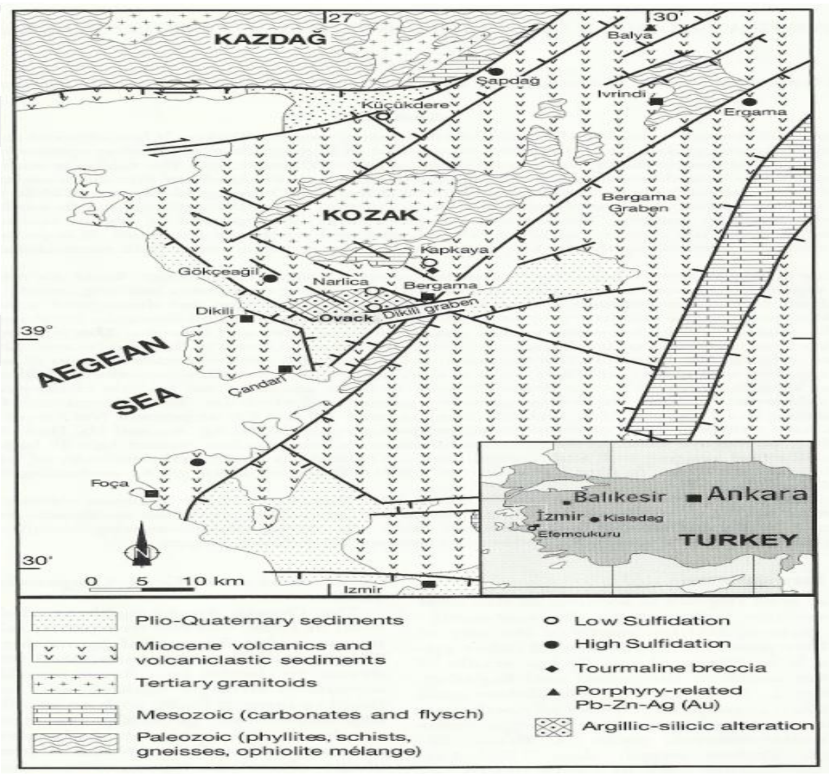

Figure 3.1. *Regional Geology and mineralized zones of Ovacık Gold deposits (Yılmaz et al., 2001)*

3.2.2. Local geology

The Ovacık epithermal gold mineralization and its neighboring minerals are mainly surrounded by porphyrite biotite andesite and slightly andesite breccia and debris flow (Yılmaz, 2002). The Ovacık epithermal gold deposit is adjacent to the east-northeasttrending Bergama graben. The lithologic map of Ovacık gold deposit and its surrounding is shown in Figure 3.2.

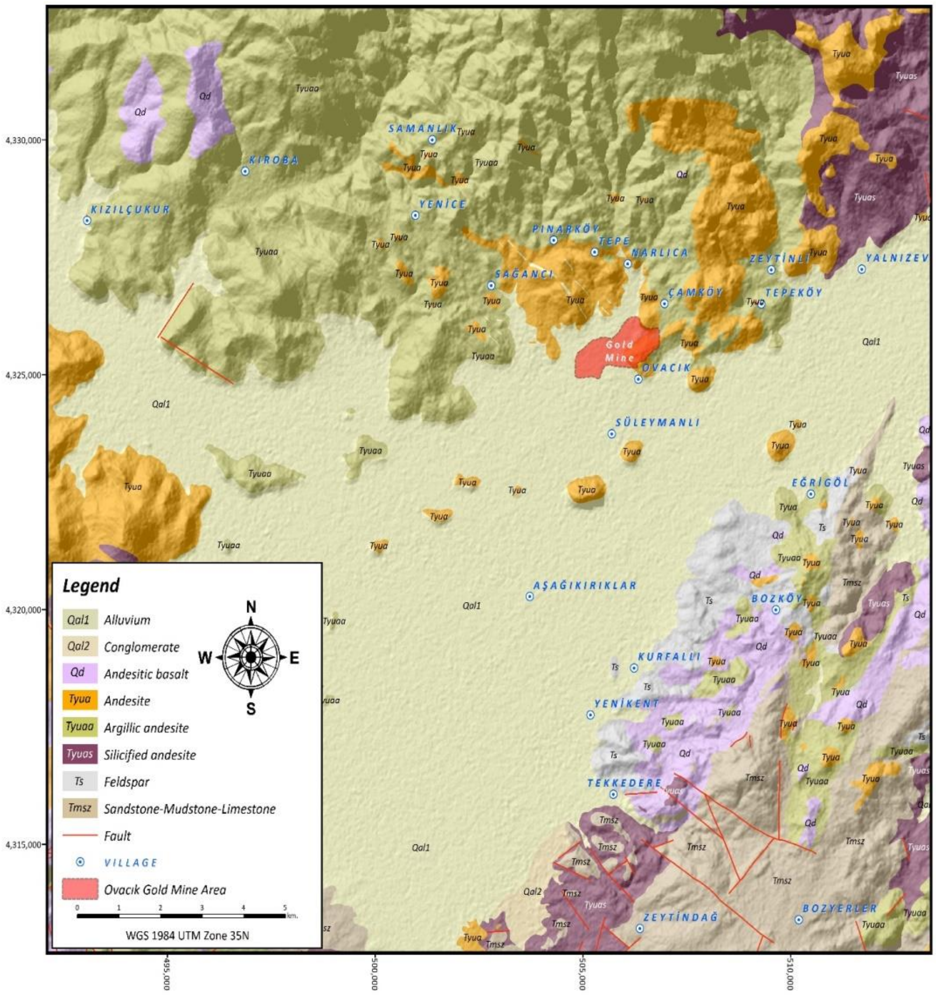

Figure 3.2. *Geologic map of Ovacık and Bergama areas (Originated from Yılmaz, 2002)*

The main minerals of the Ovacık area are feldspar, hornblende, phenocrysts of altered plagioclase and biotite. The volcanic rocks in the Ovacık area are calc-alkaline (Ercan et al., 1984).

The four epithermal quartz veins of Ovacık epithermal Au-Ag deposits are shown in Figure 3.3. The epithermal quartz veins comprise of two main quartz-adularia veins which have common textural and morphologic characteristics. These veins are named as M and S vein. They have sharp borders with an average grade of 13.g/t and 8.1g/t M and

S vein are respectively (Yılmaz, 2002). In the M vein, the quartz-adularia veins are well-formed whiles quartz-adularia vein and quartz-cemented breccia are formed completely in the S vein. The S vein contains high Au-Ag grade than M vein. Generally, the M and S veins contain high gold grades when compared to the other two veins (D and G vein).

The D and G veins mostly consist of fluidized breccia and massive chalcedonic quartz and some slightly quartz-adularia and quartz-cemented breccia. The gold grades in these two veins are very low and economically non-profitable.

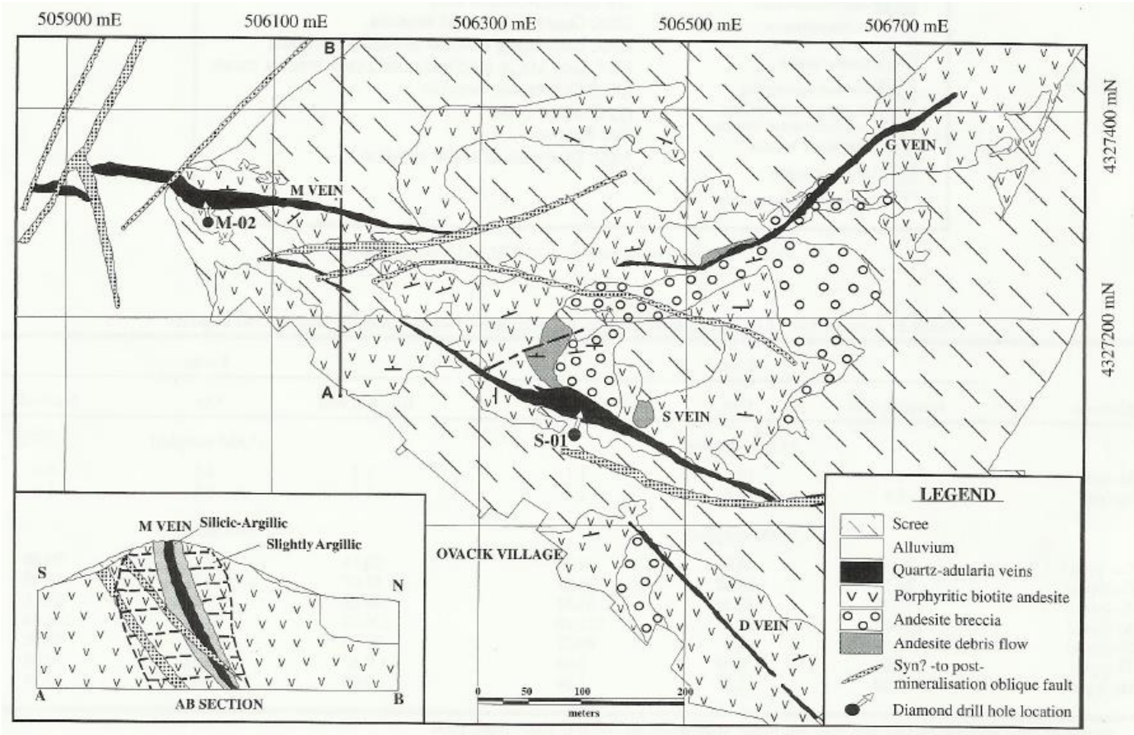

Figure 3.3. *Geology of Ovacık deposit (Yılmaz, 2002)*

3.2.3. Hydrothermal alteration of Ovacık deposit

Hydrothermal alteration is more intense close to the veins but decreases steadily a few meters away from the veins (Yılmaz, 2002). The alteration around these veins consists of silica occurring symmetrically as a wrapper around the main veins. The silicified zones around the veins are also covered with argillic alteration. The gold-silver deposits are related to the veins alteration.

The main minerals linked with argillic alteration around the veins are smectite, illite, interlayered illite/smectite and illite/chlorite, adularia, chalcedonic quartz, and chlorite. Illite was the only mineral to be detected easily through X-diffraction analysis. Other minor alterations associated with the Ovacık deposit are propylitic alteration and supergene alteration. Kaolinite and limonite are the dominant minerals of the supergene alteration and are observable in both surface samples and in core drill samples.

3.2.4. Ovacık Gold Mine

The Ovacık Mine is in the north of İzmir province about 100km from İzmir. The nearest village to the mine is Ovacık and the closest town is Bergama about 15km away from the mine. The Ovacık gold deposits were discovered in 1989 but mining operations started later in June 2001.

The type of mineral deposit at Ovacık Mine is of low sulfide epithermal deposit. The deposits comprise of both gold and silver with a total ore reserve of about 3 million tons. Gold exists freely as a combination of the gold-silver composite with an average size of 0.005 mm in the fractures within quartz veins.

The mine operates in both open pit and underground but currently, only the underground mine is fully operational. The average ore production for both open pit and underground operations are 200,000 t/y and100,000t/y respectively. Drilling activities are still ongoing for the discovery of more ore deposits. The Google Earth image of Ovacık Mine is shown in Figure 3.4.

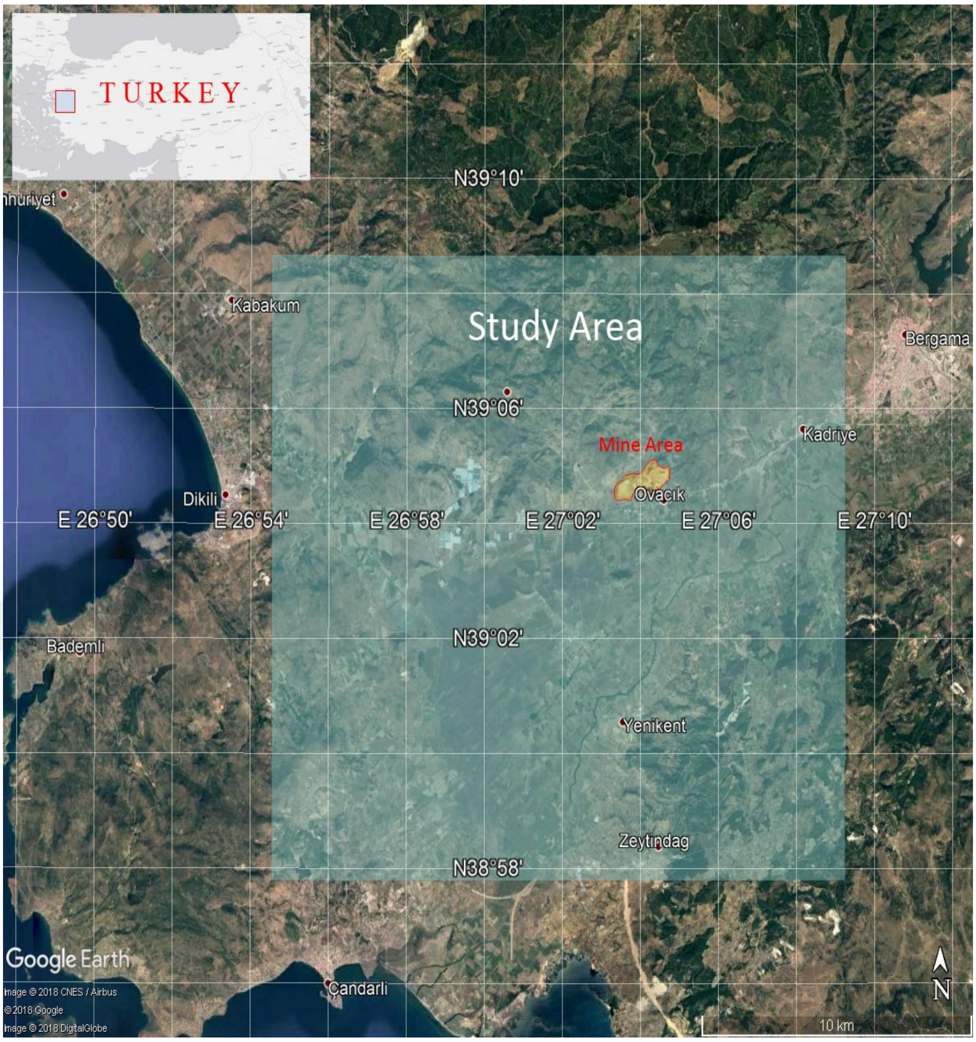

Figure 3.4. *Location of Ovacık Mine*

3.3. Materials Used

Conducting any research work requires the use of some materials. These materials can be data and software and using them would help in achieving objectives of the research. Proper analysis of the materials especially the data is crucial in achieving the expected results. In this research, the data and the reasons for their usage are explained in the sections below;

3.3.1. ASTER image

ASTER image is mostly used in hydrothermal alteration mapping because of its numerous infrared bands. The multiple SWIR bands of ASTER are useful for mapping soil, rock, and minerals. Over the years, different types of ASTER data keep emerging with the recent one being the ASTER Level 1T (AST_L1T). The AST_L1T was the data type used to map the hydrothermal alteration in this study.

In March 2015, the processing of ASTER L1A into ASTER L1T product was started by the Land Processes Distributed Active Archive Center (NASA LP DAAC) of NASA. The AST_L1T is radiometric and geometrically corrected; free of cross-talk effect and at-sensor radiance data. Precision terrain correction is being applied and projected onto north-up UTM coordinate system.

AST_L1T comprises of 14 at-sensor scaled radiance spectral bands in Hierarchical Data Format-Earth Observing System (HDF-EOS) format and embedded HDF metadata file in XML format (NASA LP DAAC, 2015). The 14 spectral bands include 3 VNIR bands, 6 SWIR bands, and 5 TIR bands. The characteristics of the 14 spectral bands are explained Table 3.1. The AST_L1T data can be obtained from any of these sites; Reverb, GloVis, Data Pool, EarthExplorer and NASA Earthdata Search at no charge. From April 2008, because of some technical problems, the SWIR portion of AST_L1T data is no more available.

Table 3.1. *Properties of the spectral bands of AST_L1T image (NASA LP DAAC, 2015)*

Band Name	*Spectral Range (μm)*	*Spatial Resolution(m)*	*Units*	*Data Type*
		Visible near infrared band		
Band 1	0.52-0.60	15	Radiance	8-bit unsigned
Band 2	0.63-0.69	15	Radiance	8-bit unsigned
Band 3N	0.78-0.86 7	15	Radiance	8-bit unsigned
		Shortwave infrared band		
Band 4	1.600-1.700	30	Radiance	8-bit unsigned
Band 5	2.145-2.185	30	Radiance	8-bit unsigned
Band 6	2.185-2.225	30	Radiance	8-bit unsigned
Band 7	2.235-2.285	30	Radiance	8-bit unsigned
Band 8	2.295-2.365	30	Radiance	8-bit unsigned
Band 9	2.360-2.430	30	Radiance	8-bit unsigned
		Thermal infrared band		
Band 10	8.125-8.475	90	Radiance	16-bit unsigned
Band 11	8.475-8.825	90	Radiance	16-bit unsigned
Band 12	8.925-9.275	90	Radiance	16-bit unsigned
Band 13	10.25-10.95	90	Radiance	16-bit unsigned
Band 14	10.95-11.65	90	Radiance	16-bit unsigned

3.3.2. USGS digital spectral library

The digital spectral libraries provide spectral information when performing studies related to features or objects identification (Baldridge et al., 2009). The main purpose for compiling the digital spectral libraries is to serve as a platform or spectral base for spectral analysis (Clark et al., 1990). The spectra of rocks, minerals, or any materials from the fieldwork or the spectra extracted from the multispectral image can be matched with the spectra from the digital spectral library to identify the type of rock or mineral. Without the digital spectral libraries, the matching and identification of the extracted spectra from the image or from the field work would very difficult and even impossible.

In the ASTER spectral library, there is only one spectrum for a file with a unique name which gives information about the sample type, the measured spectrometer type, the laboratory of measured sample and other useful information about the sample (Baldridge et al., 2009). An ancillary is normally associated with the spectrum file which gives further explanations about the spectrum file e.g. X-ray diffraction information. The spectrum file contains the spectral information about the sample and ends with "spectrum.txt" suffix. This spectrum files can be plotted in ENVI software or in Microsoft Excel application after which it can be matched with the spectra obtained from the fieldwork or the image.

In this study, the USGS Digital Spectral Library was used when matching and identifying the spectra extracted from the ASTER image of the study area. The USGS Digital Spectral Library is already embedded in ENVI software for easy matching of the extracted image spectra. The spectral range of the USGS Digital Spectral Library lies within 0.2 to 3.0 µm and this made the matching of the spectra extracted from ASTER than using the other spectral library such as JPL and JHU.

3.3.3. Digital elevation model (DEM)

The topography of any place can be best depicted by using a digital elevation model. The DEM can provide a 3-dimensional view for easy visual understanding and interpretation of the topography. With the free availability of DEM covering the whole world, its applications are beginning to take a central role in geosciences and natural sciences. The usage of DEM with satellite imagery can provide a better picture of the scenario under investigation.

In Geology and mineral exploration studies, DEM can provide vital information in identifying and defining the type of mineral or rock because of the strong correlation between relief and geologic structure and lithology. Structural lineaments and faults can be extracted after performing slope analysis on the DEM. In mineral exploration, an outcrop of rocks and minerals play vital roles and they are easily captured by the sensors of the satellites when they occur in high relief areas. Hydrothermal alteration zones of minerals are best depicted with DEM.

The DEM of the study area (Figure 3.5) was downloaded from the USGS Earth Explorer. The DEM served as the purpose of the topographic map over which the hydrothermal alteration zones and other features were overlaid to create the 3-D picture of the argillic alteration distribution.

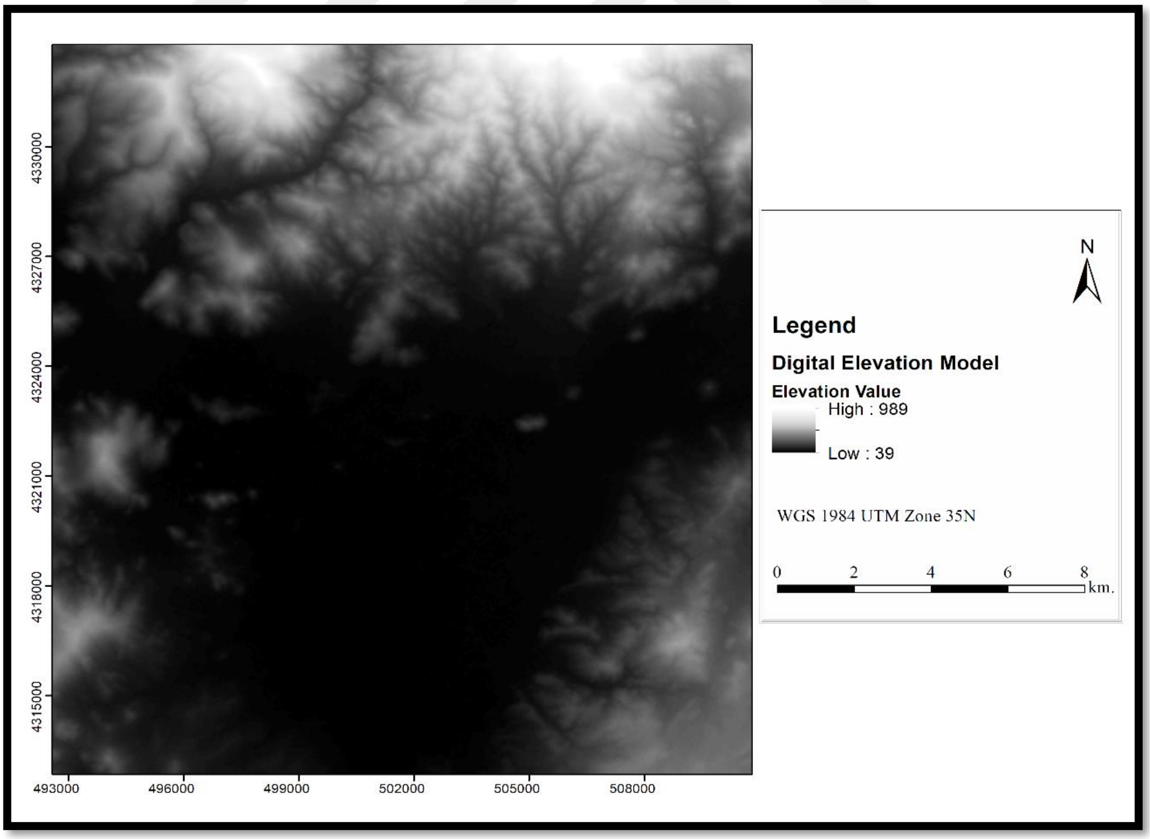

Figure 3.5. *Digital elevation model (DEM) of the Study Area*

3.3.4. Geologic map of Ovacık mine

The geologic information of a mineral exploration area is very important. This geologic information serves as a guiding knowledge in performing the exploration activities. The lithological types, the structure, fault, and other prominent geologic features all play some vital roles in the discovery of new ore deposits. The importance of geologic map goes beyond the exploration stage, during mining operations, geologic map serves as a vital data and information for the projection of assay information outside the sample points.

The surface reflectance from the multispectral and hyperspectral image can offer vital information on lithology, alterations, structure, and faults more easily than field geological mapping. Mineral deposits do not occur in an isolation but are generally associated with some geologic features such as hydrothermal alteration and lithology. Integration of the surface reflectance from remote sensing image with geologic information from the geologic map would make the prediction of the potential ore deposits more accurate. Geographic information systems can provide the platform for the integration of multiple datasets for mineral exploration purpose.

3.3.5. Methods

Methods are the procedures followed in the achievement of the set goals in any research work. The method section is the most vital part of any research work as it serves as the basis for the judgment of the research's validity.

In this study, the steps and procedures used to achieve the objectives of the study are outlined chronologically, and the reasons for using them are also explained for easy follow-up and understanding. Screenshots of procedures were captured in addition to the word descriptions to enhance the representation and the readability of the write-up of this study.

3.3.5.1. *Preprocessing of ASTER image*

Image preprocessing is required for accurate analysis and interpretation of the image. Image preprocessing is the basic requirement for any image analysis but the number of operations to be performed at the preprocessing stage depends on the type of image analysis to be carried out. When the right preprocessing operations are not performed, the result of the analysis and interpretation might be different from the expected result. After downloading the image, the first required operation to be performed was the preprocessing. The image preprocessing increases the quality of the data and prepares the image for further image extraction analysis. The image preprocessing operations performed on the ASTER image to obtain the surface reflectance for further analysis are elaborated below.

3.3.5.2. *Importing ASTER imagery*

The downloaded ASTER image is normally in the hierarchical data format (HDF) with three separate groups of visible-near infrared files, shortwave infrared files, and thermal infrared files. These groupings of ASTER image exist because of the difference in spatial resolution of the VNIR, SWIR and TIR datasets. The HDF format of ASTER dataset can be opened or imported in an ENVI software environment by following the instructions in Figure 3.6.

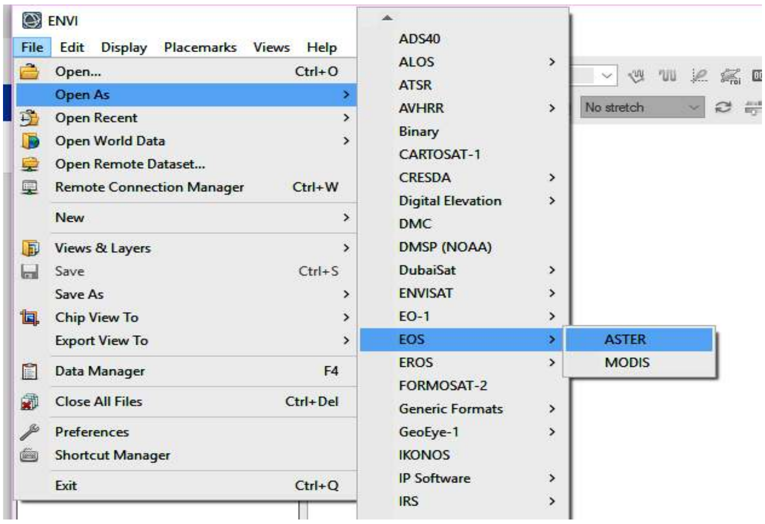

Figure 3.6.*Steps for importing ASTER image*

After importing the ASTER image, ENVI software generates three groupings for the ASTER image, all the three VNIR files are grouped under one heading, the six SWIR files are also grouped under the same heading and finally, all the five TIR files are grouped under one heading. The various groupings of the ASTER dataset can be accessed by opening the Data Manager option under the file menu of ENVI software. The three datasets of ASTER image are shown in Figure 3.7.

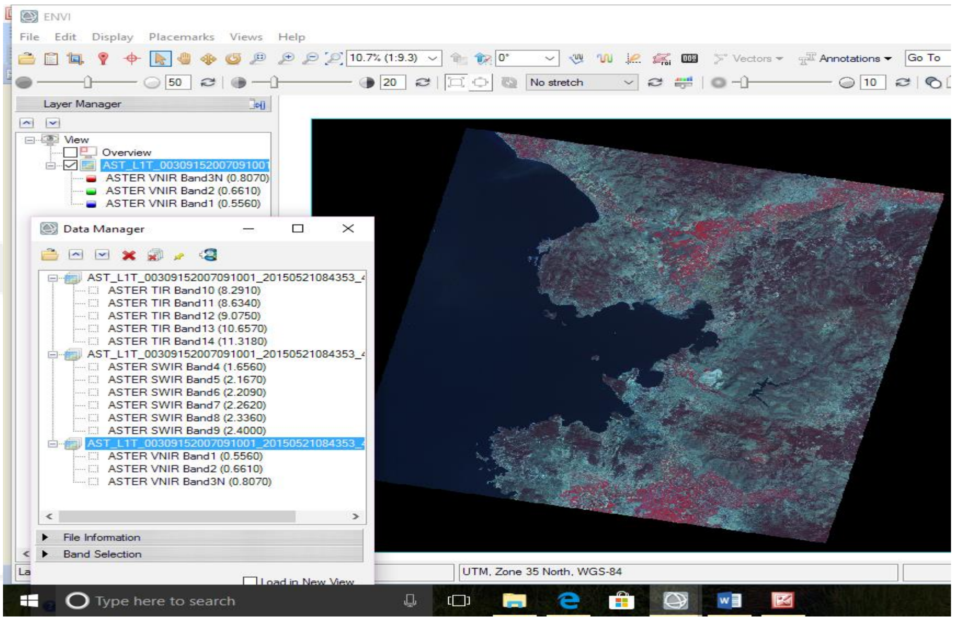

Figure 3.7. *Three datasets of ASTER image*

3.3.5.3. *Layer stacking*

The process of combining two or more greyscale images as a single image is called layer stacking. The satellite images are generally made up of individual greyscale bands. Each of these bands is sensed in different wavelength and might contain different level of information for a specific feature or object. Stacking these bands together can help in performing analysis involving all the different bands or layers of the image. The advantage of multispectral imaging can be utilized properly after stacking the bands together. Normally, bands or layers with the same spatial resolution are stacked together as a single dataset. However, bands with different spatial resolutions must be resampled to the same spatial resolution unit before stacking them together or a common spatial resolution unit can be defined for the different bands when stacking in ENVI software.

Stacking of bands increases the size of the stacked image, it is, therefore, important to stack the only bands to be used in performing the analysis.

In this study, the visible near-infrared bands and the shortwave infrared bands of ASTER image were stacked together for further image processing. Because of the difference in spatial resolution, the common spatial resolution of 15m was chosen for all the stacked bands. This means that only the 30m spatial resolution of the SWIR bands was resampled to 15m since the VNIR dataset was already in 15m spatial resolution unit. The process for stacking the bands of the ASTER AST_L1T image is indicated in Figure 3.8.

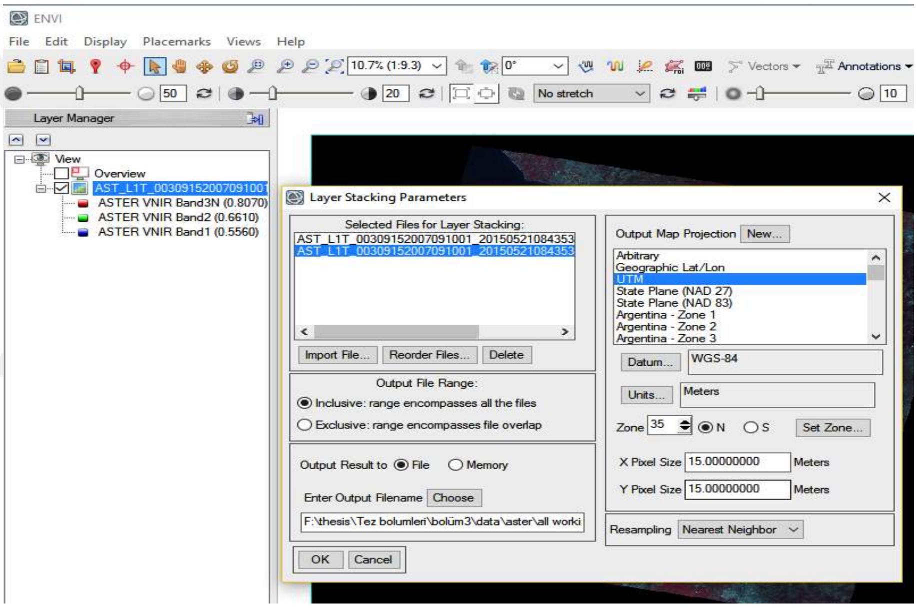

Figure 3.8. *Layer stacking parameters*

3.3.5.4. *Dark pixel subtraction*

Radiometric calibration was not performed on the dataset because the AST_L1T product is already in radiance and therefore there was no need to do the conversion from digital numbers to radiance. The dark pixel correction is a type of theoretical atmospheric correction that suppresses the effect of atmospheric scattering.

The dark pixel subtraction was done after the layers were stacked together. Three methods of dark pixel subtraction are incorporated in ENVI software and for this study, the band minimum subtraction option was chosen because the pixel values of the atmospheric scattering particles are assumed to be the least minimum values within the image scene in band minimum subtraction method. The screenshot of the dark pixel subtraction process is shown in Figure 3.9.

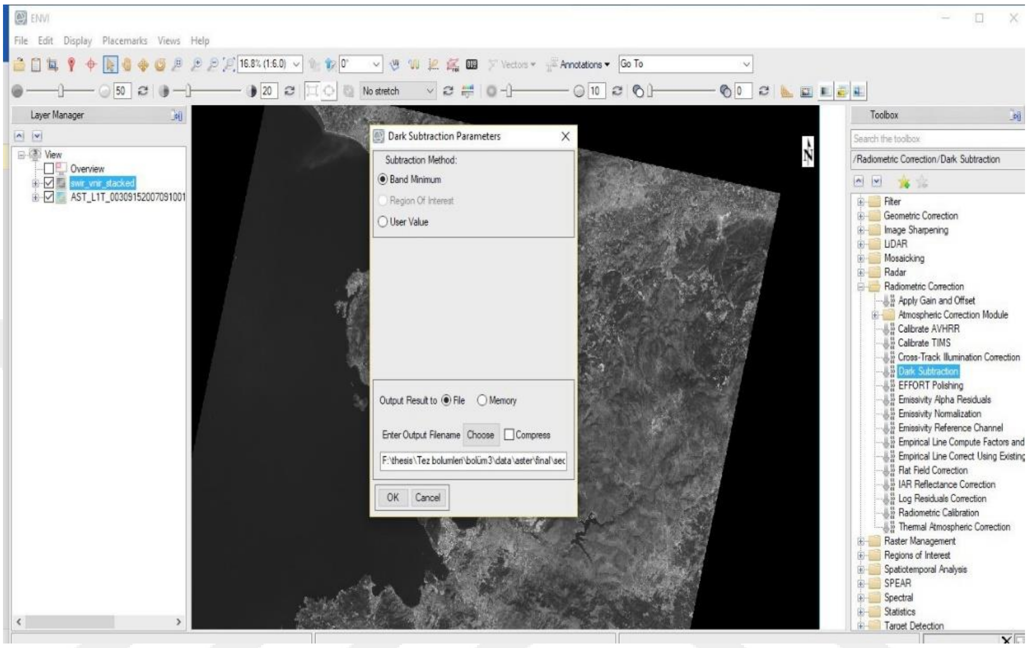

Figure 3.9. *Dark pixel subtraction process*

3.3.5.5. *Log residual atmospheric correction*

Atmospheric effects on the surface reflectance are the main factor that can lead to mismatching of the image spectra against the known spectra of minerals measured in the field or laboratory.

The issue of atmospheric effect can impede the attempts of using remote sensing for mineral exploration if it is not well addressed. In line with this reason, after applying the dark pixel subtraction correction, which is based on image statistics, there was also the need to perform another atmospheric correction based on empirical data to make sure that at least the effect of the atmosphere is reasonably removed or suppressed.

The log residual correction was chosen against the other empirical methods because the log residual generates pseudo reflectance image which is very important for mineral-related absorption diagnostic analysis. The log residual creates a reflectance image freed from effects such as solar irradiance, instrument gain, atmospheric transmittance, topographic and albedo effects. The log residual atmospheric correction and Internal Average Relative Reflectance are similar as they both utilized in-scene statistics to generate the reflectance image. The procedure for applying the log residual is illustrated in Figure 3.10.

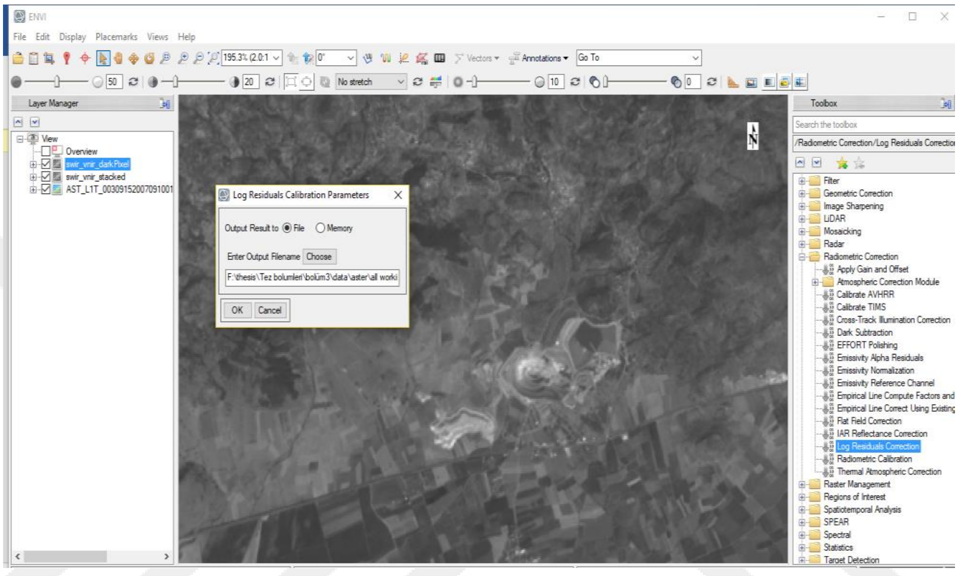

Figure 3.10. *Log residual calibration parameters*

There was a great improvement in the surface reflectance of the image after the log residual calibration was applied. The brightness values of the image in Figure 3.11 were more noticeable than those in Figure 3.10. With the appropriate atmospheric correction applied on the image, the issue of spectra mismatching will be minimal and further image analysis such as the band ratio can be performed to produce the hydrothermal alteration zones associated with the epithermal gold-silver deposits in the study area.

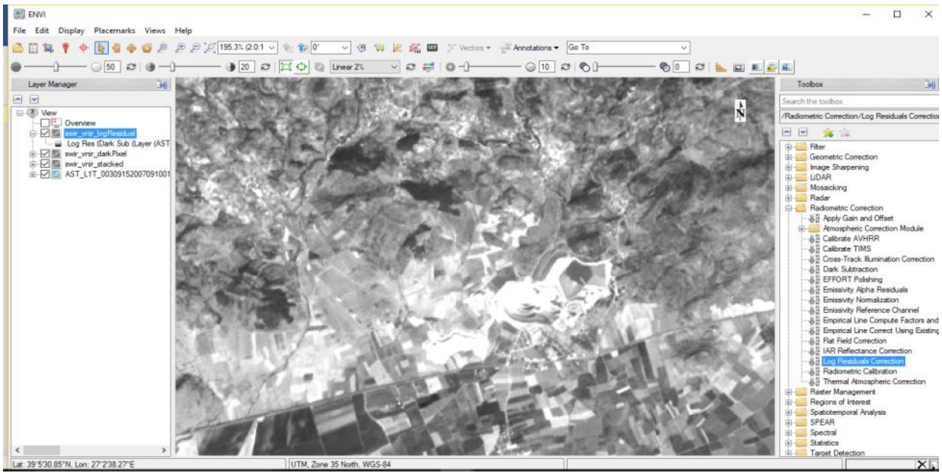

Figure 3.11. *Pseudo reflectance image of Ovacık Gold Mine*

3.3.5.6. *Subsetting*

To focus the analysis and interpretation only on the area of interest, the area of interest must be clipped out or subset from the whole image scene. Using only the clipped part for the analysis would help to improve the processing speed of the data and reserves some amount of storage space than when the whole image scene is being used.

To perform the subsetting operation in ENVI software or in any other image processing software, the region of interest (ROI) file must be created first or any vector file of the area of interest must be available to define the boundary of the study area. The area of interest was created from the image and then used as a boundary for clipping the interest area. Figure 3.12 displays the clipped image of the area of interest.

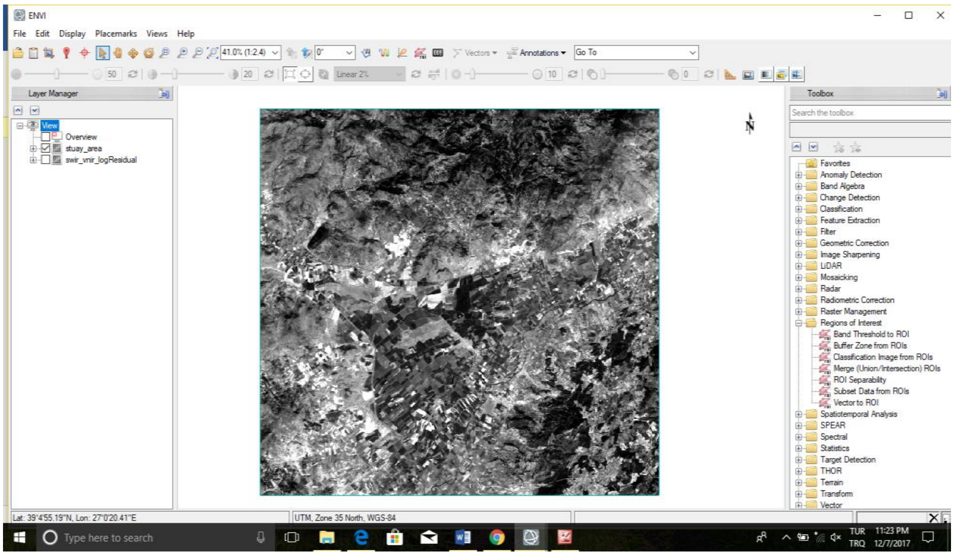

Figure 3.12. *Clipped image for the Area of Study*

3.3.5.7. *Masking*

The presence of reflectance of certain features which might not be needed for the analysis may cause some interference to the analysis of the reflectance of the feature under-investigated. For instance, the presence of dense vegetation can cause some interference in hydrothermal alteration analysis which can result in misclassification. To avoid the problem of interference of reflectance, the unwanted feature's reflectance must be excluded from the analysis and this process is termed as masking.

In this study, the presence of vegetation was masked by first performing normalized difference vegetation index on the image to highlight the vegetated areas. A vector file was then created from the normalized difference vegetation index ratio image using a threshold value of 0.2-0.6. The areas of vegetation cover after applying the threshold were highlighted in Figure 3.13.

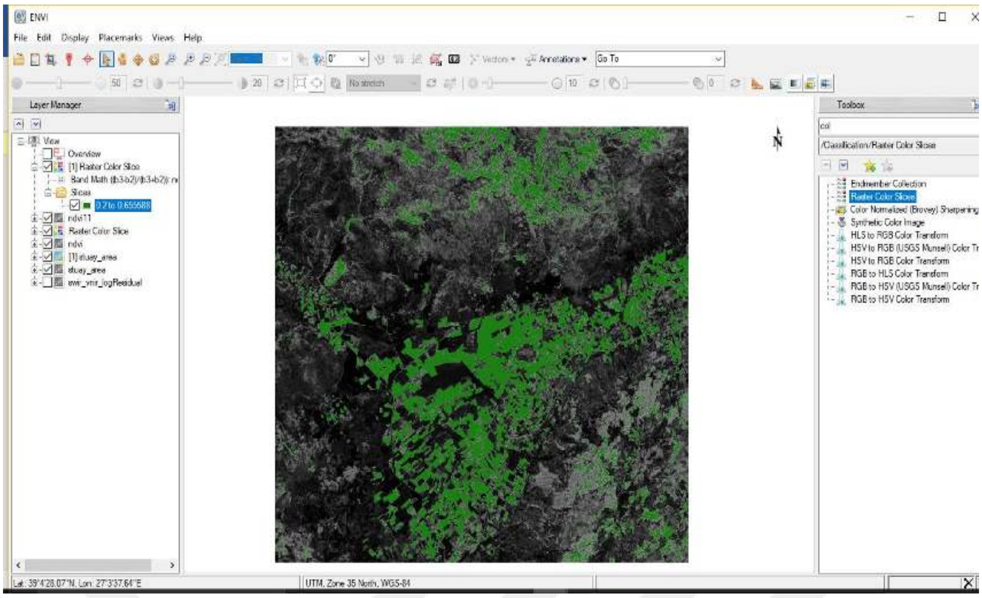

Figure 3.13. *Vegetated zones within the Study Area*

After the mask was applied these vegetated zones can be excluded from the hydrothermal alteration analysis because the reflectance values for the vegetated zones were defined as zero (0) values. Image processing will only occur in areas with reflectance values greater or less than zero.

3.3.5.8. *Spectral signature generation*

The concept of the spectral signature is the main backbone of multispectral and hyperspectral remotes sensing techniques. The difference in feature types can be easily distinguished with their spectral signatures. The spectral signature of features plays a vital role in image classification because similar features exhibit the same spectral patterns.

3.3.5.8.1. Selection spectral endmembers

Spectral endmember is 'pure' spectra representing a unique feature class type. Selection of the spectral endmembers is very crucial for the image classification because improper selections can lead to mixed pixels which in terms affect the accuracy of the classification.

Geologic map of the Ovacık deposit was overlaid on the AST_L1T image after which the regions representing the spectral endmembers were defined using the creating vector tool in ENVI. At least two areas of interest were sampled from each of the rock types within the mine area as illustrated in Figure 3.14.

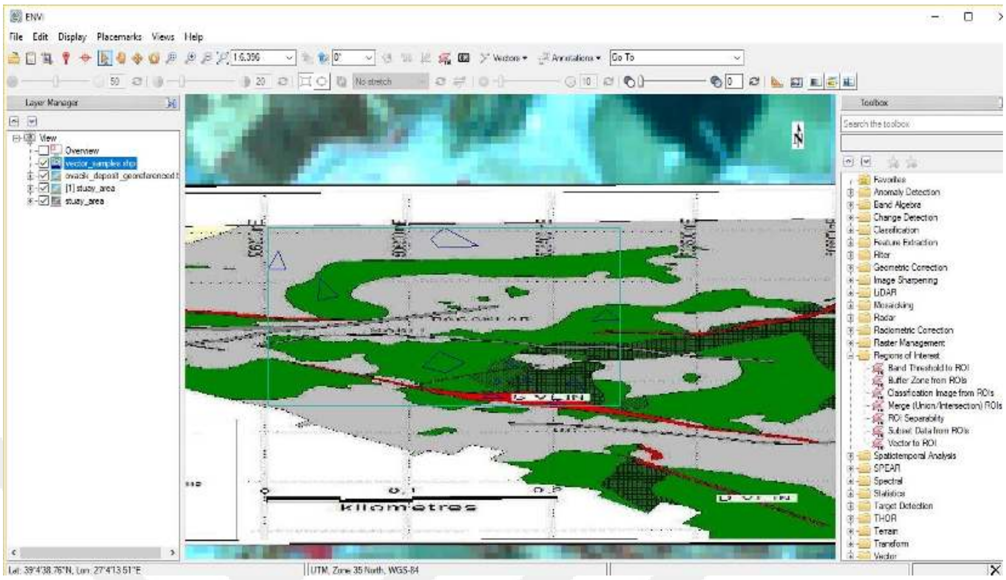

Figure 3.14. *Sampling of Areas of Interest from the Geologic map of Ovacık Mine*

The gold mineralization veins picked from the geologic map of Ovacık mine were transferred onto the AST_L1T image in Figure 3.15, using the converted vector to ROI tool in ENVI software. The ROI file is suitable for performing image processing such as the extraction of statistics for classification and the extraction of mean spectra from the image.

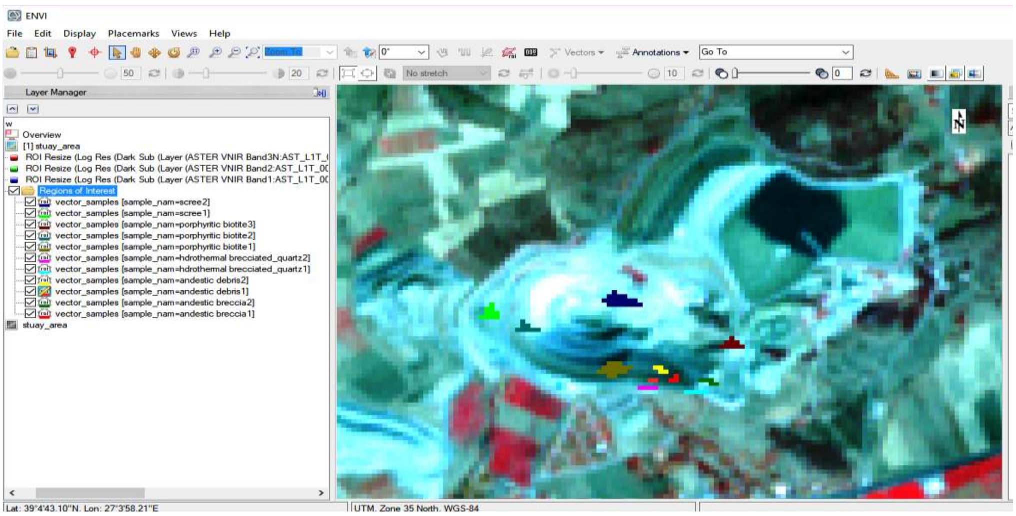

Figure 3.15. *ROI samples defined on the Mine Area*

The mean spectra for each of the sampled points on the image were extracted from the ROI file and exported as a text file. The spectral signature curve for each of the sampled point was plotted in Microsoft Excel from the text file.

3.3.5.8.2. Spectral matching

The USGS digital spectral library was used as a reference source for identifying the mineral types of the spectra extracted from the image. The spectra of the suspected mineral from the USGS digital spectral library and unknown image spectra were plotted together in Microsoft Excel for easy matching and identification. The spectral patterns of the unknown image spectra were matched against the spectra from the USGS digital spectral library. The absorbing points of the spectral curves were used as the reference point for the comparison and identification of the unknown spectra. The plot of spectral response curves for the sampled points and the spectra from the USGS spectral library are shown in Figure 3.16.

From the spectra matching, most of the unknown image spectra were identified to be illite mineral. The illite was the abundant in study area according to XRD diffraction analysis (Yılmaz et al., 2013). Most often, illite minerals are associated with low sulfidation epithermal gold deposits.

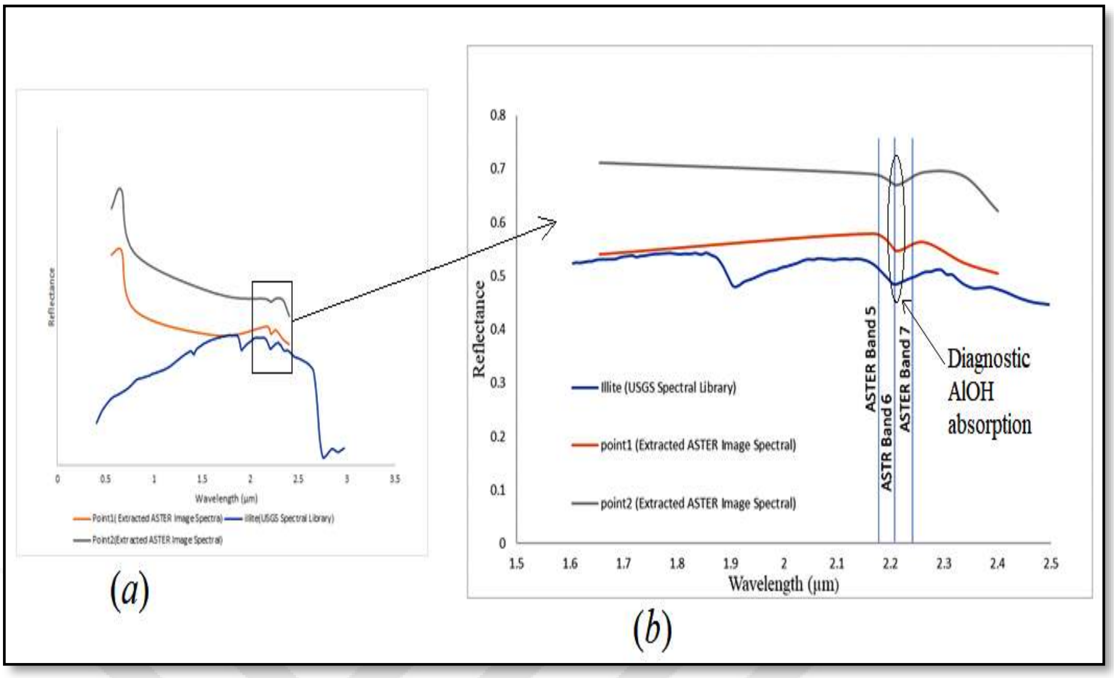

Figure 3.16. *Extracted ASTER image spectra within the (a) VNIR-SWIR and (b) SWIR region and the USGS Illite spectra*

3.3.5.9. *Hydrothermal alteration mapping*

Associating of hydrothermal alteration with mineral deposits has been one of the main concepts in mineral exploration. The introduction of multispectral and hyperspectral remote sensing has contributed significantly to mapping alteration associated with minerals. Mapping hydrothermally altered rocks or minerals with remote sensing technique could provide the exploration geologists the basic information to start the exploration work with.

Different methods have been employed by many authors to map hydrothermal alteration zones associated with mineral deposits. Among the most used methods are the band ratio technique, the spectral angle mapping technique, the principal component analysis, and the constraint energy minimization. Each method has its own advantages and disadvantages and is for this reason that more than one method was applied in identifying the alteration zones associated with a gold deposit in the study.

3.3.5.9.1. Band ratio technique

The difference between the high and low spectral reflectance of a feature can be easily highlighted by applying the band ratio technique. The band ratio indexes have been used to identify the different land cover type, rocks, and minerals. Minerals may show some high absorption characteristics at some wavelengths and at the same time exhibit high reflectance at different wavelengths.

The critical examination of the spectral response curves in Figure 3.16 revealed bands where the reflectance was high and band where the reflectance was low or high absorption for illite mineral. The illite mineral which is a component of argillic alteration was highlighted by dividing band 7 by band 6. There was high absorption of the incident energy in band 6 and high reflectance of energy by illite mineral in band 7. A simple illite index was proposed from the illite mineral spectral signature is shown in equation 3.1.

$$\text{Illite index} = \frac{band\ 7}{band6} \tag{3.1}$$

The Illite index was used to highlight the argillic alteration zones associated epithermal gold-silver mineralization in the study area. The process of performing the band ratio analysis in ENVI software is illustrated in Figure 3.17 and its resulting argillic alteration image is in Figure 3.18. The argillic alteration zones are highlighted in grey color.

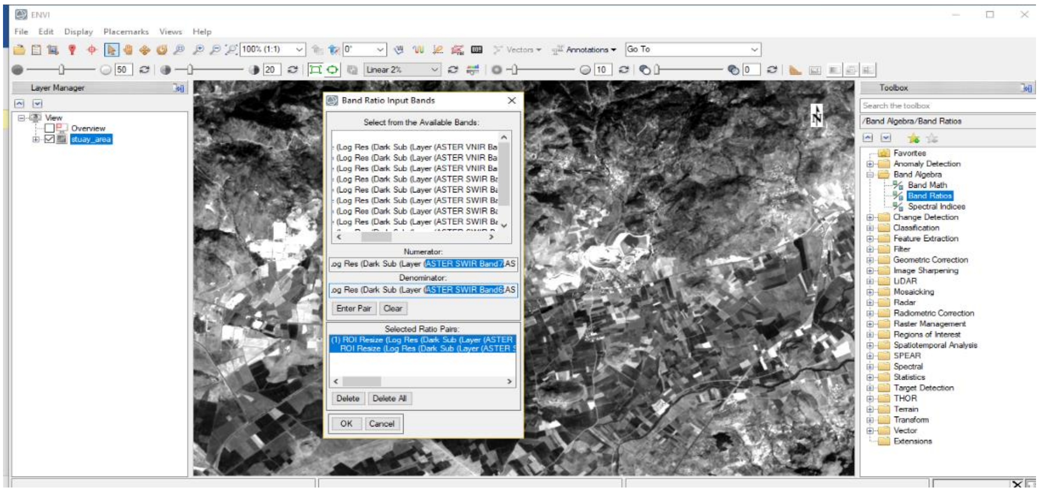

Figure 3.17. *Applying the band ratio of band 7 to band 6 on the image*

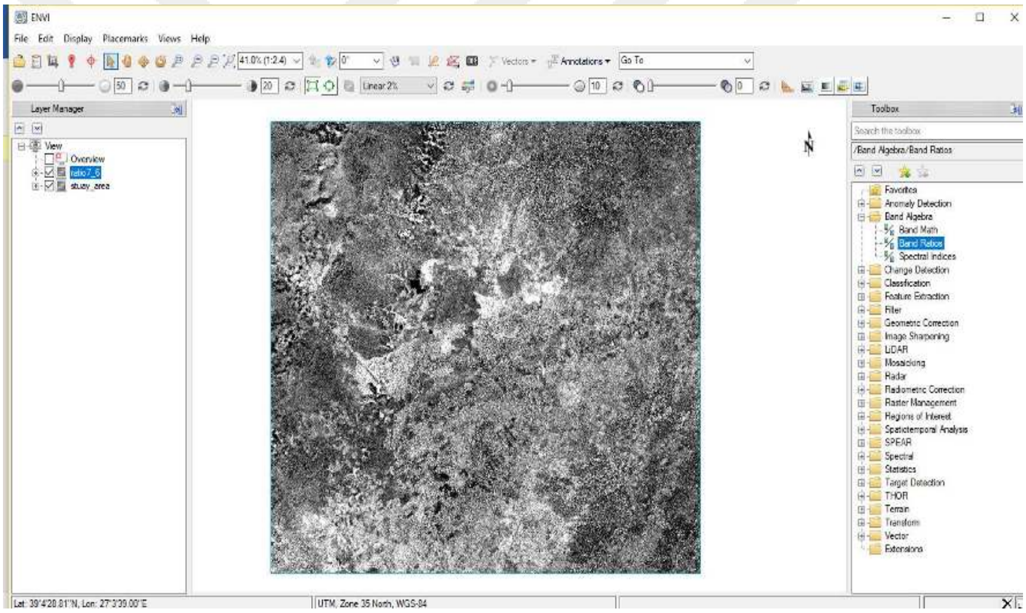

Figure 3.18. *Resulting image of band 7 over band 6*

The next processing step after the band ratio image was application of the already created vegetation masked vector file on the band ratio image. This was done to prevent the vegetated areas from taking part in the analysis. In other words, all the alteration zones that fall within vegetation zones were excluded from the image because they were assigned pixel values of zero during the masking process. The resulting image after applying the mask is shown in Figure 3.19. The black colored zones are the vegetated areas and grey color are argillic alteration zones.

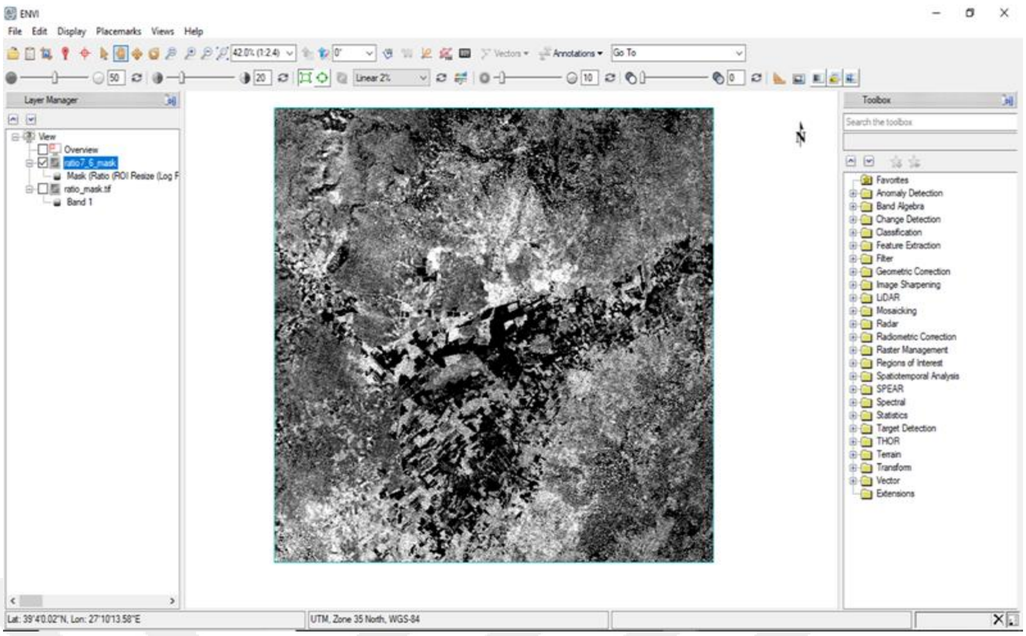

Figure 3.19. *Band ratio image after applying vegetation mask*

The statistics of the band ratio image and the band ratio image after applying the vegetation mask is showed in Figure 3.20. Defining a threshold value for extracting the argillic alteration zones from the ratio image was based on the statistics of the ratio the image.

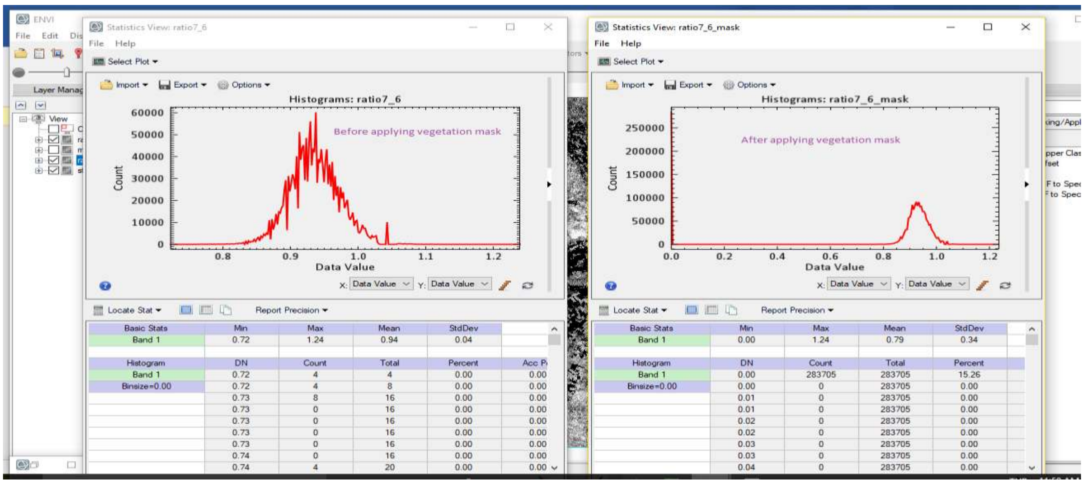

Figure 3.20. *Statistics of the band ratioed image and the band ratio image after applying the vegetation mask*

With reference to the statistic results in Figure 3.20, the threshold (background) value and subsequently the expected argillic alteration anomaly of the band ratio image was obtained by using one of the following equations:

$$\text{Threshold value} = \text{mean} + 3 * \text{standard deviation (confidence 98\%)} \qquad (3.2)$$

$$\text{Threshold value} = \text{mean} + 2 * \text{standard deviation (confidence 95\%)} \qquad (3.3)$$

$$\text{Threshold value} = \text{mean} + \text{standard deviation (confidence 92\%)} \qquad (3.4)$$

A threshold value of 1.06 was determined by using equation 3.2 and was used to extract the argillic alteration anomaly within the study area. Values ranging from 1.06 and above were considered be argillic alteration anomaly and values below 1.06 were considered as background. The raster color slices tool in ENVI was used to extract the anomaly once the threshold value was known. The defined argillic alteration anomaly was export as a vector file for field validation. The argillic alteration anomaly associated gold mineralization in the study area is indicated in red color in Figure 3.21.

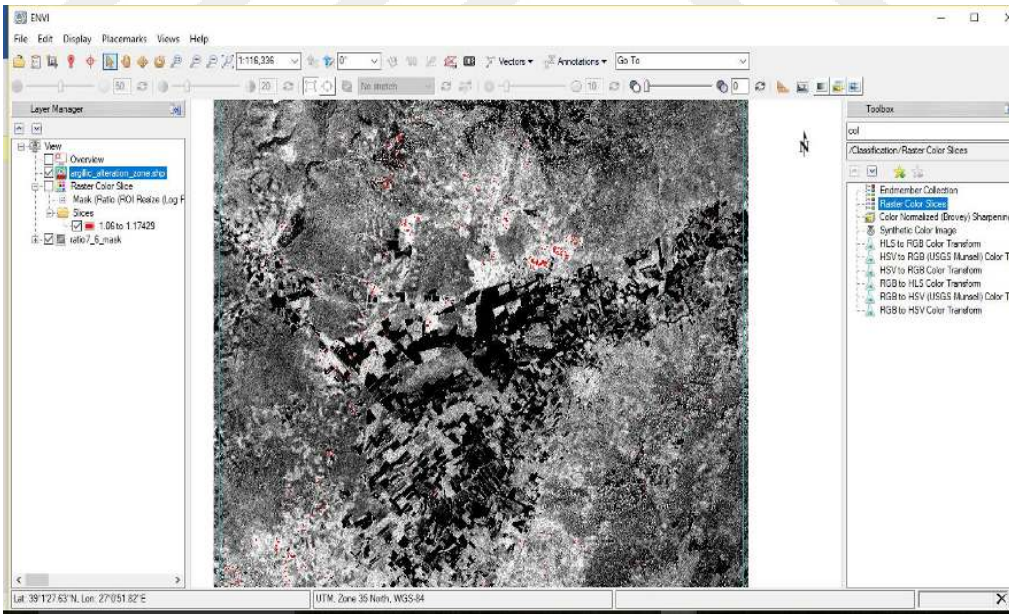

Figure 3.21. *Argillic alteration zones within Ovacık Mine*

3.3.5.9.2. Principal component analysis

The principal component analysis is one of the methods used for mapping hydrothermal alteration in most part of the world. Principal component images can be used to provide colorful composite images for easy identification of hydrothermal alteration zones. The principal component analysis utilizes the scene statistics to classify the spectral difference within the multispectral image. The Principal component analysis reduces the dimensionality of the data without any information loss.

In this study, all the three types of principal component analysis were applied, and comparison was also made among the results from each type of the principal component analysis. The concept of the three forms of principal component analysis used in this study are explained as follows:

3.3.5.9.3. Standard PCA

The standard principal component analysis normally utilizes all the bands of the image and for this study, only the visible near infrared and the shortwave infrared bands were used. The VNIR and SWIR bands were used because they exhibit some diagnostic spectral characteristics of most minerals such as clay and hydroxyl minerals.

In total 9 bands were used, 3 VNIR bands and 6 SWIR bands. A total of 9 principal component images were produced from the 9 bands used in the principal component analysis. Many color composite images can also be produced from these 9 principal component images by combining any three of the principal components in the RGB guns or channels. The standard principal component analysis has the advantage of producing more principal component images than the other two methods of principal component analysis. The procedure for performing the standard principal component analysis in ENVI software is captured in Figure 3.22.

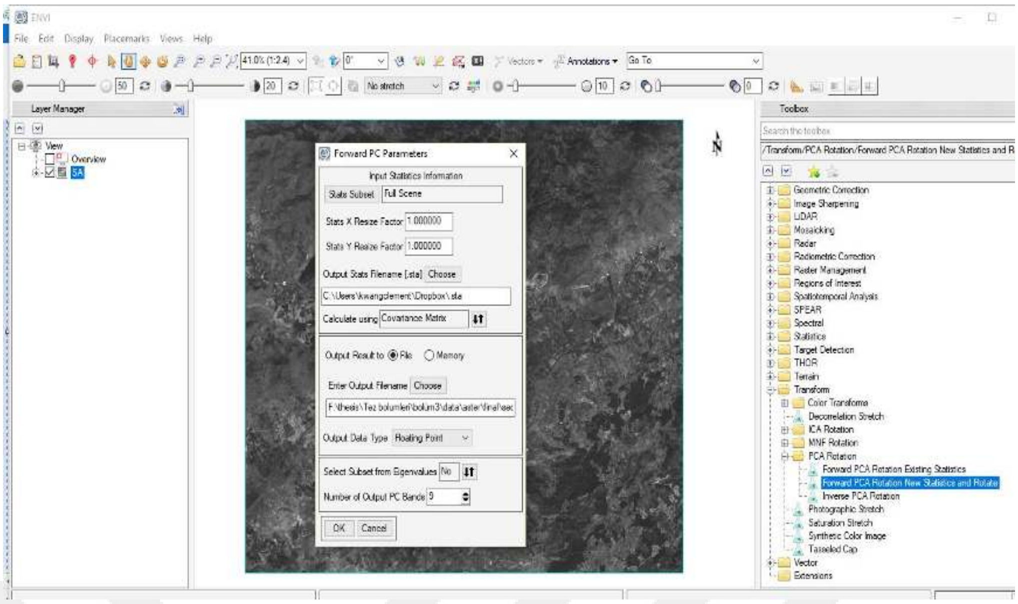

Figure 3.22. *Procedures of the standard principal component analysis*

3.3.5.9.4. Selective PCA

The selective principal component analysis utilizes only two selected bands of the multispectral image. The material or mineral under investigation determines which bands are to be selected for the analysis. One of the bands should show a high spectral reflectance while the seconded band should exhibit high spectral absorption characteristic of the feature under study.

In this research, the mineral under investigation was illite mineral and the selected bands for highlighting the illite mineral through selective principal component analysis were the band 6 and band 7 of ASTER image. The band 7 shows high spectral reflectance of illite mineral while band 6 shows a high absorption. The reason for choosing band 6 and band 7 was that the band ratio 7/6 was able to highlight the presence of illite minerals in the study area. Figure 3.23 and 3.24 illustrates the steps used in performing the selective principal component analysis in ENVI software.

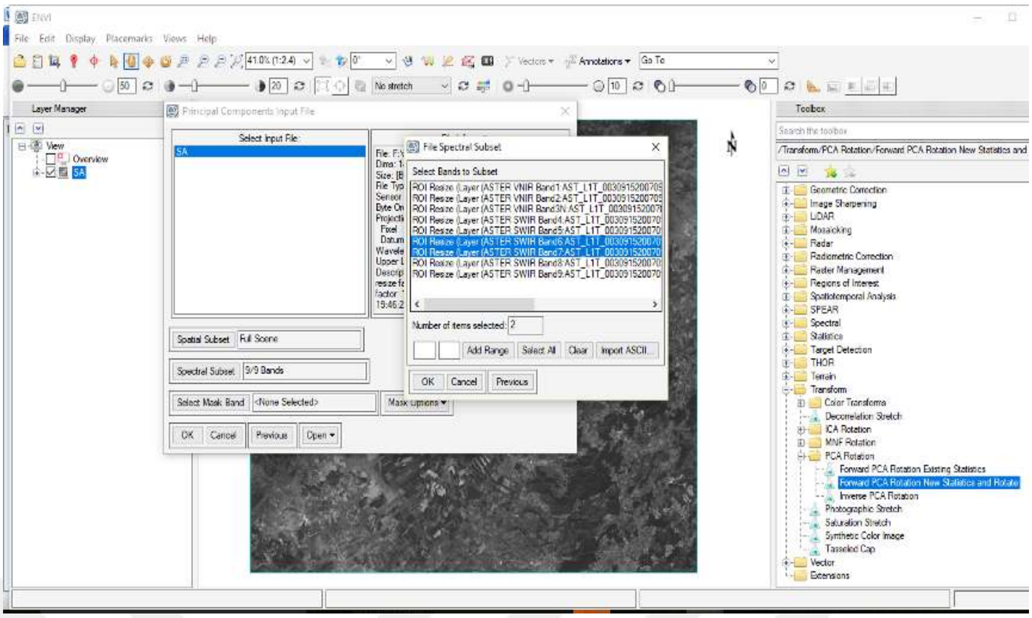

Figure 3.23. *Steps used in performing the standard component analysis*

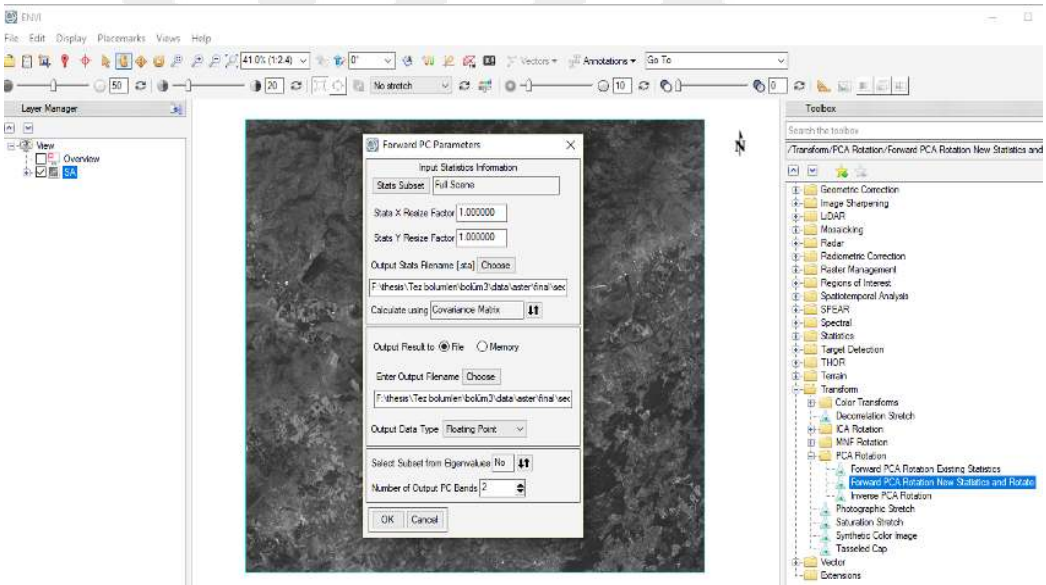

Figure 3.24. *Steps used in performing the standard component analysis*

3.3.5.9.5. Crosta Technique

The Crosta Technique identifies or detects the spectral difference among features based on the examination of the magnitude and sign of the principal components or the eigenvector loadings. Normally, four bands are required for the principal component analysis and the selection of the bands are based on the spectral response of the feature under investigation.

The spectral response characteristics of the target feature must be examined critically to detect bands which show either high reflectance or high absorption. Previous knowledge on how the target feature was mapped through either band combinations or band ratio analysis can also be of great contribution in the selection of the four bands for the Crosta Technique. Using the reduced number of bands could increase the chances of detecting the target feature within a principal component.

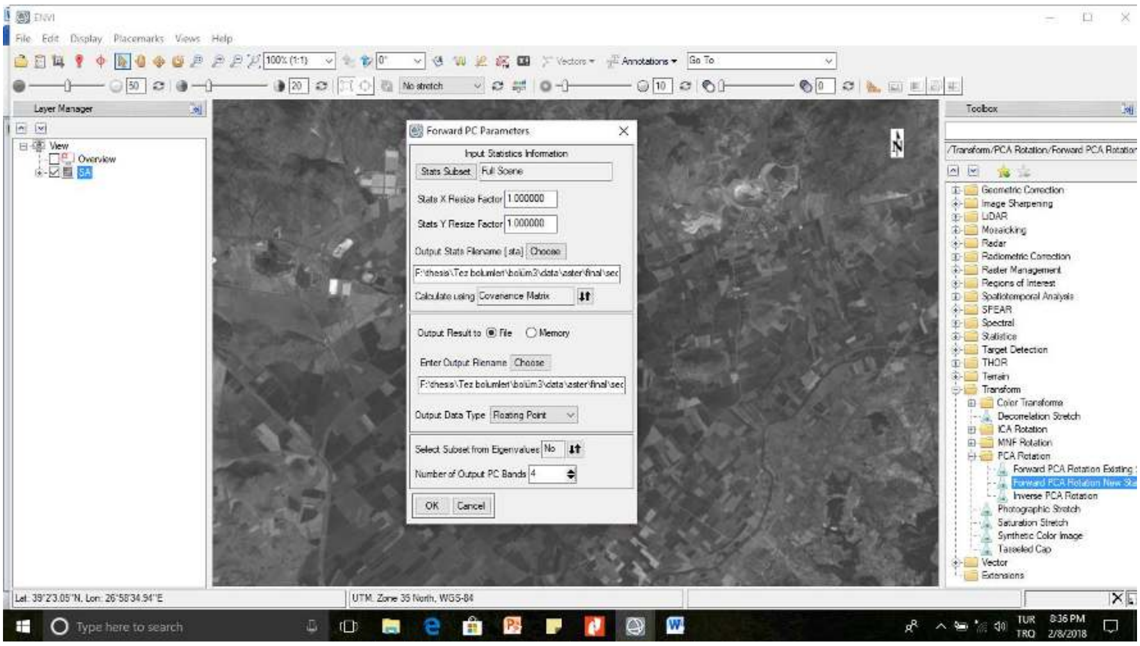

Figure 3.25. *Steps used in performing the standard component analysis*

3.3.6. Methodology of potential gold mapping

3.3.6.1. *Software and data sources*

This section provides information on the software and datasets used in predicting the potential Gold-Silver locations in the study area.

3.3.6.1.1. *Software*

The ArcGIS version 10.6.1, under a continuing educational license with Spatial Data Modeler for ArcGIS (ArcSDM)[2] extension was the software used for predicting potential gold locations within the study area. The ArcGIS version 10.6.1 served as the working environment for the ArcSDM tools and geoprocessing and spatial analysis. The ArcSDM tools were first developed an extension for ArcView version 3 by Graeme Bonham-Carter (formally of Geological Survey of Canada) and Gary Raines (USGS). The ArcSDM 5 was however developed Tero Rönkkö and Janne Kallunki (Geological Survey of Finland) and hosted at https://github.com/gtkfi/ArcSDM/. ArcSDM 5 is compatible with ArcGIS desktop and ArcGIS pro. The ArcSDM 5 was downloaded from the above link and added as Arctool in ArcGIS 10.6.1 and ArcGIS pro 2.1. The ArcSDM 5 tools consist of Fuzzy logic, Neural network, ROC Tool, Utilities, and weights of Evidence as shown in Figure 3.26.

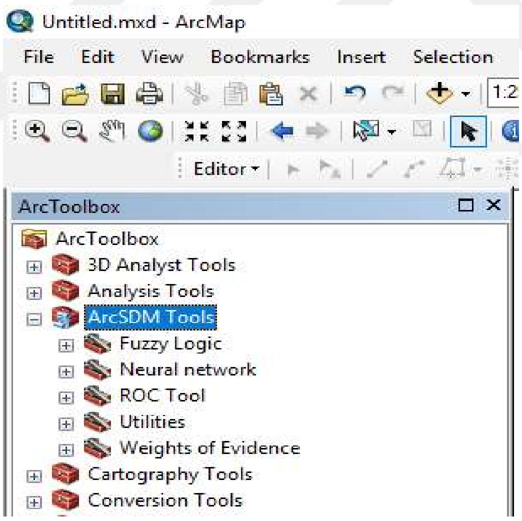

Figure 3.26. *ArcSDM tools*

In this study, only the fuzzy logic and weights of evidence tools were used in predicting the potential Gold-silver deposits. The sub-tools of fuzzy logic and weights of evidence models are shown in Figure 3.27. The functions of each of sub-tools of Fuzzy logic and weights of evidence tools were explained in detail in the method section.

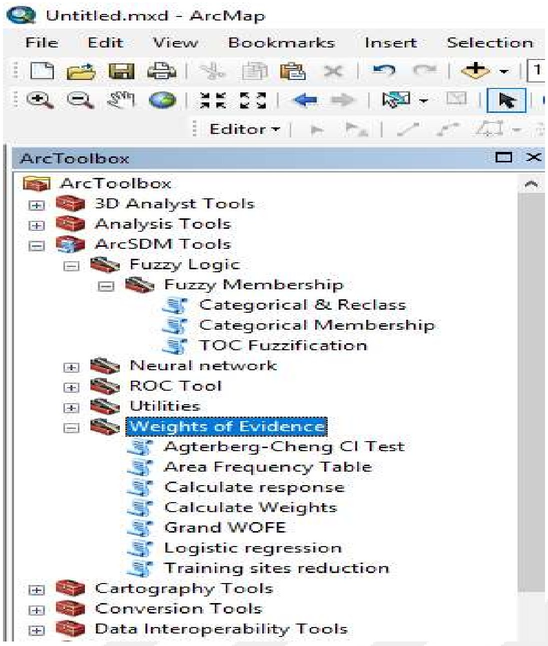

Figure 3.27. *Sub-tools of fuzzy logic and weights of evidence models*

3.3.6.1.2. Data Sources

Table 3.2 shows the list of datasets and the sources used in this study. The projection of all the datasets was in UTM Zone 35N, WGS 84 datum.

Table 3.2. *Lists of datasets used and their source*

Dataset	Data Type	Purpose	Source
Hydrothermal alteration	Raster	Evidential layer	Obtained from this study
Geological map	Raster	Evidential layer	Koza Altn Işletmeleri, 2015
Fault	Polyline	Evidential layer	Koza Altn Işletmeleri, 2015
Drill points	Point	Training and validation points	Koza Altn Işletmeleri, 2015

3.3.6.2. *Methods*

The weights of evidence and fuzzy logic modeling tools in ArcSDM 5 work only with raster evidential layers. This means that all the vector evidential layers must be converted into integer raster format. The training points and validation points were not converted into raster format. The raster conversion and the other spatial analysis performed before obtaining some of the evidential layers are described under the data preprocessing section.

3.3.6.2.1. Data preprocessing

The geologic map of the study area was first georeferenced and the various rock types were digitized. The digitized geology map was converted to an integer raster format based on the various rock types using the Polygon to Raster tool in ArcGIS 10.6.1. The rock types were reclassified further in six classes to obtain the lithology evidential layer in Figure 3.28.

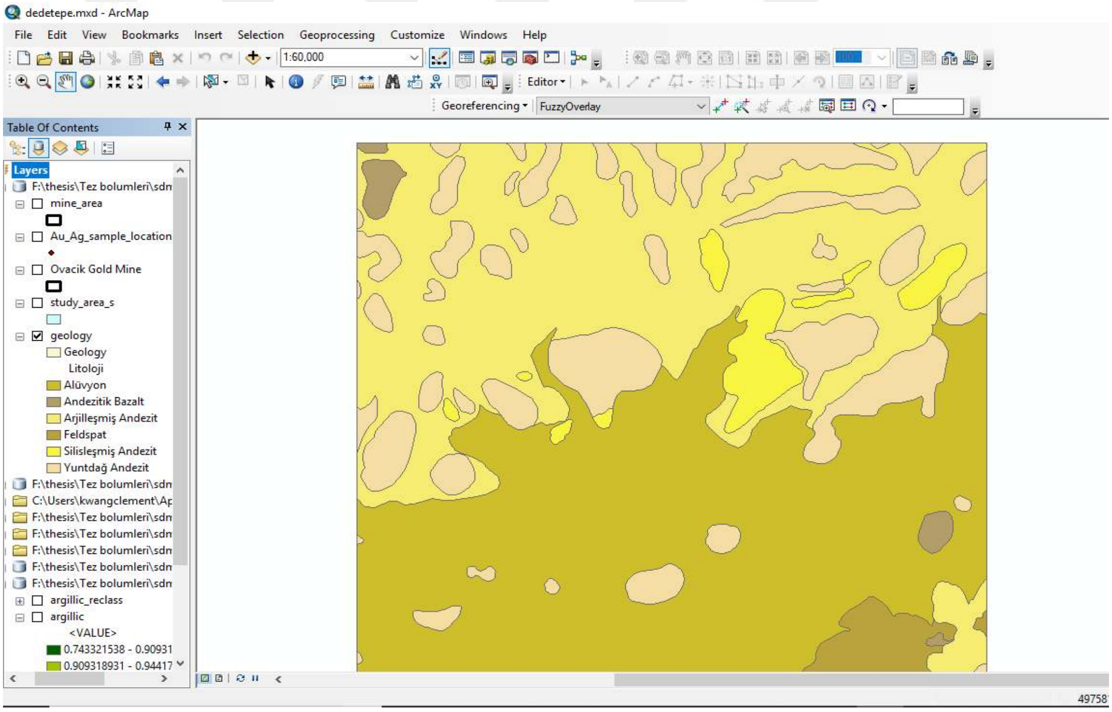

Figure 3.28. *Lithology evidential layer*

Analyzing faults is one of the main techniques used in identifying new deposits as they provide vital information on the geological contacts within an area (Phani, 2014). The strong correlation between faults and mineral deposits have been emphasized by many authors (Rajesh, 2004). They can reveal the configuration of the basement rocks and expose their mineralization types (Phani, 2014). The locations of minerals normally coincide with the faults even though some may exist away from the faults (Phani, 2014). Buffer zones are created around faults to take into consideration of that mineralization away from the faults. The faults used in this study were extracted from the exploration report of Koza gold company. Buffered zones of 100m, 200m, 300m, 400m, and 500m were created around the faults using the multi-ring buffer tool in ArcGIS. The buffered distances to faults were then converted into integer raster using a polygon to raster tool to obtain the distance to faults evidential layer (Figure 3.29).

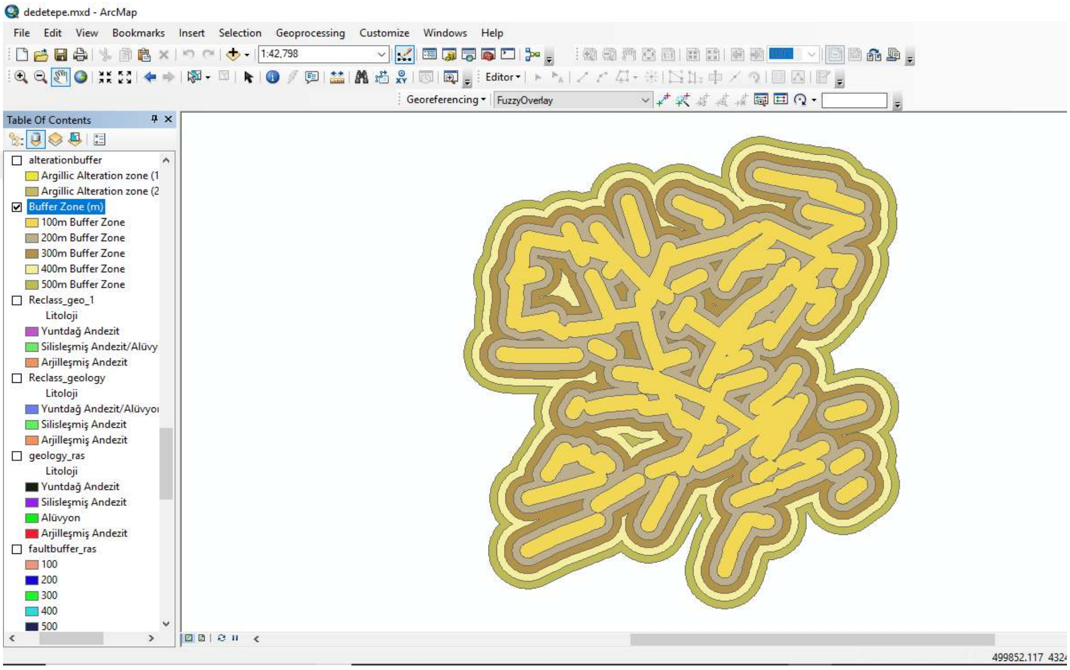

Figure 3.29. *Distance to faults evidential layer*

The argillic alteration zones are hydrothermal alteration zones associated epithermal Gold deposits in the study area and therefore plays a vital role in the prediction of new location Gold deposits. The hydrothermal alteration zones layer was obtained from the first part of this of study. The high reflectance areas of hydrothermal alteration map produced from the İllite index were digitized to obtain the argillic alteration zone within the study. The two ring buffer zones of 100m, 200m, 300m, and 400m were then created around the digitized argillic alteration zones (Figure 3.30). The buffer zones were created to make sure all the possible argillic alteration zones within the study area were captured in the mineral prospectivity modeling.

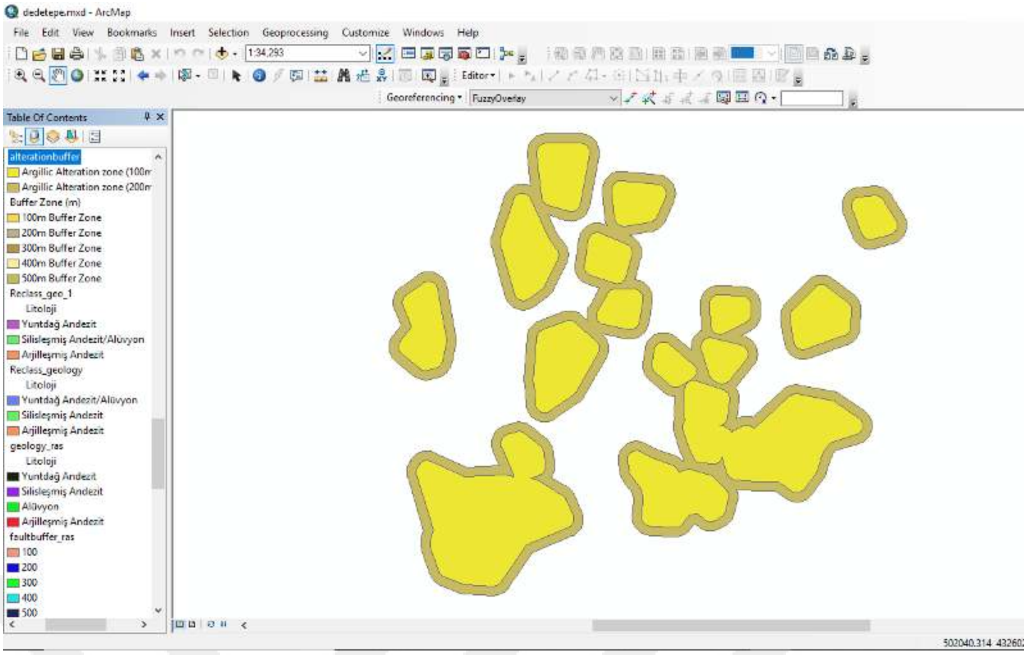

Figure 3.30. *Buffer zones around the argillic alteration zones*

3.3.6.2.2. Training points

The training and validation points used in this study represent known gold occurrences obtained from drill holes. The training points were used to calculate the weights of the evidential layer which measures the spatial association between the known gold occurrence and the evidential layers. 80 points were used as training points and 70 points for validation of the gold potential map. The locations of the training points within the study area are shown in Figure 3.31.

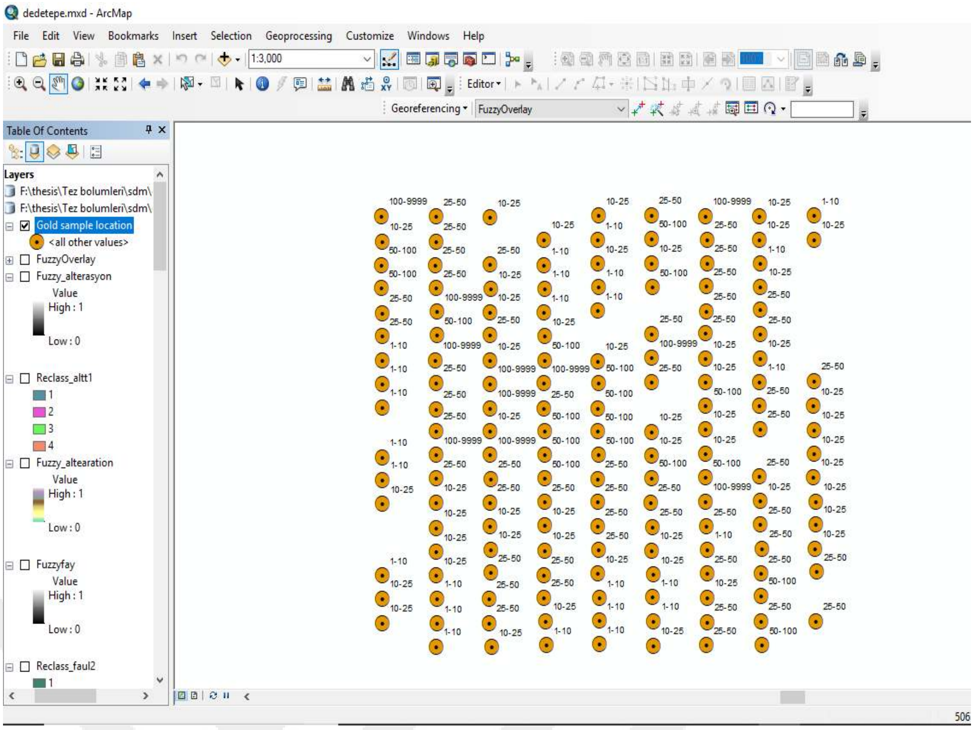

Figure 3.31. *Locations of the training points within the Study Area*

3.3.6.2.3. Weights of evidences method

The weights of evidence involve two main steps; estimating weights for each evidential layer and combining the weighted evidential layers to predict the new gold deposit locations. Before using the weights of evidence tool of ArcSDM 5 in both ArcGIS desktop and ArcGIS pro, the environment setting must be performed first. The study area should be in raster format and its unit cell size be specified. In this study, the unit cell size was set to 1km^2 based on the map scale, after consideration of Carranza (2009). Figure 3.32. show the environment setting for ArcSDM 5.

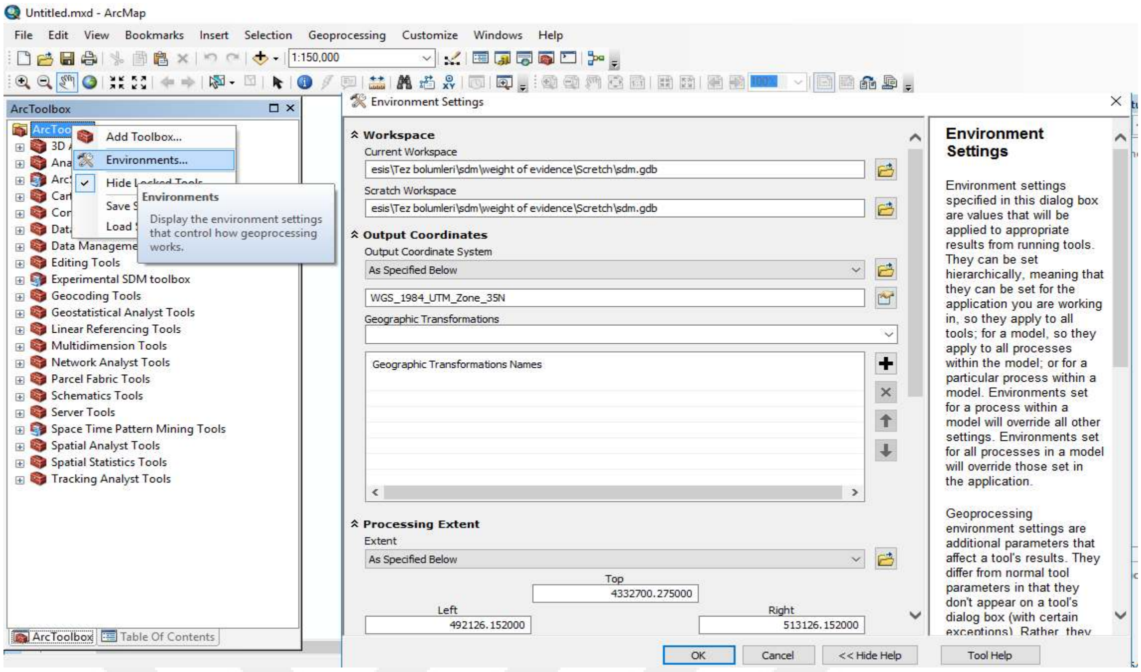

Figure 3.32. *Environment setting for ArcSDM 5 tool*

The Calculate weights tool in ArcSDM 5 was used to compute the weights for each of evidential layer. The Calculate weights as shown in Figure 3.33 required some input parameters such as evidence raster layer, training points, type, the confidence level of studentized contrast, and unit area cell size. The evidence raster layers for this study are geology (lithology evidence layer), hydrothermal alteration layer and fault proximity layer. Under the Type, Categorical was chosen for all the evidence layers because they grouped the layer into classes. The ratio of contrast to the standard deviation of the underlying weights gives the studentized contrast (Hartley, 2014). The confidence level of studentized contrast measures the confidence level of studentized contrast. For a limited number of training point, low confidence is more appropriate. A confidence level of studentized contrast of 2 represents 98% confidence which is the default value for Calculate weights tool. For this study, a confidence level of studentized contrast of 68% which corresponds to a value of 1.7 was chosen because of the size training points. The unit cell size was set to $1km^2$ based on the map scale and after consideration of Carranza (2009). The Calculate weights tool estimates the weights and stores them in the output weights table. The weights (w) will either indicate the presence (w+) or absence (w) of training points within the classes of the evidential layer.

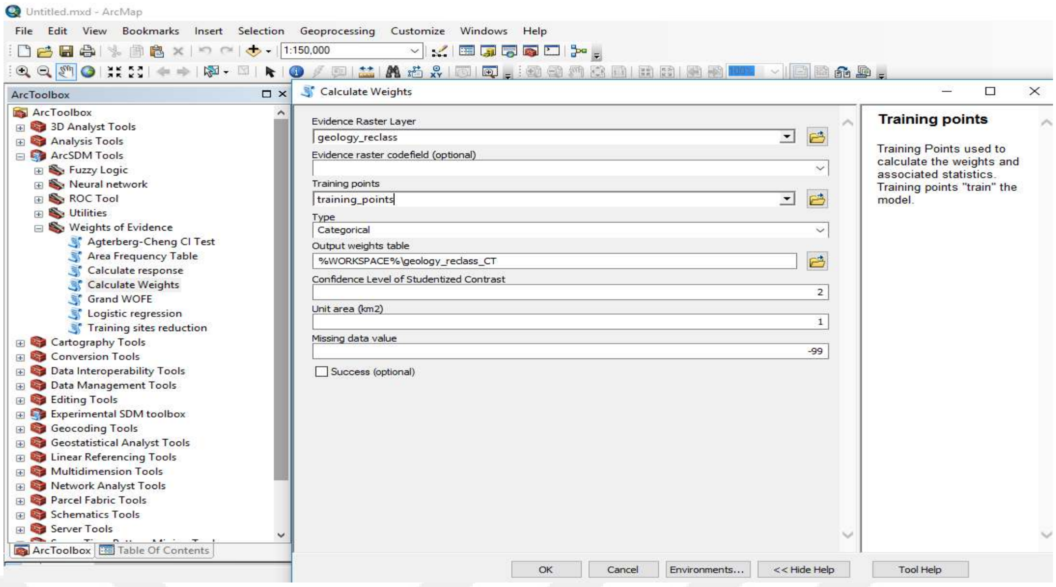

Figure 3.33. *Calculate weights tool of ArcSDM 5 tool*

The Calculate response tool was used to combine weighted evidential layers to produce the posterior map showing the locations of unknown gold occurrences with probabilities. The input parameters for Calculate response tool are training points, evidential layers, and their associated calculated weight tables. As shown in Figure 3.34, Calculate response tool outputted posterior raster map, standard deviation raster map, missing data variance raster map, total standard deviation raster map, and confidence raster map.

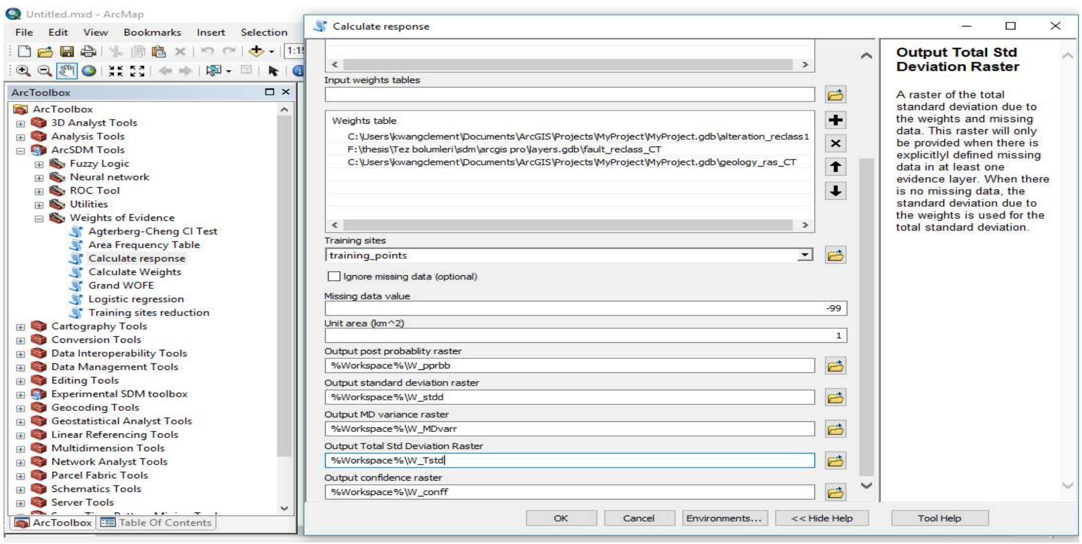

Figure 3.34. *Calculate Response tool of the ArcSDM 5 tool*

3.3.6.2.4. Fuzzy logic modeling

The fuzzy logic was also used to predict the occurrence of gold deposit because, in the fuzzy logic models, possibilities (degree, certainty, or credit level) are used instead of mathematical probabilities in resolving the complex and poorly characterized geological problems relating exploration (Quadros et al., 2006). The fuzzy logic comprises of two main processes; fuzzification of the evidential layer and combining of the fuzzified layers to produce the mineral prediction map. The classes of the evidence layers were classified based on the studentized contrast results obtained from the weights of evidence before performing the fuzzy logic model.

In this study, the linear algorithm was used to transform the evidential layers into a 0 to 1 scale using Fuzzy Membership tool (Figure 3.35). 0 indicates a low possibility of gold occurrence and 1 shows the high possibility of gold occurrence. The linear algorithm estimates the possibility of gold occurrence based on the linear transformation of the evidential layer. In a linear algorithm, the minimum value is assigned a favorable value of 0 and the maximum value is assigned a favorable value of 1.

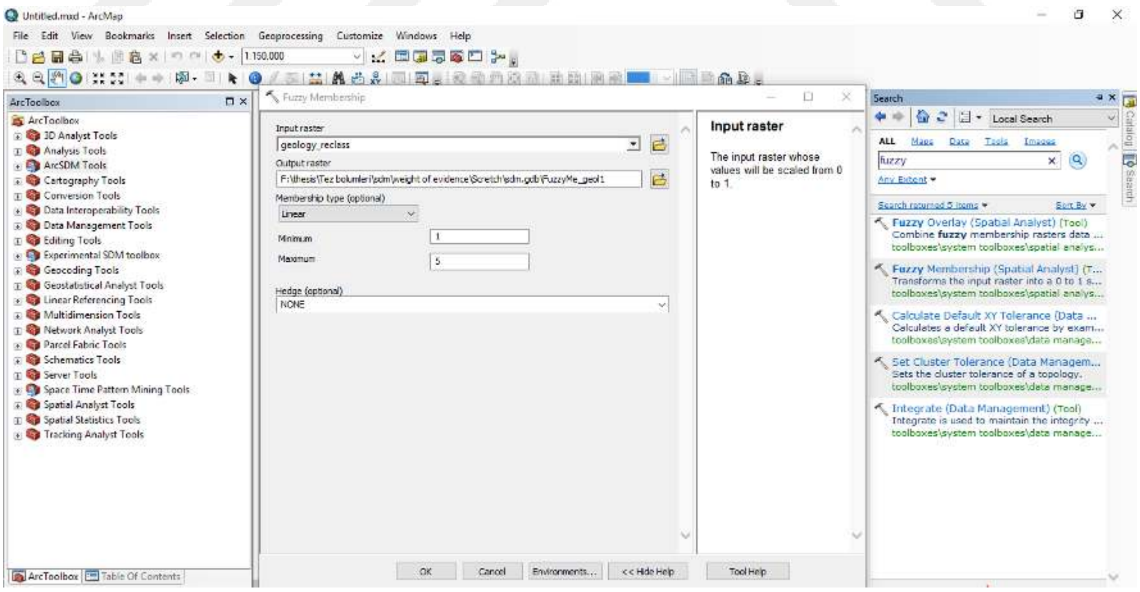

Figure 3.35. *Fuzzification of the evidential layers*

The Fuzzy Overlay tool was used to combine the fuzzified layers (Figure 3.36). The combination of the fuzzified data can be done with one of the following basic fuzzy operators such as fuzzy AND, fuzzy OR, fuzzy algebraic product, fuzzy algebraic sum and fuzzy gamma (An et al., 1991). In this study, all the fuzzy operators were tried but fuzzy gamma yielded the optimal result.

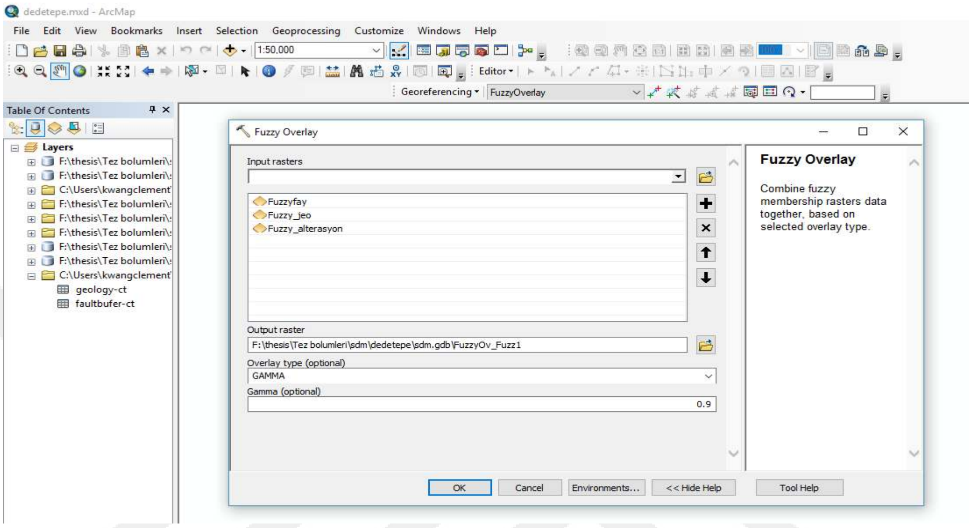

Figure 3.36. *Combining of the fuzzified layers with fuzzy gamma operator*

4. RESULTS AND DISCUSSIONS

The chapter talks about the interpretations of the results of this study. It tries to interpret the meaning and essence of the results. The chapter has two main sections viz; the results of argillic alteration detection and results from mineral potential mapping. Under each of the main sections are subsections.

4.1. Results of Band Ratio Analysis

This section deals with results and discussions of the proposed band ratio index, the illite index. It also highlights the applications of illite index in the exploration of argillic alteration of epithermal gold-silver mineralization. Band ratios and principal component analysis have been successfully applied in detecting hydrothermal alteration in the early stages of mineral exploration works. The band ratio technique identifies and maps the hydrothermal alteration associated with mineral by using the diagnostic absorption features of the alteration mineral. The diagnostic absorption feature is very important in identifying any material through the band ratio technique. The first requirement for proposing any band ratio index is the identification of the diagnostic absorption band of the mineral under study.

4.1.1. Illite index

The illite index was proposed by using band 6 and band 7 of the ASTER image. The band 6 and band 7 are all shortwave infrared bands. The band 6 was the absorption band while band 7 was the reflectance band. The absorption in the band 6 was due to the absorption of the electromagnetic radiations by Al-OH molecules in the illite mineral (Pontual, 2008). The absorption feature occurs at 2.20µm which corresponds to the wavelength range of band 6 of ASTER image.

It can be deduced from the illite spectral signature that the illite mineral within the study area have higher reflectance values being displayed in band 7 around a spectrum range of 2.235-2.285 µm and being absorbed in band 6 around 2.20µm. Therefore, by dividing the higher reflectance band by the lower reflectance or the absorption band, the anomaly of illite mineral was emphasized or highlighted in the image as bright pixels. The illite index is given in equation 4.1 as follows;

$$\text{Illite index} = \frac{\text{Band 7}}{\text{Band 6}} \tag{4.1}$$

The extracted spectral signatures from the ASTER image and the USGS spectral signature of illite were used as a guide in proposing the illite index. The illite index was proposed based the 2.20μm absorption spectral feature of illite although there are other absorption spectral features along the USGS illite spectral profile, the most visible absorption spectral feature from the image extracted illite spectral profile was the 2.20μm absorption spectral feature.

Band ratio is one of the main techniques used in identifying and mapping the hydrothermal alterations associated with minerals. Band ratio technique has been used to identify and discover most minerals in the world. Pour and Hashim (2011) used a band ratio technique to identify new deposits of epithermal gold in Iran. Gabr et al. (2010) utilized 4/8, 4/2, and 8/9 in RGB to discover high-potential gold mineralization in Abu-Marawat, Egypt. Arindam et al. (2015) used their proposed band indexes to identify chromitite and meta-ultramafite. Band ratio technique has also been used to identify and map altered rocks (Rowan et al., 2006; Tommaso and Rubinstein, 2007). The above-mentioned authors are only of the researchers who have used the band ratio technique in mapping and identifying hydrothermal alteration zones associated with minerals.

The argillic alteration zones identified by the illite index can serve as the first reference point to start gold mineral exploration. The index will reduce the exploration work to the most probable mineralized zones thereby saving cost, time and energy of the exploration team.

The application of band ratio, in general, is not only limited to the identification and mapping of hydrothermal alteration associated with minerals but it is applicable in other areas such as water bodies mapping, vegetation, and soil studies. Numerous band ratio indexes have been developed to identify and map water bodies from remote sensing images. The most popular ones for water bodies mapping are the modified normalized water difference index (MNDWI) and normalized water difference index (NDWI). The normalized difference vegetation index (NDVI) and vegetation index are the common indexes used to identify vegetated areas from remote sensing image.

The main advantage of band ratio is that the effect of topography and solar illumination is suppressed whiles at the same time the anomaly of the target material is highlighted. Also, the interpretation of a band ratio image is simple and straightforward. However, the selection of the bands for the ratio is not simple and may depend on other factors such as the target material and the surrounding features. Deciding which bands to be used in the band ratio technique is not simple work as Jensen (2005) rightly put it.

4.1.2. Illite index ratio image

The result obtained from the illite index is a surface reflectance image because the radiance of the image was first converted into surface reflectance by using the log residual correction algorithm in ENVI software. The higher reflectance of illite mineral in the band ratio image was the bright pixels in Figure 4.1. The illite index suppressed all other features and highlighted the presence of illite minerals (argillic alteration) within the study area as bright pixels.

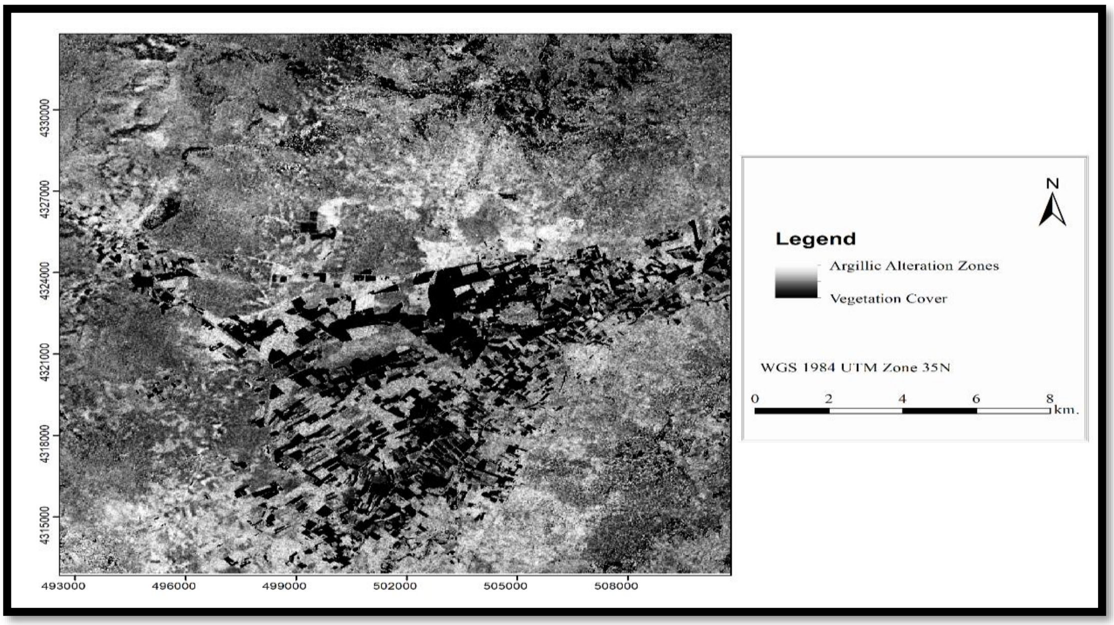

Figure 4.1. *The Illite index ratio image*

The dark pixels are the vegetation areas. The Ovacık gold mine was captured within the bright pixel zones. All the areas highlighted as bright pixels might not show the presence of argillic alteration as associated with the epithermal gold in the study area but the brightest pixels, however, indicate the presence of argillic alteration produced illite mineral. Illite mineral is one of the main minerals of argillic alteration and it is normally found in a place where epithermal gold mineralization occurred.

To indicate the most likely argillic alteration zones associated with epithermal gold mineralization, the band ratio image was classified based on the brightness pixel values. The classification result is illustrated in Figure 4.2. The classification helped in identifying the argillic alteration zones from the non-argillic alteration zones. The argillic alteration zones have undergone transformation after the interaction of the hydrothermal fluid and the gold deposit hosting rocks. The red colored zones in Figure 4.2 are the argillic alteration zones associated with the epithermal gold deposits. The Ovacık gold mine was identified within the red areas. These identified argillic alteration zones can aid further gold deposit exploration works. The green parts in Figure 4.2 are the vegetation cover and the yellow areas are places where the likelihood of discovering epithermal gold deposits is very less.

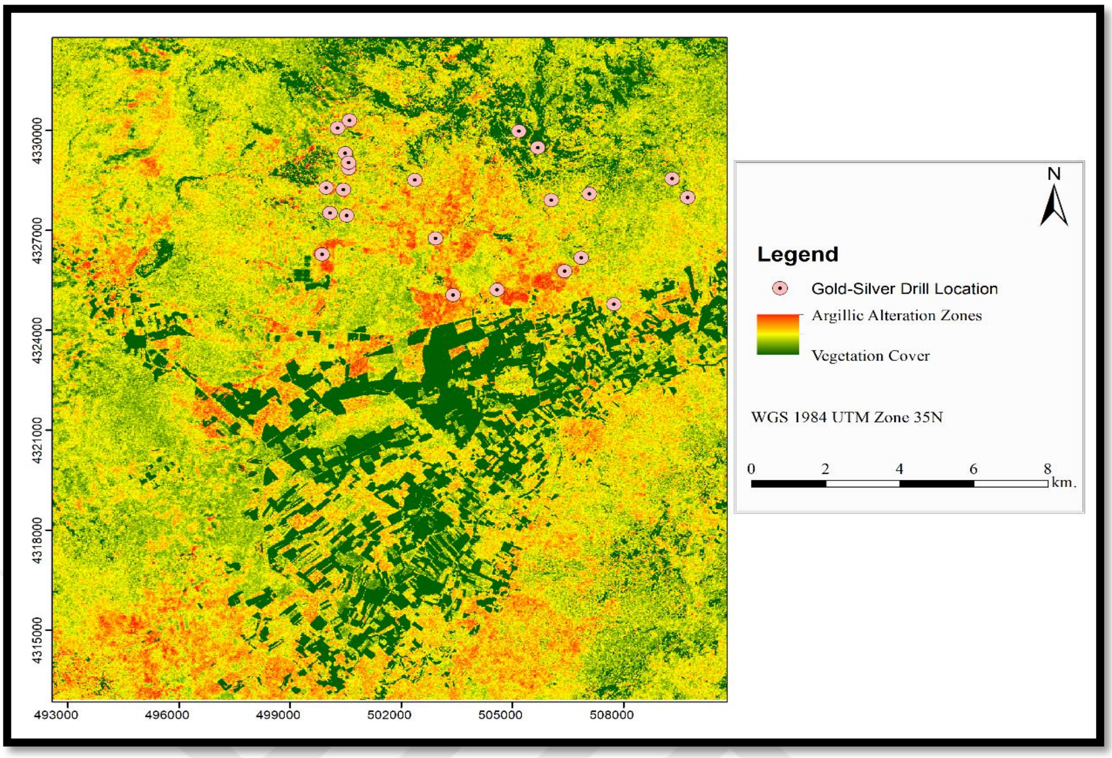

Figure 4.2. *Classification of argillic alteration zones after applying the Illite index*

4.2. Results of Principal Component Analysis (PCA)

The principal component analysis and band ratio are commonly used in identifying and mapping hydrothermal alteration zones. The principal component analysis uses the statistics of the image bands to produce uncorrelated principal component images. The results for the three different types of principal component analysis applied in identifying the hydrothermal alteration zones of gold mineralization of the study area are explained in the following subsections. The results obtained from the principal component analysis were used to compare and validate the hydrothermal alteration zones produced by the illite index.

4.2.1. Results of standard PCA

The standard PCA utilized all the bands from the visible infrared and the shortwave infrared portion of the ASTER image. The thermal infrared bands were excluded from the standard principal component analysis because clay minerals such as illite do not show any spectral diagnostic characteristics in the thermal infrared region of the electromagnetic spectrum. In the standard PCA, no priority was given to any of the bands in identifying the argillic alteration within the study area and hence there was no need to choose any group of bands. The standard PCA used 9 bands, three from the visible-near infrared region and 6 shortwave infrared bands.

4.2.1.1. *Statistical results from the Standard PCA*

The general statistics of 9 bands used in the standard PCA is illustrated in Table 4.1. The maximum pixel values for the first three bands (Band 1, 2 and 3) are very high as these bands have dynamic ranges greater than 200. The dynamic ranges for the other six SWIR bands are quite low. They have maximum pixel values less than 160. From these six bands, the one with the highest maximum pixel value is band 8 whiles the rest of the bands have relatively the same maximum pixel values. The bands with high dynamic range contain a wider and evenly spread variation of bright and dark pixel values than those with low dynamic range. In terms of reflectance, the bands with high maximum pixel values have high reflectance than those with low maximum pixel values.

The mean digital number shows the average brightness value of each band within the multispectral image. The VNIR bands (the first three bands) have an average brightness value greater than 75 whiles the SWIR bands (last six bands) have mean pixel values less than 66. The band with the highest mean pixel value is band 1 and this means that its reflectance and dynamic range are high and better. Band 9, on other hands, has the lowest average brightness value of 45.91 and this indicates poor reflectance and poor dynamic range value.

The standard deviation for 9 bands is given in Table 4.1. The standard deviation is used as a measure to assess the variability or spread of the pixel values within the bands from their central tendency and in this case the mean brightness values. Band 2 has the highest standard deviation value of 22.8, followed by band 1 with 17.76. The band with the least standard deviation value is band 9. This, therefore, means that the pixel values or the reflectance values within band 9 are consistent and alike to each other.

The consistency and similarity among the pixel values within the bands with low standard deviation values may mean that the reflected energy recorded by these bands came from objects or features of the same type. However, bands with moderate to high standard deviation values indicate high variability and dissimilarity among pixel values and this may mean these bands were able to capture objects with different spectral responses. Band 4 and band 6 had almost the same standard deviation (13.79 for band 4 and 13.50 for band 6) whiles band 7 and band 8 also had almost similar standard deviation values (band 7 = 12.14 and band 8 = 12.51).

Table 4.1. *Basic statistics for the 9 bands (VNIR + SWIR)*

Band	Minimum	Maximum	Mean	Standard Deviation
B 1	47	255	89.16	17.76
B 2	29	255	78.44	22.86
B 3	25	219	75.18	15.67
B 4	21	131	65.30	13.79
B 5	27	135	58.31	11.87
B 6	23	138	57.34	13.50
B 7	20	141	51.43	12.14
B 8	18	158	49.62	12.51
B 9	23	131	45.91	9.07

The covariance matrix for the 9 bands used in the standard PCA technique is indicated in Table 4.2. The covariance matrix of the image bands shows how the brightness values of one band vary with the brightness or pixel values of another band. In other words, the covariance matrix compares the variances of two different bands. The diagonal values in the covariance matrix represent the variances of each band whiles the variance between each of the pair of the bands (covariance) are shown the off-diagonal position of the covariance matrix.

Table 4.2. *Covariance matrix for the 9 bands (VNIR + SWIR)*

Covariance	**B 1**	**B 2**	**B 3**	**B 4**	**B 5**	**B 6**	**B 7**	**B 8**	**B 9**
B 1	315.41	396.01	96.95	190.30	167.94	188.62	171.20	175.68	124.21
B 2	396.01	522.54	99.04	255.18	224.56	253.51	228.94	235.57	167.77
B 3	96.95	99.04	245.59	57.64	21.95	25.12	23.20	19.98	9.37
B 4	190.30	255.18	57.64	190.12	156.46	179.30	159.08	161.84	115.46
B 5	167.94	224.56	21.95	156.46	140.85	158.62	142.49	146.46	105.16
B 6	188.62	253.51	25.12	179.30	158.62	182.36	161.68	166.05	119.70
B 7	171.20	228.94	23.20	159.08	142.49	161.68	147.28	150.43	107.73
B 8	175.68	235.57	19.98	161.84	146.46	166.05	150.43	156.57	111.72
B 9	124.21	167.77	9.37	115.46	105.16	119.70	107.73	111.72	82.27

All the visible near-infrared bands (band 1-3) had higher variance values than the bands within the shortwave infrared regions (band 4-9). Band 2 had the highest variance value of 315.41 and the least variance value of 82.27 was displayed by band 9. This means that pixel values in band 2 are highly spread out than all the pixel values of the other bands. The covariance values for all the bands were positive and this means that a higher pixel value of one band corresponding to a higher pixel value of the other band. A negative covariance value indicates that a higher pixel value of one band corresponds to a lower pixel value of the other band. However, a zero-covariance value means that there is no predictable relationship between the pixel values of the two bands.

The values of the covariance matrix are very difficult to interpret because they are not normalized. The normalized form of the covariance matrix is the correlation matrix. The correlation matrix standardized the covariance values to a range of -1 to +1 and this makes them easy for the comparison. Correlation matrix can depict the relationships between the pixel values of one band and the other bands in a stronger way than when using the covariance matrix. The correlation matrix for the 9 bands used in the standard PCA technique is indicated in Table 4.3.

Table 4.3. *Correlation matrix for the 9 bands (VNIR + SWIR)*

Correlation	B 1	B 2	B 3	B 4	B 5	B 6	B 7	B 8	B 9
B 1	1.00	0.98	0.35	0.78	0.80	0.79	0.79	0.79	0.77
B 2	0.98	1.00	0.28	0.81	0.83	0.82	0.83	0.82	0.81
B 3	0.35	0.28	1.00	0.27	0.12	0.12	0.12	0.10	0.07
B 4	0.78	0.81	0.27	1.00	0.96	0.96	0.95	0.94	0.92
B 5	0.80	0.83	0.12	0.96	1.00	0.99	0.99	0.99	0.98
B 6	0.79	0.82	0.12	0.96	0.99	1.00	0.99	0.98	0.98
B 7	0.79	0.83	0.12	0.95	0.99	0.99	1.00	0.99	0.98
B 8	0.79	0.82	0.10	0.94	0.99	0.98	0.99	1.00	0.98
B 9	0.77	0.81	0.07	0.92	0.98	0.98	0.98	0.98	1.00

All the correlation coefficient values are positive values and range between 0.07 and 1.00. The correlation values along the diagonal of the correlation matrix are 1 and are the highest correlation values. The correlation of a band and itself always has a perfect correlation and hence the correlation value of 1. There was a high correlation among the shortwave infrared bands with the least correlation value of 0.92 and the highest correlation value of 0.99. However, there was a high correlation value of 0.98 between band 1 and band 2 even though there were low correlations among the visible infrared bands. A high correlation (0.99) existed between these bands; band 5 and band 6, band 5 and band 7, band 5 and band 8, band 6 and band 7, and band 7 and band 8. Normally, there exists a good correlation among bands of the same region of the electromagnetic spectrum even though it may happen among bands of different regions of the spectrum.

To better illustrate the relationships among the bands, the correlation coefficient values from the correlation matrix were plotted. With the correlation relationship plot in Figure 4.3, comparing the relationships among the bands were simple and easy to interpret.

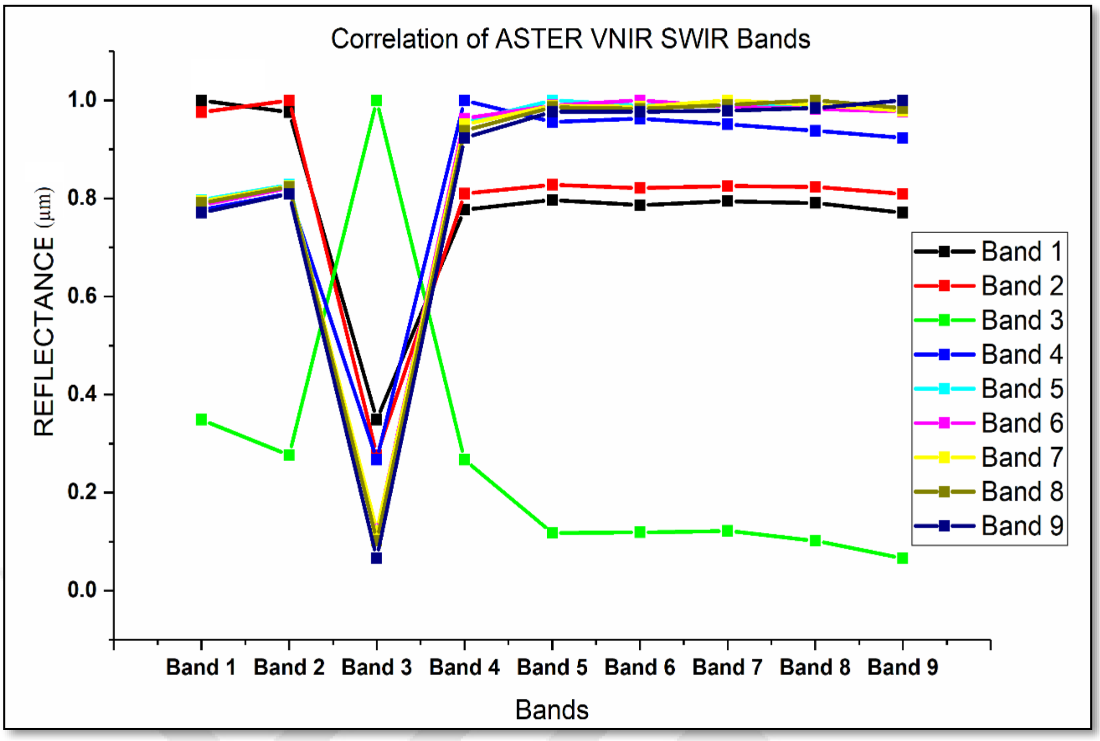

Figure 4.3. *Plot of correlation between the 9 bands*

Band 3 had the least correlation with all the bands. After band 3, the next worst correlation existed between band 1 and band 2. Among the shortwave infrared bands, the band with the worst correlation was band 9. The plot also indicated strong correlation among band 5, 6, 7 and 8. Bands which are highly correlated have similar reflectance or pixel brightness values than bands with low correlations.

There are two ways to obtain the eigenvector matrix. One way is through the correlation matrix and the other way is through the covariance matrix. The eigenvector loadings produced from the correlation matrix range between -1 and +1. In this study, the eigenvector loadings were produced from the correlation matrix and are standardized principal component loadings (Table 4.4). The principal component loadings produced from the covariance matrix are not normalized or standardized because the eigenvector loadings do not range between -1 and +1.

Table 4.4. *Eigenvector matrix for the 9 bands (VNIR + SWIR)*

Eigenvector	B1	B2	B3	B4	B5	B6	B7	B8	B9
PC 1	-0.42	-0.55	-0.11	-0.32	-0.28	-0.32	-0.29	-0.30	-0.21
PC 2	-0.21	-0.15	-0.89	0.07	0.16	0.19	0.17	0.18	0.15
PC 3	0.41	0.53	-0.42	-0.36	-0.21	-0.26	-0.22	-0.21	-0.15
PC 4	0.39	-0.36	0.09	-0.69	0.12	-0.01	0.22	0.34	0.24
PC 5	0.66	-0.50	-0.13	0.40	0.05	0.06	-0.08	-0.24	-0.25
PC 6	0.00	0.00	0.04	-0.21	0.06	0.69	-0.44	-0.40	0.35
PC 7	-0.12	0.08	0.03	-0.29	0.50	0.26	0.27	-0.22	-0.68
PC 8	-0.02	0.01	0.00	0.05	0.76	-0.46	-0.37	-0.08	0.24
PC 9	0.00	0.01	0.00	0.00	-0.01	-0.19	0.62	-0.66	0.38

There are nine principal components or eigenvector with different weighting or magnitude of variance as displayed by the nine different bands used in the standard principal component analysis. The principal components are displayed in the rows of Table 4.4 whiles the loadings are displayed in the columns. The band(s) with high weighting or loading dominate the corresponding principal component. The sign of the loading only indicates the direction in which the data was transformed.

PC1, PC2, PC3, and PC5 were dominated by the visible-near infrared bands with band2, band3, band2, and band1 respectively. PC4, PC6, PC7, PC8, and PC9 were dominated by the shortwave infrared bands with band4, band6, band9, band5, and band8 respectively. The characteristics of the dominant band in terms of pixels would be displayed most in its corresponding principal component images.

Each principal component has its corresponding variance. The variance indicates the amount of information contained within the principal component. The higher the variance values the more information being contained by the principal component. The order of information from highest to lowest follows the ordering of the principal component. Generally, the first principal component contains the highest variance, followed by the subsequence principal components. The variances in terms of percentage produced by the nine principal components are illustrated in Figure 4.4. The first principal component (PC1) has 79.2% of the total variance, followed by the seconded and third principal component with 13.2% and 6.4% respectively. PC4 through to PC9 has a variance value of less than 1% and therefore may contain spectral information specific to only one feature type.

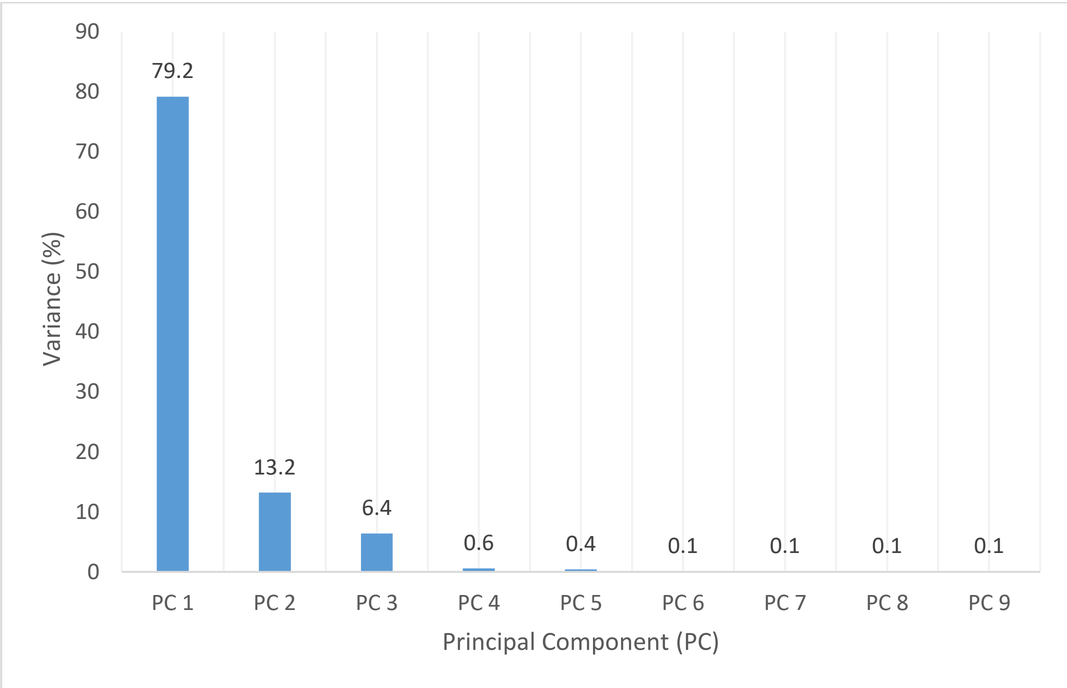

Figure 4.4. *Variance for the 9 principal component images*

4.2.1.2. *Standard PCA component images*

The principal component images were also produced from the correlation matrix. The principal component images contain the same information as the eigenvector matrix just that the principal component images displayed that statistical information in the eigenvector matrix as a variation of bright and dark pixel values. The eigenvector matrix gives the weightings in terms of contribution of each of the nine bands. For better interpreting of the principal component images, the loadings or weightings of the eigenvector matrix are needed.

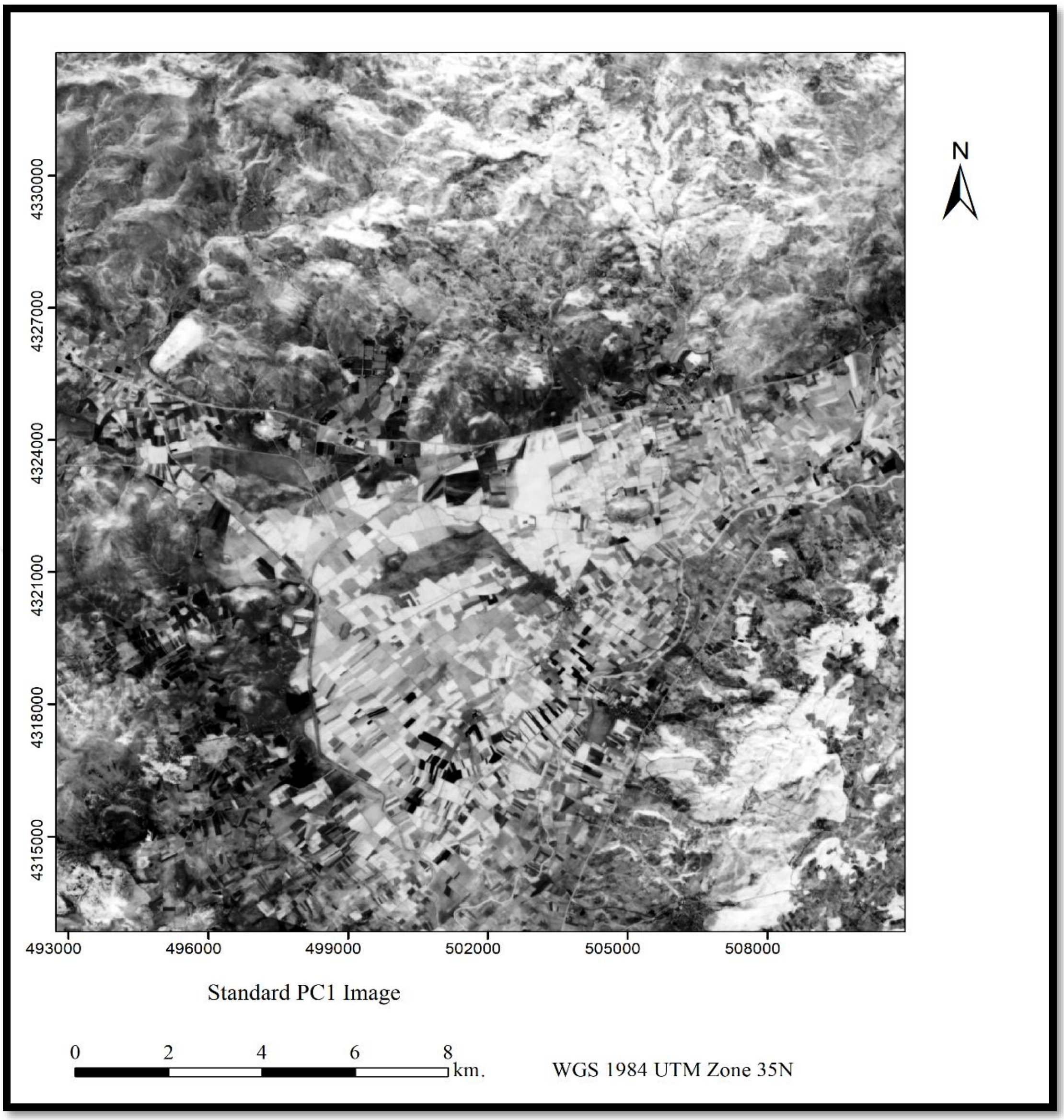

Figure 4.5. *PC 1 image of the standard PCA*

The first principal component image normally has the highest possible variance and contains much information than any of other principal component images. The first principal component image can explain the characteristics of the dataset completely because of its detailed information. The first principal component image is useful in categorizing the general characteristic of the data set and may not be helpful in identifying the unique characteristics of the dataset. The different forms of features or object within image data were exhibited in the first principal component image. From the first principal component image in Figure 4.5, the dominant feature was vegetation cover because of the high negative eigenvectors loading value showed in the red band (band 2). The vegetation cover is showed as bright color in Figure 4.5 because of the negative eigenvectors loading value of the red band. In the red band, the absorption of electromagnetic energy is high, and, a negative loading value made the vegetation cover was displayed as bright pixels in Figure 4.5.

The principal component image that depicted the argillic alteration zones within the study area was the principal component 6 image. The principal component 6 image has the highest loading weighting at band 6 where the absorption of illite mineral is high. The dark pixels in Figure 4.6 show the argillic alteration zones produced by the illite minerals within the study area. The dark pixels in Figure 4.6 were due to the positive loading value of the absorption band 6.

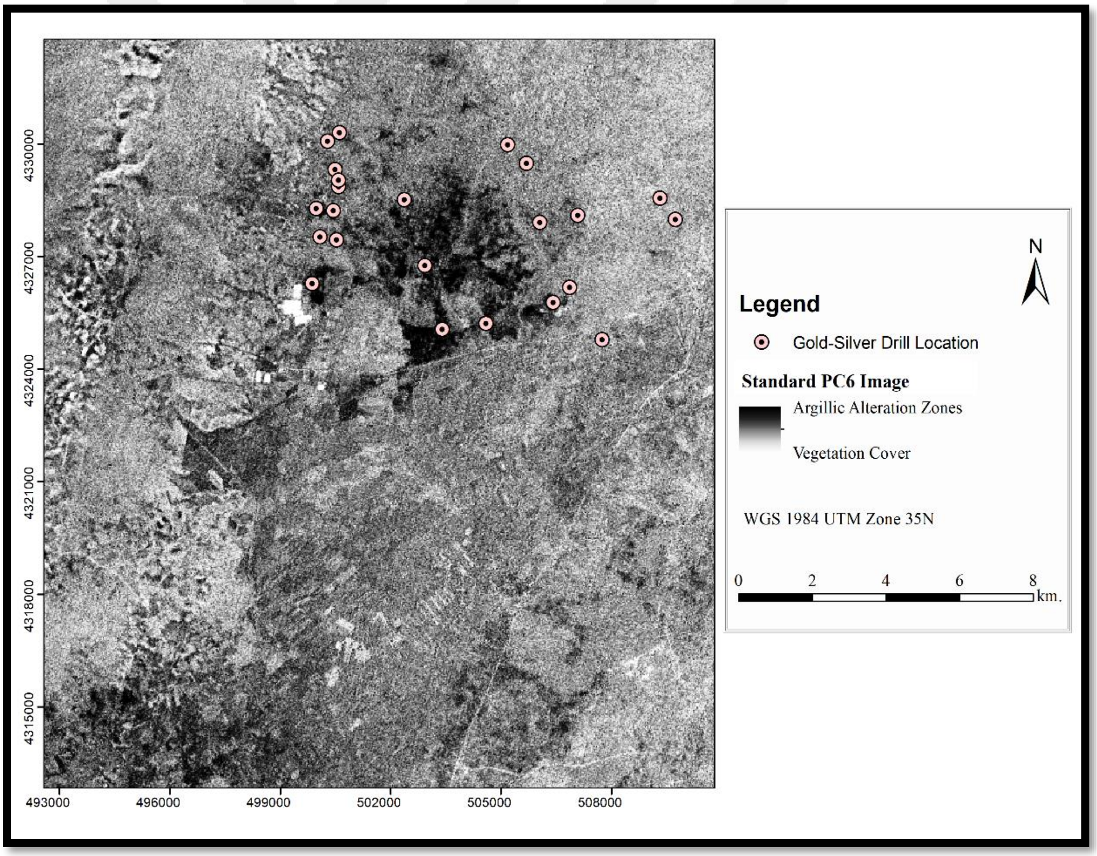

Figure 4.6. *PC 6 image of the standard PCA*

The dark pixels in Figure 4.6 were converted into bright pixels by negating the positive loading value of the absorption band 6. The resulting image from the conversion of the dark pixels of the PC6 image is shown in Figure 4.7. The bright pixels are the argillic alteration zones produced by illite mineral. The Ovacık Gold Mine was among the zones indicated by PC6 as the argillic alteration zones. The argillic alteration zones are the most probable gold- bearing zones within the study area.

The argillic alteration produced by PC6 may contain misclassified features such as vegetation cover and bare soil and this made the areas identified as argillic alteration zones a little bigger. This problem can be overcome by thresholding or classifying the pixel values of PC6 to contain only the most probable argillic alteration zones. The standard principal component analysis was, however, able to produce the argillic alteration zones within the study areas through the sixth principal component image.

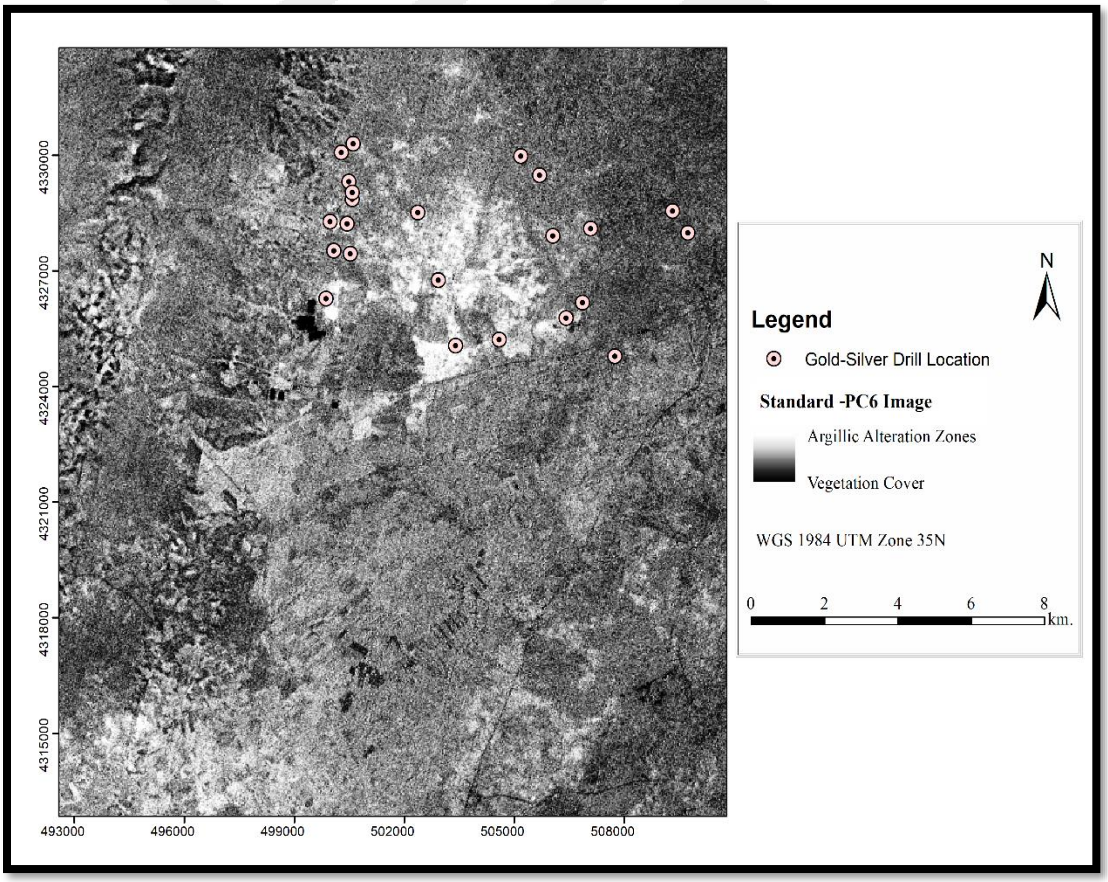

Figure 4.7. *Negative PC6 image of the standard PCA*

The last two principal component images (PC8 and PC9) do not contain any information and the noise levels in these principal components are very high. The last principal components are normally ignored for any analysis because of their high level of noise.

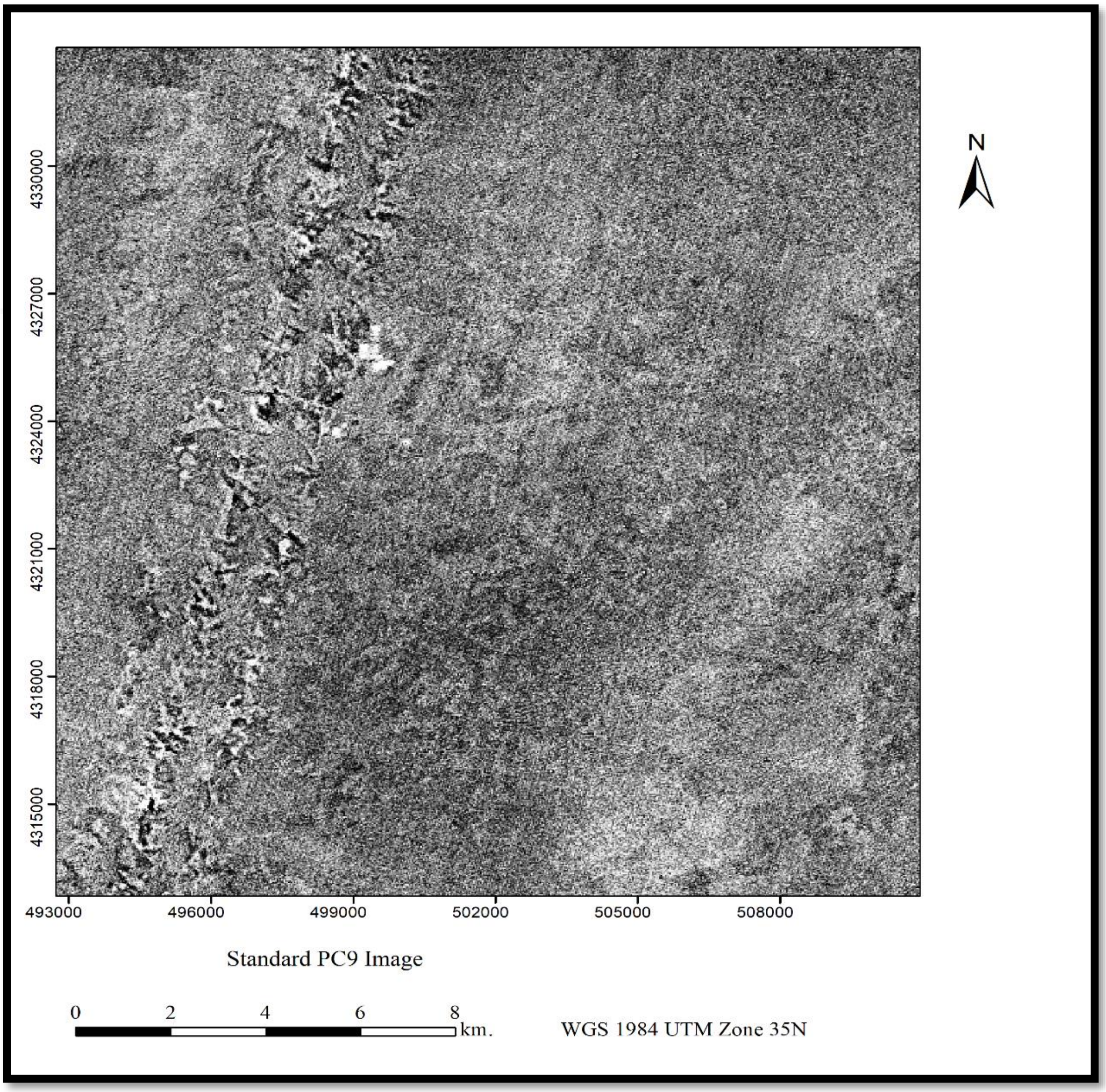

Figure 4.8. *PC 9 image of the standard PCA*

4.2.1.3. *Standard PCA color composite image*

The color composite image is formed to highlight features which could have been very difficult to detect from the single image. The color composite image uses distinguishable colors to depict different features, thereby making visual interpretation easy. The color composite image is not only formed from greyscale bands or band ratio images but also from the principal component images. The color composite images were formed by placing three of the principal component images into the red, green, blue channels. The color composite image can provide information about the hydrothermal alteration of mineral. Forming the color composite image from the principal component images can enhance the exposure of the altered rock. The color composite may also provide the opportunity to combine three different principal component images and this would help in bringing out hydrothermal alteration glues from the three principal component images.

In this study, several color composite images were produced by combining the principal component images to highlight argillic alteration zones within the study area. Some of the color composite images were not able to highlight the presence of an argillic alteration in the study area. The few color composite images which highlighted the argillic alteration are provided in Figure 9-12.

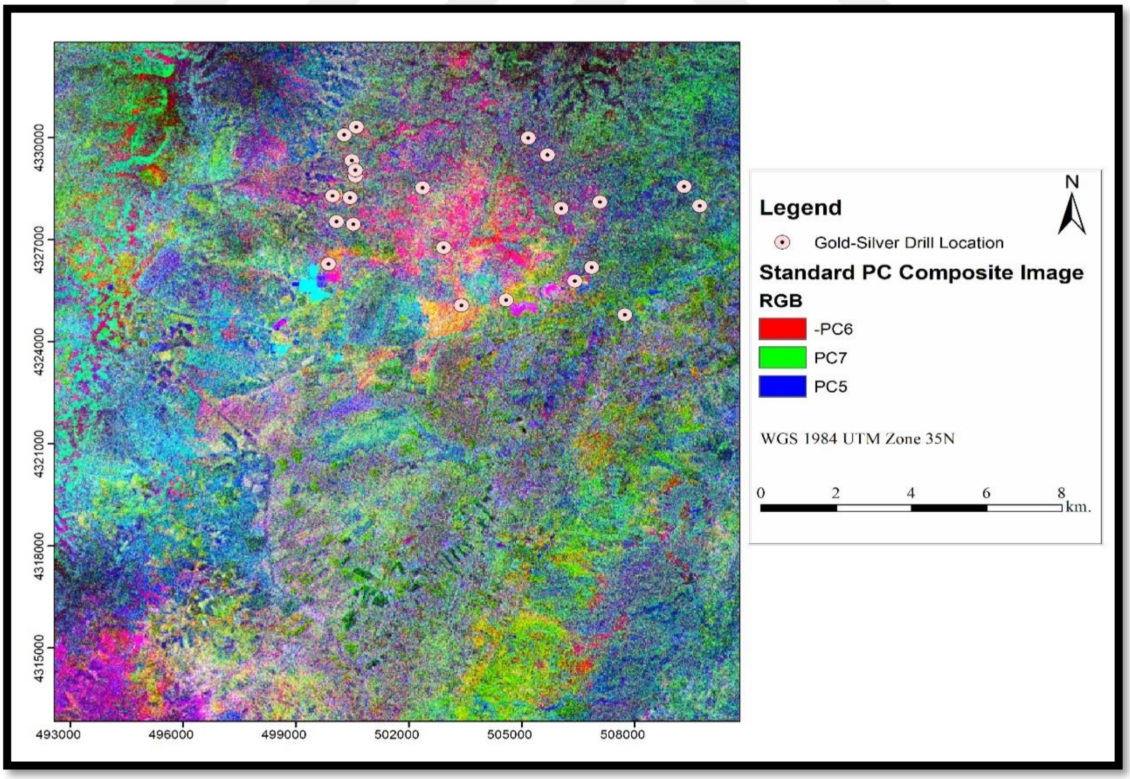

Figure 4.9. *Color composite image of the standard PCA (-PC6, PC7, & PC5)*

In Figure 4.9, the argillic alteration zones produced by the illite mineral are highlighted in the purple color. The areas identified as argillic alteration zones are quite smaller than the one produced in the PC6 image. The argillic alteration zones associated with the epithermal gold in the study area is however indicated as a green color in Figure 4.10 and this combination produced fewer alteration zones as compared to the combination in Figure 4.9.

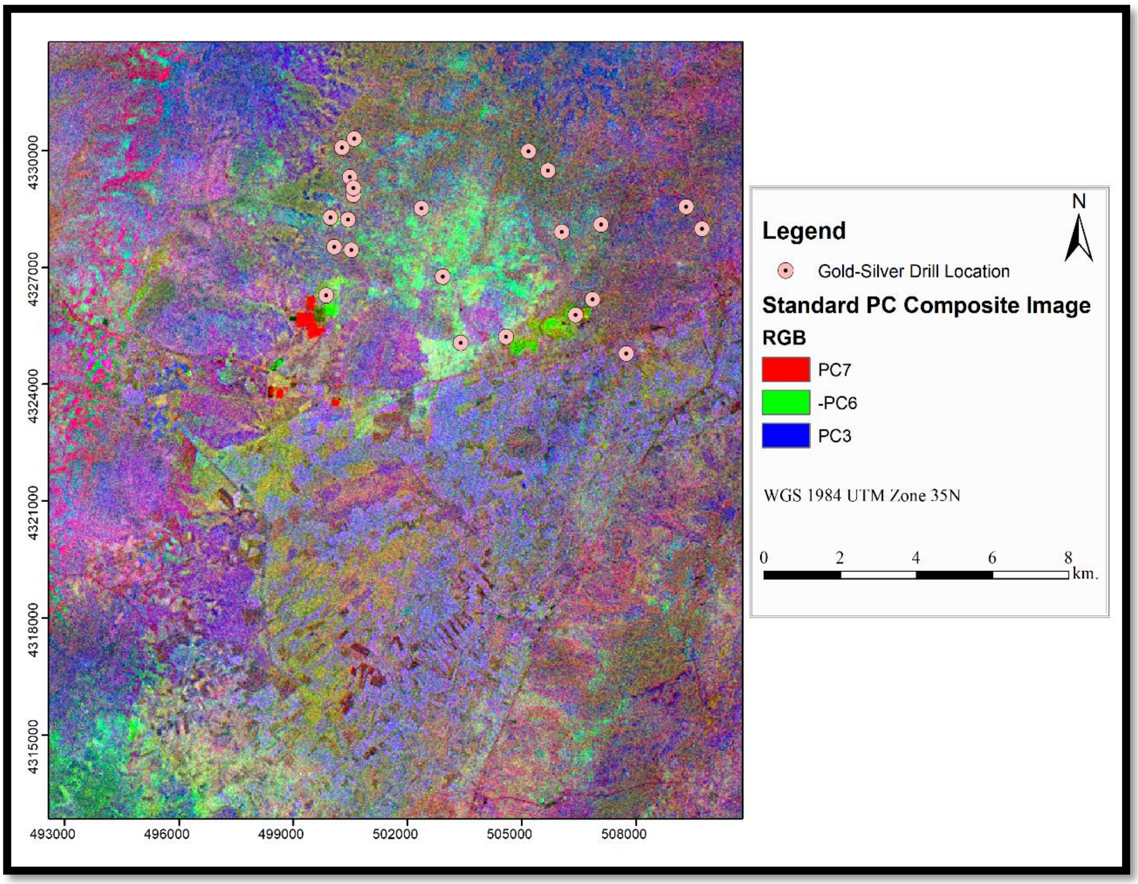

Figure 4.10. *Color composite image of the standard PCA (PC7, -PC6 & PC3)*

The principal component image combination in Figure 4.11 produces a similar result as the combination in Figure 4.9 in terms of coverage of the argillic alteration zones. In both combinations, the red channel contains the principal component image (PC6) that depicted the argillic alteration from the standard principal component analysis.

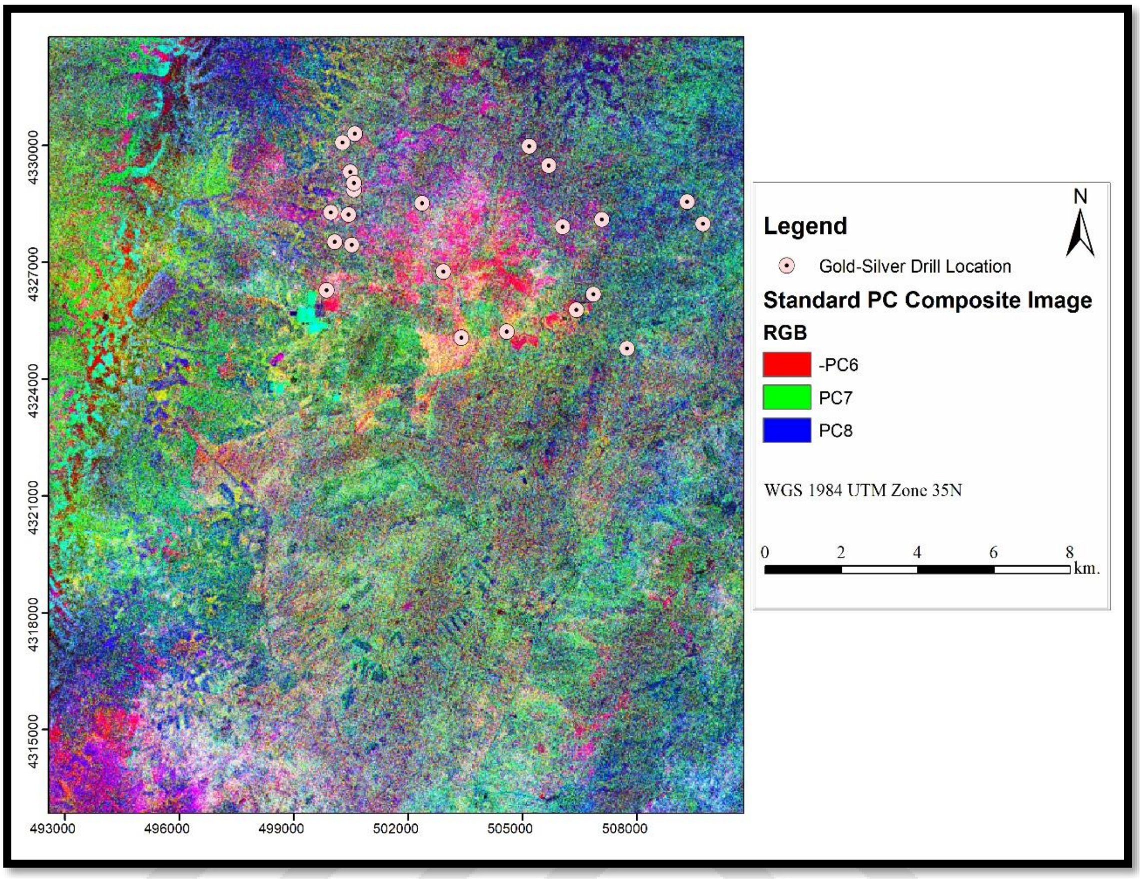

Figure 4.11. *Color composite image of the standard PCA (-PC6, PC7 & PC8)*

The combination of the individual principal component images helps in visual enhancement of the argillic alteration produced from the standard principal component analysis. Apart from delineating the argillic alteration zones associated with the epithermal gold-silver mineralization, other features such as vegetation, and bare soil were equally well identified. The color composite provided the opportunity for combining three different principal component image in delineating the argillic alteration in the study area.

4.2.2. Results of Crosta Technique

The Crosta technique is the commonly used type of principal component analysis in hydrothermal alteration mapping. The Crosta technique uses only 4 bands and as a result, only 4 different principal components are possible. The bands used in the Crosta technique must include the absorption and reflectance bands of the feature or mineral under-investigation. The absorption bands used in this Crosta principal component analysis in mapping illite mineral were band 4 and 6 as the absorption bands while the reflectance bands were band 7 and 8. The general statistics of these bands are shown in Table 4.5. The calculation of the principal components was based on the statistics of these 4 bands.

Table 4.5. *Basic statistics of the bands used in the Crosta technique*

		General statistics		
Band	Minimum	Maximum	Mean	Standard Deviation
Band 4	21.00	131.00	65.30	13.79
Band 6	23.00	138.00	57.34	13.50
Band 7	20.00	141.00	51.43	12.14
Band 8	18.00	158.00	49.62	12.51
		Covariance matrix		
Covariance	Band 4	Band 6	Band 7	Band 8
Band 4	190.12	179.30	159.08	161.84
Band 6	179.30	182.36	161.68	166.05
Band 7	159.08	161.68	147.28	150.43
Band 8	161.84	166.05	150.43	156.57
		Correlation matrix		
Correlation	Band 4	Band 6	Band 7	Band 8
Band 4	1.00	0.96	0.95	0.94
Band 6	0.96	1.00	0.99	0.98
Band 7	0.95	0.99	1.00	0.99
Band 8	0.94	0.98	0.99	1.00

Only one of the 4 bands (band4) was a visible-near infrared band, the rest of the bands were shortwave infrared bands. Band 4 had the highest standard deviation among the four bands and band 7 with the least standard deviation value. The high the value of the standard deviation, the high the amount of information contained within the band. Therefore, the band with the highest information was band 4 and the one with the least information was band 7.

Table 4.5 contains other information such as the covariance and correlation matrix of the bands used in the Crosta technique. The covariance matrix and correlation matrix were calculated from the standard deviations of the four bands. The correlation matrix is the normalized form of the covariance matrix and is easy to interpret. Both the covariance matrix and the correlation matrix indicate the level of relationships between the pixel values of the bands. The diagonal of the covariance matrix shows the variance of each of the band. Band 4 has the highest variance value of 190.12, followed by band 6 (182.36), band 8 (156.57) and band 7 (147.28). The trend of the variance is the same as the standard deviation since the square root of the variance values will produce their corresponding standard deviation values. The correlation values of the bands used in the Crosta technique range from 0.94 to 1. The correlation value of 1 shows a perfect relationship. The correlation between the bands is plotted in Figure 4.12 for easy interpretation and visualization.

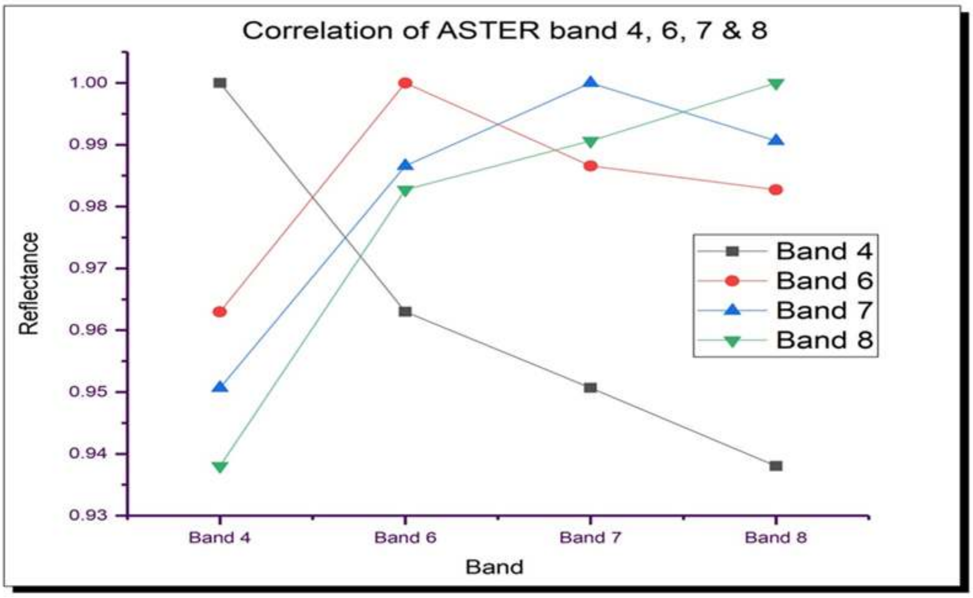

Figure 4.12. *Plot of correlation between the bands 4, 6, 7 & 8*

From the correlation plot, band 4 is less correlated with the other three bands. The relationships between band 6, 7 and 8 are however stronger. Band 6 has the strongest correlation, followed by band 7 and band 8. A stronger correlation indicates that the pixel values of the two bands are identical and may contain the reflectance from the same feature and in this case illite mineral.

Table 4.6. *Eigenvectors loadings and variance values of the Crosta technique*

Principal component	**Band 4**	**Band 6**	**Band 7**	**Band 8**	**Eigenvalues**	**Variance (%)**
PC 1	0.52	0.52	0.47	0.48	659.86	97.57
PC 2	0.82	-0.12	-0.31	-0.47	12.83	1.90
PC 3	0.22	-0.84	0.28	0.40	2.35	0.35
PC 4	0.07	0.05	-0.78	0.62	1.28	0.19

The eigenvector loadings and variance value for each of the principal components are shown in Table 4.6. The principal component with the highest variance is PC1. Principal component 2 follows with a variance value of 1.90%. The third and fourth principal components have low variance values of 0.35 and 0.19 respectively. There is a relationship between variance and spectral response or the pixel values produced by the material (Loughlin, 1991).

Bands or principal components with high variance values contain high pixel values and the distribution of the pixel values are evenly spread out. The first principal component contains pixel values from all the features in the study area and cannot map out any distinguishable feature. However, the first principal component can be used to represent all the features within the study area.

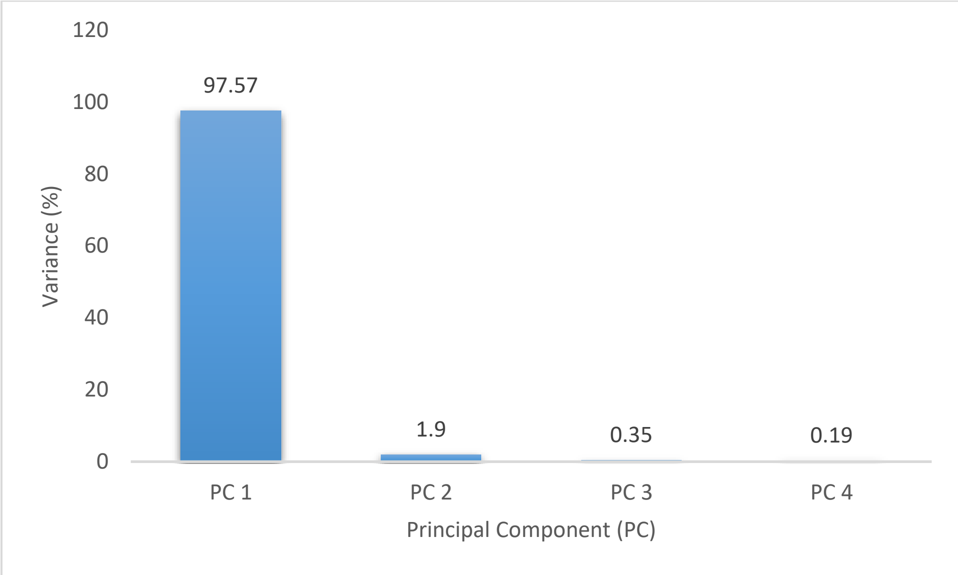

Figure 4.13. *Variance of each principal component*

The Crosta technique identifies the principal component for defining the target feature by examining the eigenvector loadings produced from the principal component analysis (Loughlin, 1991). The target feature is predicted as a bright or dark pixel in the principal component image based on the sign of the highest loading of the principal component. In the Crosta tenhique, the sign and magnitude of the eigenvector loading can give an indication of the type of feature that produces the variance. The band with the highest eigenvector loading value is always responsible for the variance of its corresponding principal component. The Crosta technique used highest eigenvector loading to highlight the target feature in its corresponding principal component.

From Table 4.6, the principal component that highlighted the presence of illite mineral was PC3. The negative high loading of band 6, an absorption band of illite mineral makes the illite mineralized zones in the PC3 appeared as a bright pixel. The seconded principal component (PC2) is dominated by vegetation because of the high positive loading value of band 4 where normally, the reflectance of vegetation is high. It is because of this reason that the vegetation cover in PC2 were bright pixels.

4.2.2.1. *Crosta technique component image*

Four principal component images were produced from the Crosta technique. They are shown in Figure 4.14-4.17. The first principal component image (Figure 4.14) contains the pixel values of all the features in the study areas with the dominant pixel values from the vegetation and illite mineral because of the high eigenvector loading of the near-infrared band (band 4) and band 6. The positive eigenvector loading of band 4 highlighted the vegetation cover is bright pixel and the positive loading value of band 6 make the argillic alteration (illite mineral) appear as dark pixels.

Band 6 being absorption band of illite mineral has a high positive eigenvector loading value and this is the reason why the argillic alteration zones produced by the illite mineral appear as dark pixels. In band 7, however, the reflectance of illite mineral is high and the high positive loading value made argillic alteration zones appeared as bright pixels. The first principal component image was not used for identifying the presence of an argillic alteration in the study areas because of the combined pixel values of both vegetation and illite mineral. Some of the dark pixel in the first principal component image was also bare soil.

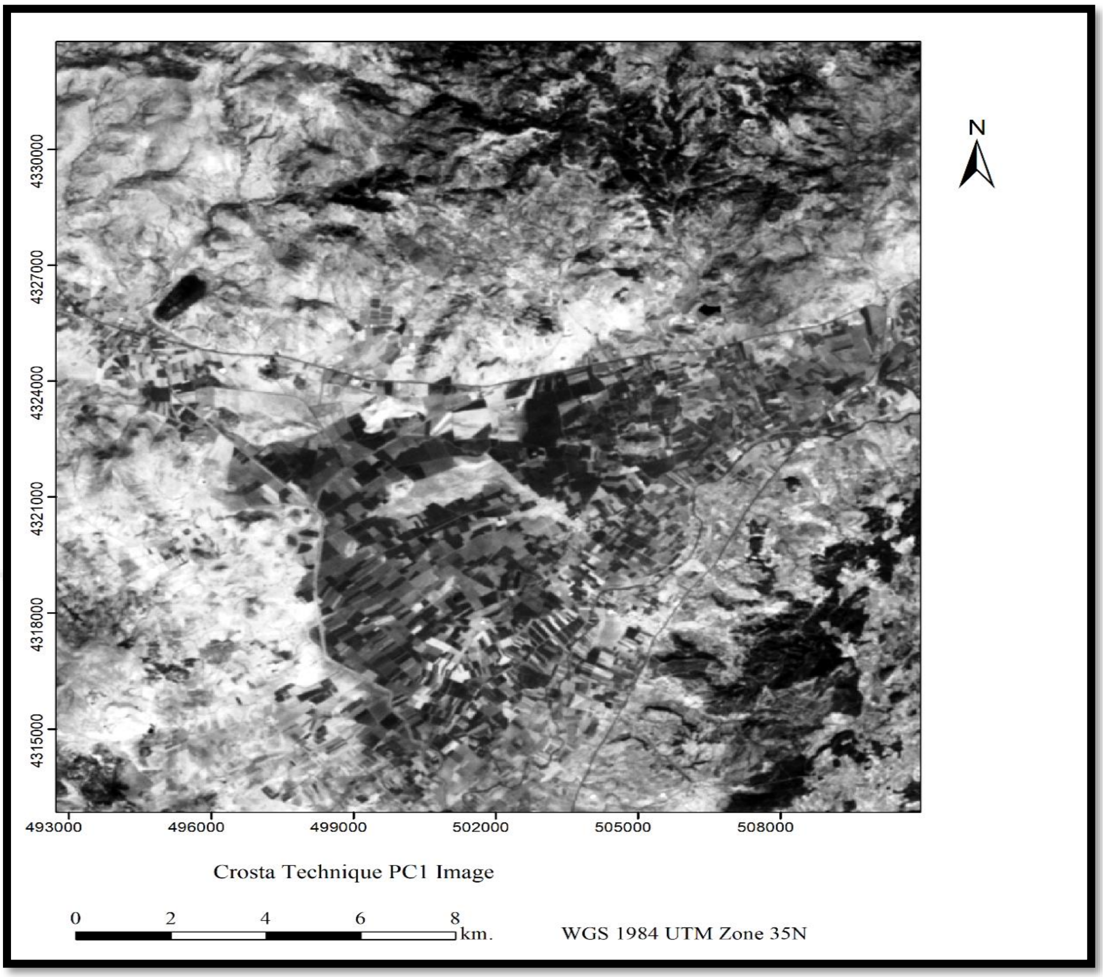

Figure 4.14. *PC1 image of the Crosta technique*

The vegetation cover was perfectly highlighted in the seconded principal component image (Figure 4.15). Vegetation was the dominant feature in the seconded principal component image (PC2) because of the high loading value of band 4, an infrared band. The vegetation was highlighted as bright pixels because of the positive value of the loading of band 4. For the vegetation cover mapping or studies, the seconded principal component image would be more appropriate than all other principal component images.

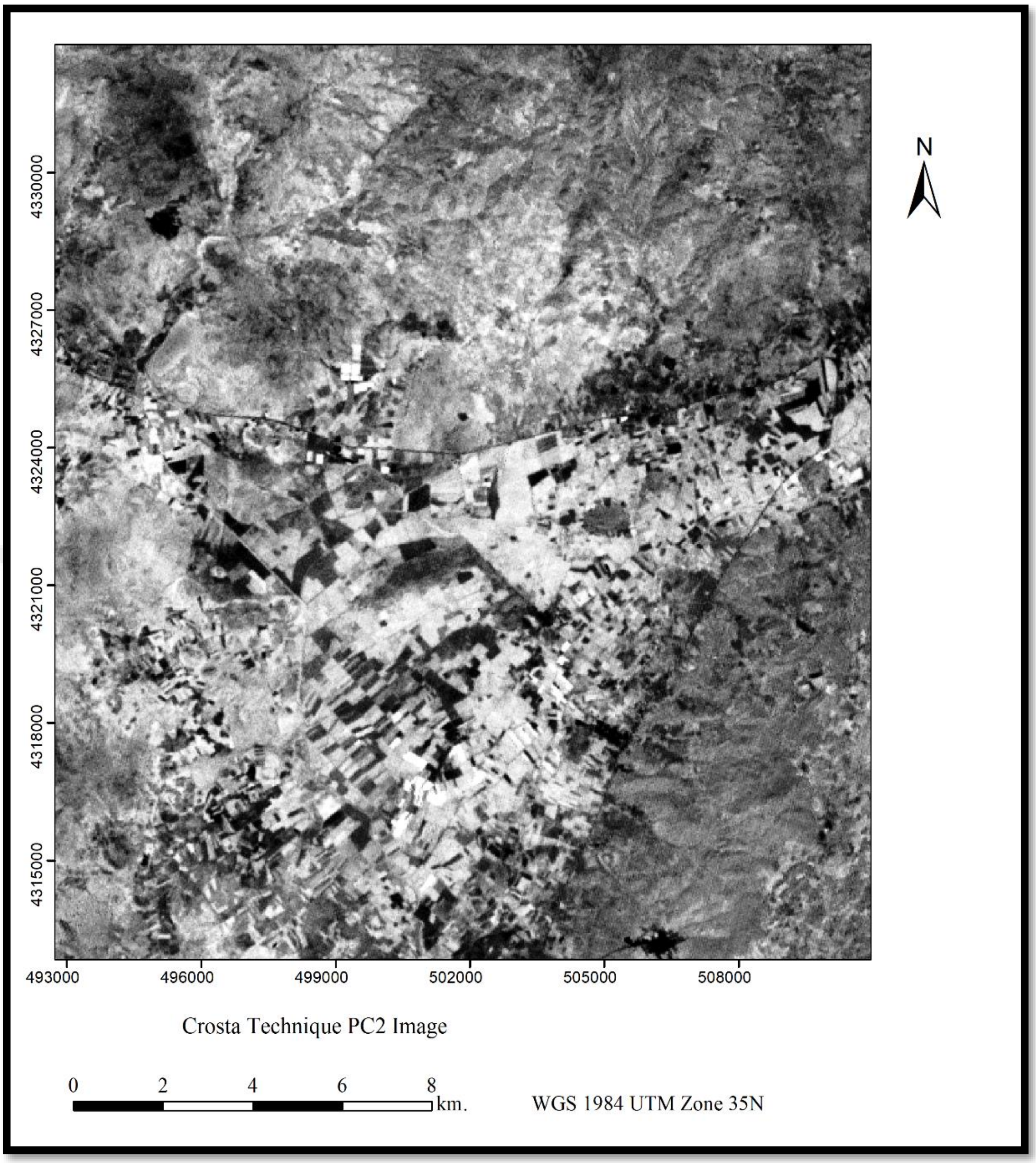

Figure 4.15. *PC2 image of the Crosta technique*

The principal component image that highlighted the argillic alteration associated with the epithermal gold mineralization in the study area was the third principal component image (PC3). The bright pixel in the third principal component image shows the argillic alteration zones. All the other features such as vegetation and bare soil were suppressed in the third principal component image. The Ovacık Gold Mine was among the areas in the third principal component image highlighted as bright pixels. The result of argillic alteration produced by Crosta principal component analysis is almost the same as the one produced by the standard principal component analysis.

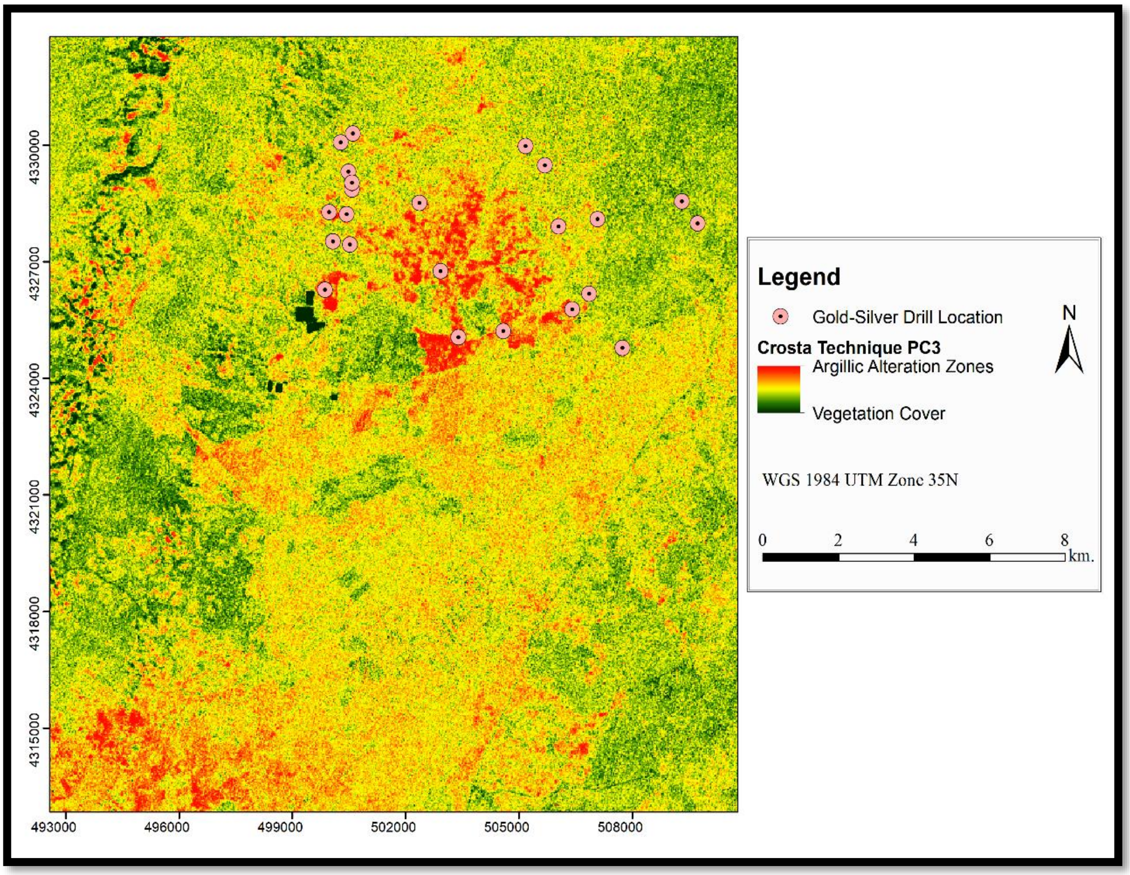

Figure 4.16. *PC3 image of the Crosta technique*

The last principal component image contains noise and would not highlight the presence of any of the features in the study area. The last principal component is normally discarded for further interpretation because of its low level of variance value and a high level of noise.

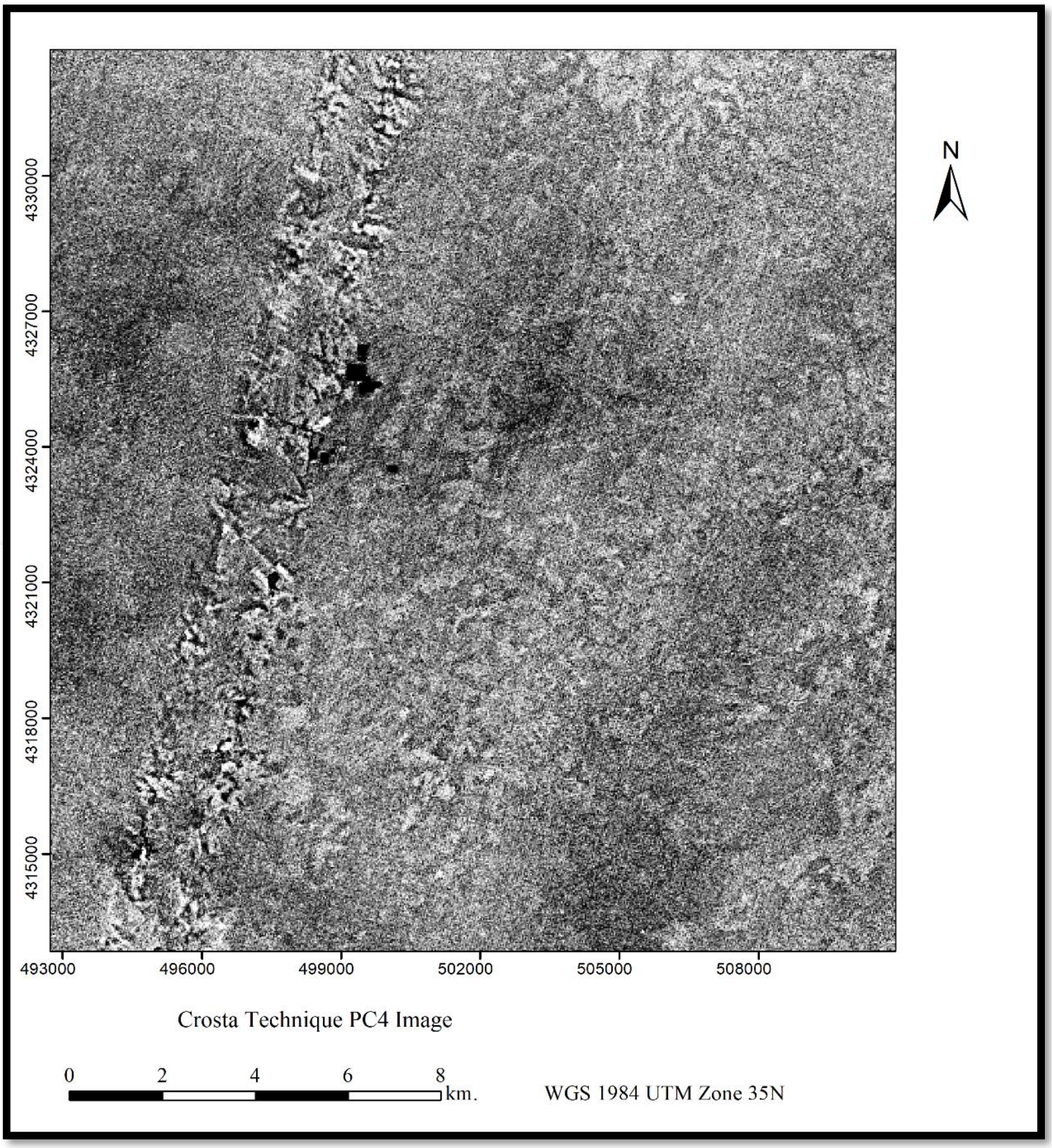

Figure 4.17. *PC4 image of the Crosta PCA technique*

4.2.2.2. *Crosta technique color composite image*

The four principal component images produced from the Crosta technique allows for some possible combinations of these principal component images in the RGB channel. The color composite images in Figure 4.18-4.20 were formed by combining the principal component image produced from Crosta principal component analysis. The yellow colored zones in Figure 4.18 are the argillic alteration zones within the study area. The green and blue color represent the vegetation cover and the purple colored areas are the bare soil. The color composite aided the interpretation of the features in the study area.

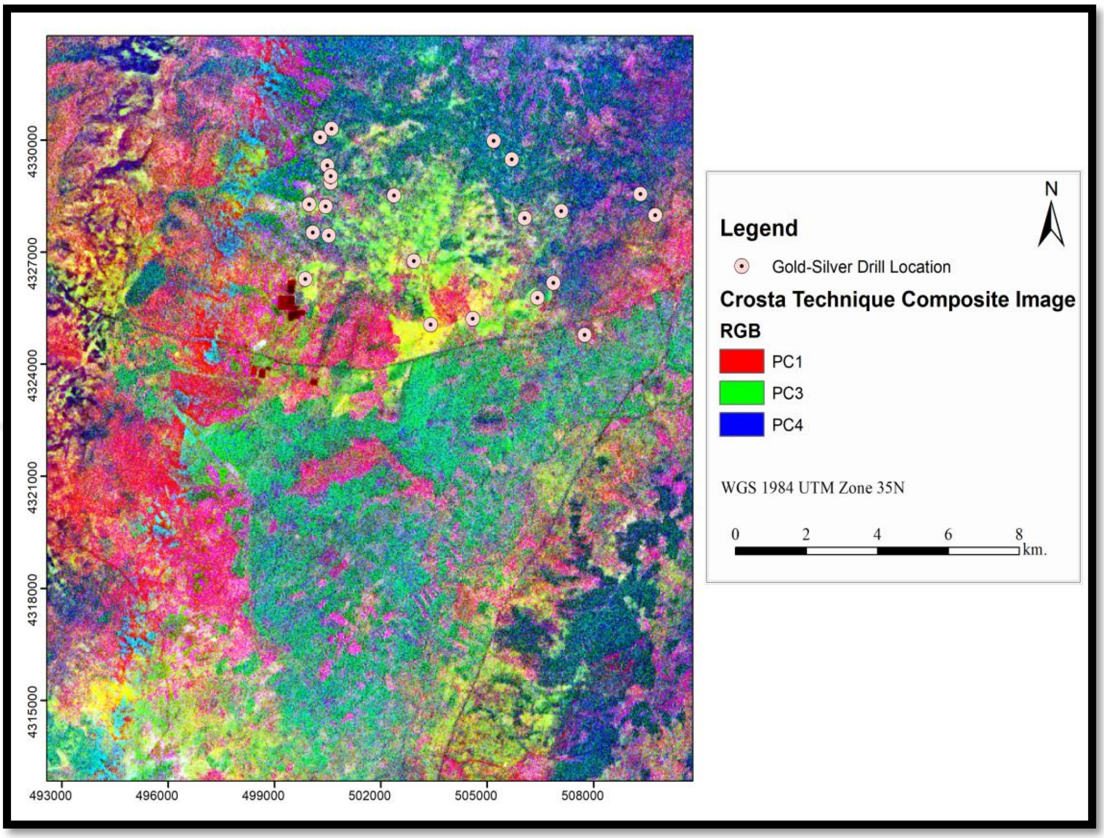

Figure 4.18. *Color composite image of the Crosta technique (PC1, PC3, &PC4)*

The argillic alteration produced by the illite mineral is indicated by yellowish green color in Figure 4.19. This combination was however not able to depict the argillic alteration as the two other combinations. The bare soil was well depicted by this combination. The brown colored areas are the bare soil.

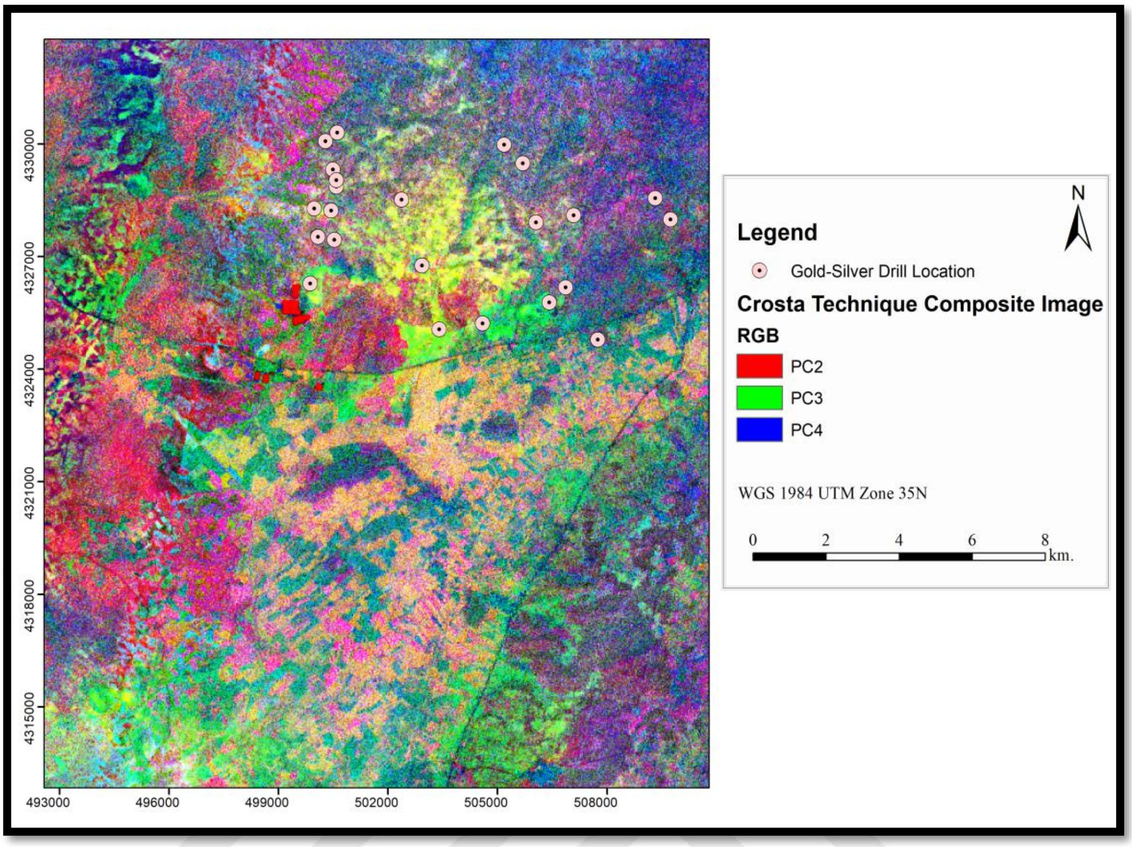

Figure 4.19. *Color composite image of the Crosta technique (PC2, PC3, & PC4)*

In Figure 4.20, the cyan colored zones were demarcated as the argillic alteration zones associated with the epithermal gold deposit in the study area. The light green colored zones are, however, the vegetated zones. The argillic alteration would help in discovering the occurrence of possible gold mineralization within the study area. It is worth noting that, all the delineated argillic alteration zones cannot lead to the discovery of gold deposits, however, the deep cyan colored zones are the most likely ones that are associated with the epithermal gold deposits in the study area and need further exploration works such drilling.

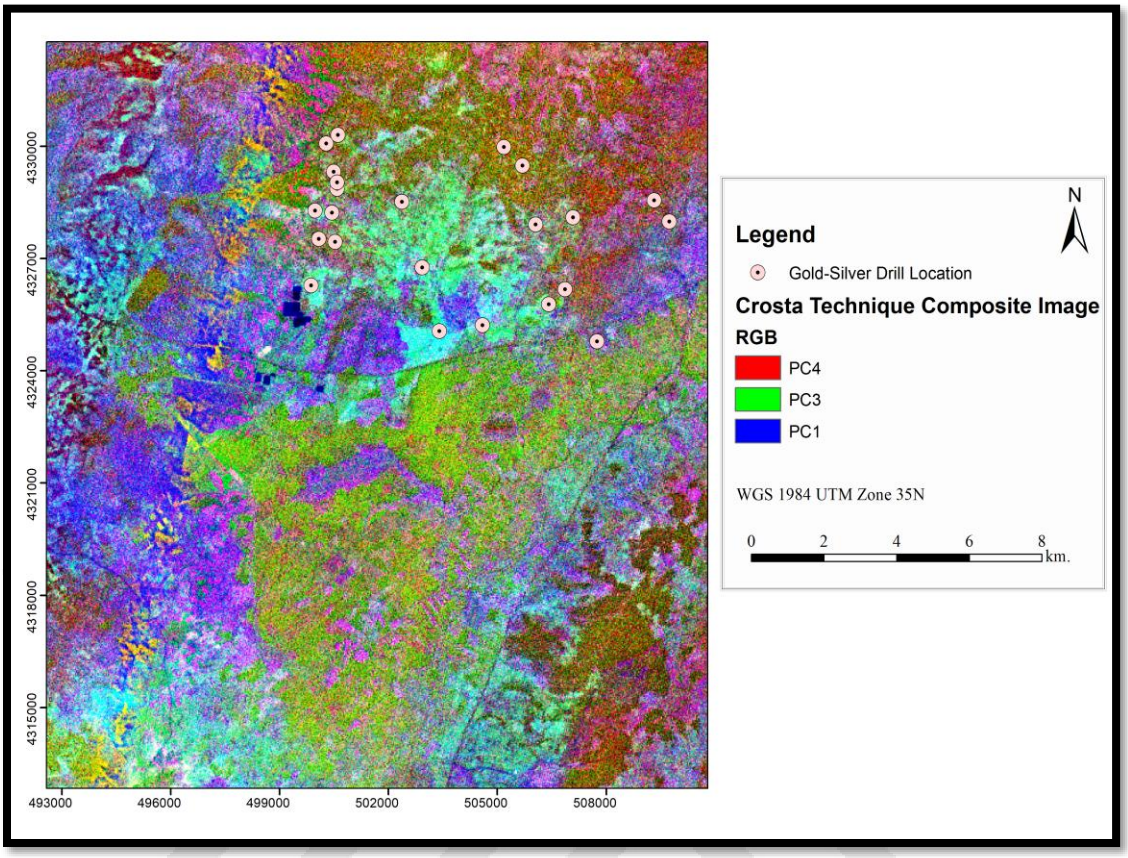

Figure 4.20. *Color composite image of Crosta technique (PC4, PC3, & PC1)*

4.2.3. Results of selective PCA

The selective principal component analysis was the last form of principal component analysis performed to highlight the argillic alteration zones in the study area. The selective principal component analysis uses only two bands. Only the absorption and reflectance bands of the illite mineral were used to perform the principal component analysis and were band 6 (absorption band) and band 7 (reflectance band). The general statistics of the two bands, the covariance matrix, and correlation matrix are illustrated in Table 4.8. Because the principal component analysis is a statistical method, the information in Table 4.7 are necessary and needed for exploring the spectral relationships among the bands.

Table 4.7. *Eigenvectors and variance values of the Crosta technique*

Principal component	**Band 6**	**Band 7**	**Covariance eigenvalue**	**Variance (%)**
PC 1	0.74	0.67	327.45	99.34%
PC 2	-0.67	0.74	2.19	0.66%

Table ***4.8.*** *General statistics of the bands used in the Selective PCA*

General statistics				
Band	Minimum	Maximum	Mean	Standard Deviation
Band 6	23.00	138.00	57.34	13.50
Band 7	20.00	141.00	51.43	12.14
Covariance matrix				
Covariance	Band 6	Band 7		
Band 6	182.36	161.68		
Band 7	161.68	147.28		
Correlation matrix				
Correlation	Band 6	Band 7		
Band 6	1	0.99		
Band 7	0.99	1		

The first principal component (PC1) contains 99.34% of the information within the study area. The spectral information in the seconded principal component is less than 1%. The first principal component is dominated by band 6 and its positive eigenvector loading makes argillic alteration zones appeared as dark pixels.

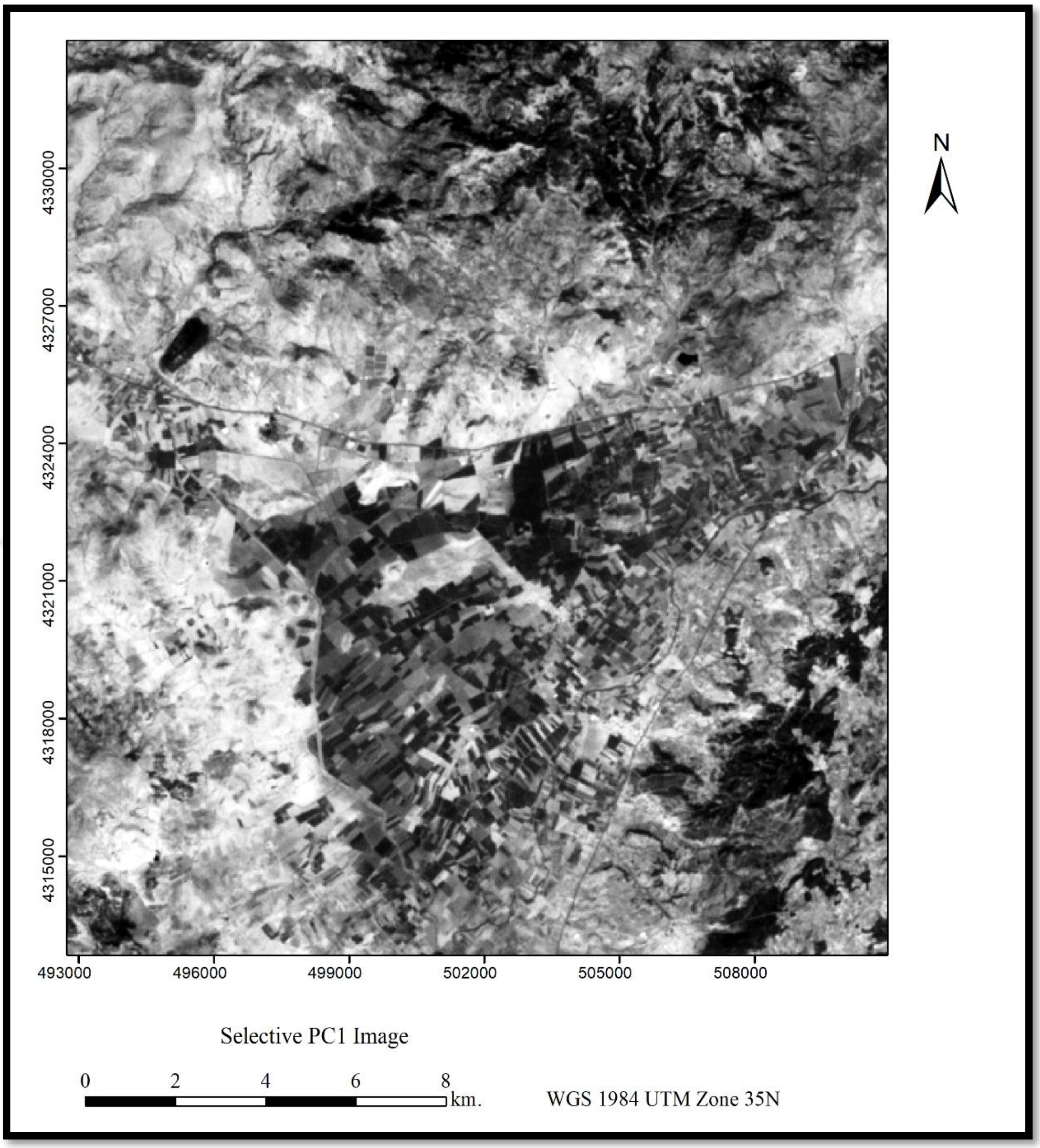

Figure 4.21. *PC1 image of the selective PCA*

The high positive loading value of the reflectance band (band 7) is the reason why the argillic alteration zones in the seconded principal component appeared as bright pixels.

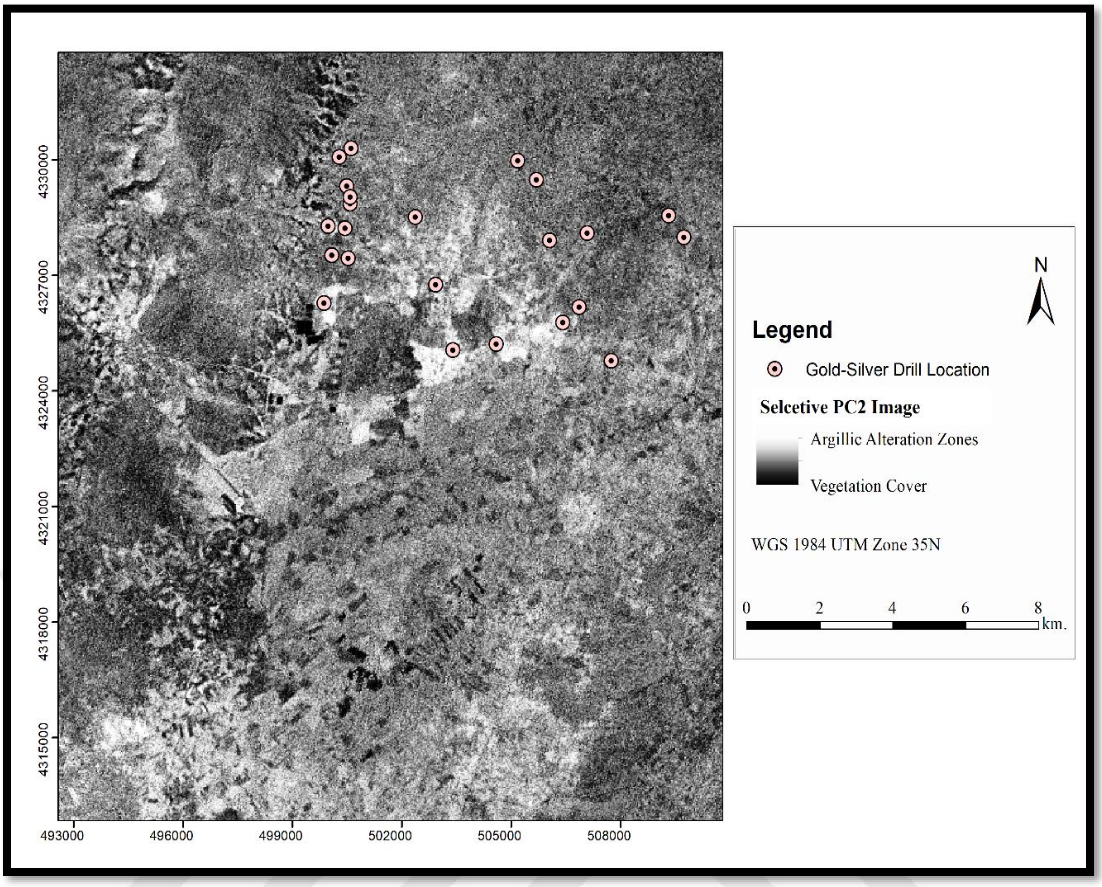

Figure 4.22. *PC2 image of the selective PCA*

4.3. Result of the GIS Integration

4.3.1. Analysis of the distance to faults

The spatial association between the faults and the known gold occurrence locations as determined by the weights of evidences analytical model is shown in Table 4.7. The Table contains information about number of training sites contained within each buffered fault zone, the positive and negative weights obtained by analysis the number of training site within each zone. The contrast (C), the standard deviation of contrast thus S (C) and the studentized contrast thus STUD (C) which was obtained by dividing the contrast by its standard deviation are also given in Table 4.7. From Table 4.7 only the first two buffer zones of the faults contain training sites. The 100m buffer zone had the highest number of training points of 128, and 26 training points for 200m buffer zone. It can be deduced from Table 4.7 that the distance closer to fault zones are more likely to host the gold mineralization. The Analysis of the buffered fault by the weights of evidence in Table has shown that there exists a spatial correlation between the distance to fault and known gold occurrences and can be considered as one of the favorable parameters for the prediction of new gold locations.

Table 4.7. *Result from weights of evidence analysis of distances to faults*

Buffer (m)	*Area (km^2)*	*#Points*	*W+*	*W-*	*Contrast (C)*	*STUD(C)*	*Rank*
100	7.63	77	2.22	-1.75	4.49	4.02	3
200	5.45	8	-2.26	1.34	-4.49	-4.01	2
300	2.85	0	0.00	0.00	0.00	0.00	1
400	1.74	0	0.00	0.00	0.00	0.00	1
500	1.38	0	0.00	0.00	0.00	0.00	1

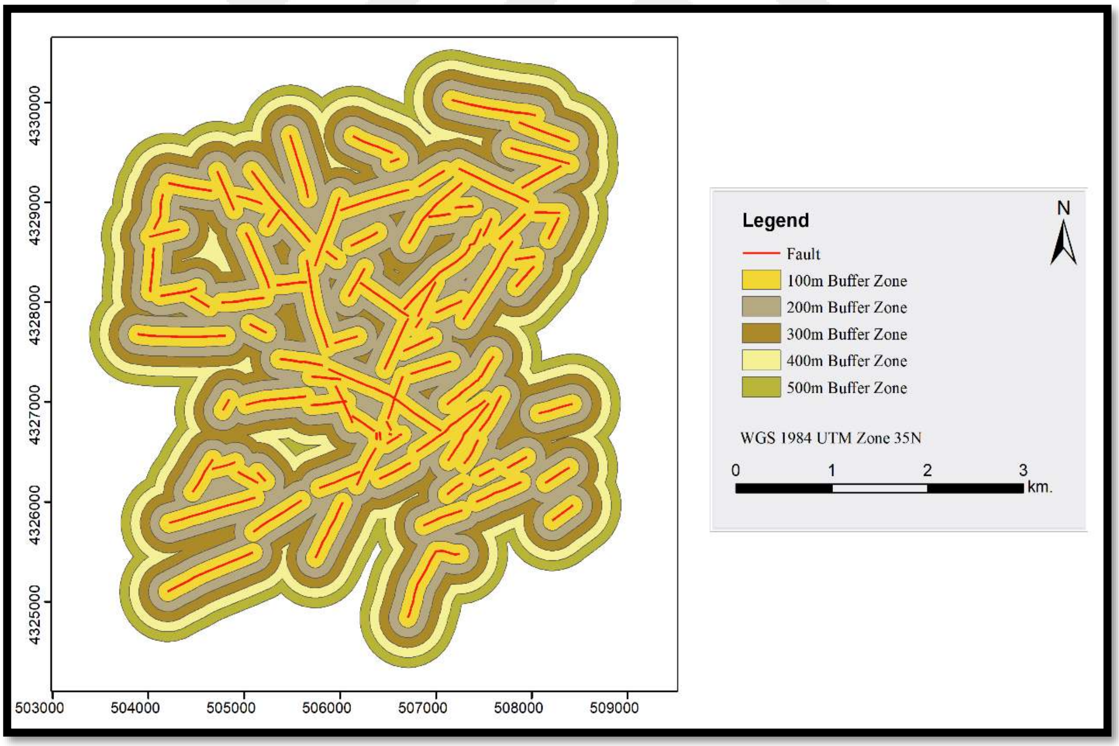

Figure 4.23. *Buffered Fault zones*

4.3.2. Analysis of hydrothermal alteration

The hydrothermal alteration can give vital information in locating the mineral. It can aid as a guide in identifying undiscovered deposits. The spatial correlation between the known gold locations used as training points and the hydrothermal zones are shown in Table 4.8 and Figure 4.24. The highest number of 146 training points were found in the hydrothermal evidential layer even though the positive weight and studentized contrast values were low. The large unit area of the hydrothermal alteration zones was the reason why the positive weight and studentized contrast values were low.

Table 4.8. *Result from weights of evidence analysis of the favorable argillic alteration zones*

Alteration *buffer* zone *(m)*	***Area (km^2)***	***#Points***	***W+***	***W-***	***Contrast (C)***	***STUD(C)***	***Rank***
100	6.69	41	1.14	-0.49	1.63	1.47	4
200	4.03	27	0.72	-0.21	0.94	0.84	3
300	3.98	13	-1.71	1.71	-3.42	-3.02	2
400	3.59	4	-2.89	1.83	-4.72	-3.92	1

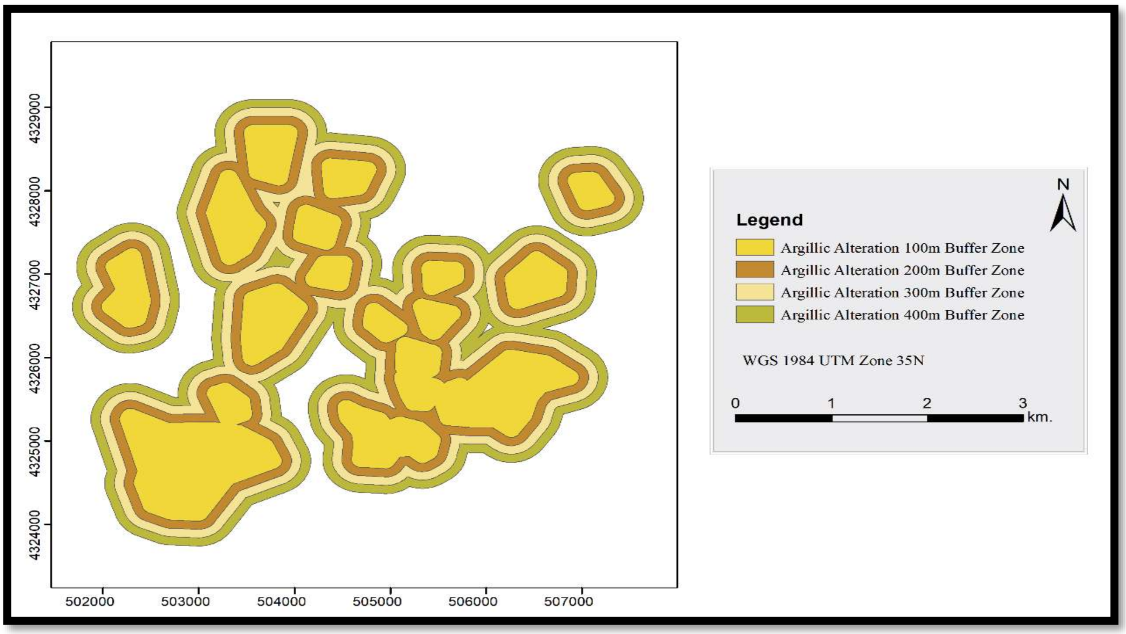

Figure 4.24. *Buffered argillic alteration zones*

4.3.3. Analysis of lithology

The weights results obtained from the spatial association of lithologies and the gold occurrence locations used as training sites are given in Table 4.9. Four different types of lithologies were used in the weights of evidence analysis. From the obtained in Table, silicified andesite had the highest training site, followed by alluvium. One hundred and forty-two of training site fell within the silicified andesite, twelve of the training points were found within alluvium zones. No training points were found argillic andesite and andesite basalt. Therefore according to the training points used in this study, the favorable lithologies for the prediction of gold deposits within the study area were silicified andesite and alluvium. It is important to notice that type of favorable lithologies for the mineral prediction can vary according to the locations of training points.

Table 4.9. *Results of weights calculation of lithology evidential themes*

Lithology	*Area (km^2)*	*#Points*	*W+*	*W-*	*Contrast (C)*	*STUD(C)*	*Rank*
Andesite basalt	6.16	0	0.00	0.00	0.00	0.00	1
Silicified andesite	2.47	80	4.56	-2.82	7.39	6.67	3
Alluvium	11.64	5	-2.19	0.68	-2.87	-5.71	2
Argillic andesite	17.06	0	0.00	0.00	0.00	0.00	1

Figure 4.25 shows the results of overlay analysis of training sites and the different lithologies within the study area. This map gives a further visual interpretation of weights of the different types of lithologies used in the weights of evidence analysis. As explained earlier, the andesitic tuff lithology contains the highest number of training sites and therefore was considered as the most favorable lithology type for the prediction of possible gold locations within the study. From Table 4.9, the highest positive weight (w+) and studentized contrast (stud (c)) of 1.02 and 3.87 respectively. The values of positive weight (w+) and studentized contrast indicate the strength of favorability of the prediction. Higher values indicate high favorability whiles a negative weight value

indicates low or no possibility of the evidential theme in contributing to the discovery of new gold mineralized locations.

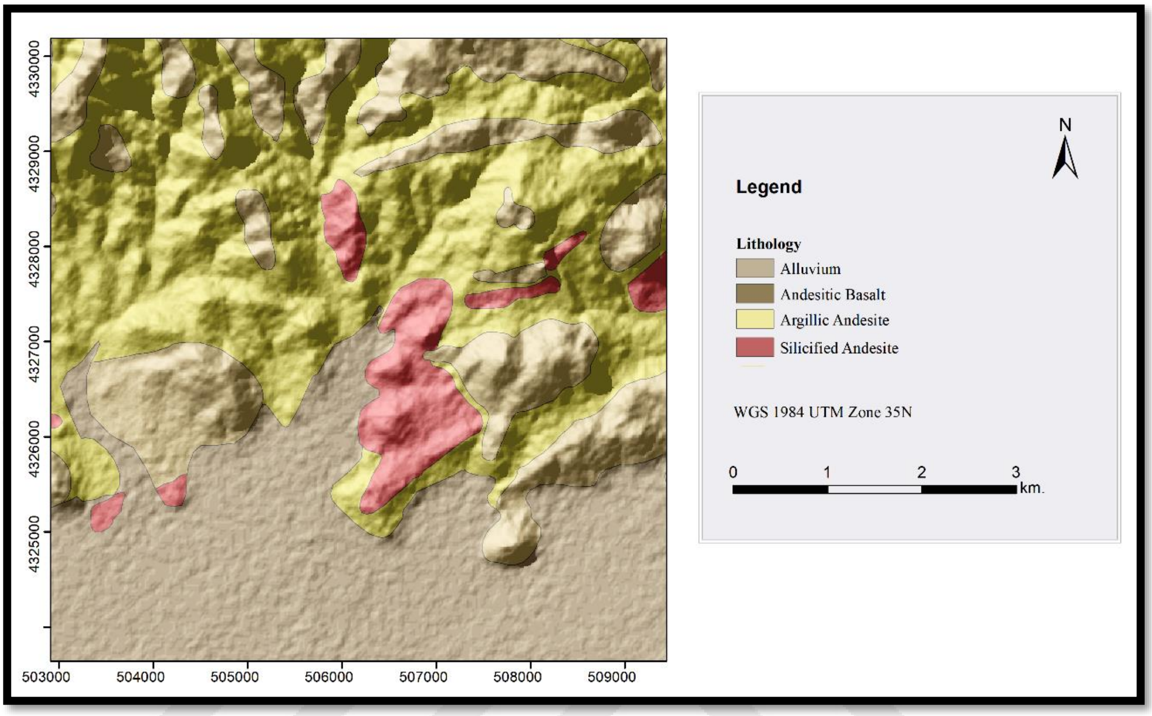

Figure 4.25. *Lithology types*

4.3.4. Result of weights of evidence model

The weights of evidence method, a data-driven approach integrates multiple exploring dataset to predict the potential mineralized zones. The weights calculated from the known gold occurrence locations and the evidential themes were used as the criteria for recognizing and predicting the new gold deposits. The gold potential locations predicted by using the weights of evidence is shown in Figure 4.26. The gold potential map was produced from the combination of all the weighted evidential layers (hydrothermal alteration zones, distance to fault lines and lithology). All the evidential layers used in the model were conditionally independent of the known gold deposit. A conditional independence ratio value of 1.02 was obtained from the assessment of conditional independence test. A conditional independence ratio value of above 1.00 shows that there is no conditional dependence among the evidential layers and the gold deposit. The conditional independence among the evidential layers is one of the main assumptions of the weights of evidence model. The occurrences of gold deposit within the study are indicated with different colors with their corresponding probabilities displayed on the legend. The red colored areas represent areas with high gold favorability probabilities, those areas with medium possibilities of gold occurrences are shown in orange color, and those areas with no or low gold occurrence possibility values are indicated in yellow color. From the gold potential map in Figure 26, most of the known gold occurrence locations fall within areas with the high conditional posterior probabilities even though there were other high conditional posterior probability zones without known gold occurrence locations. These areas are most likely the new potential gold locations discovered within the study area.

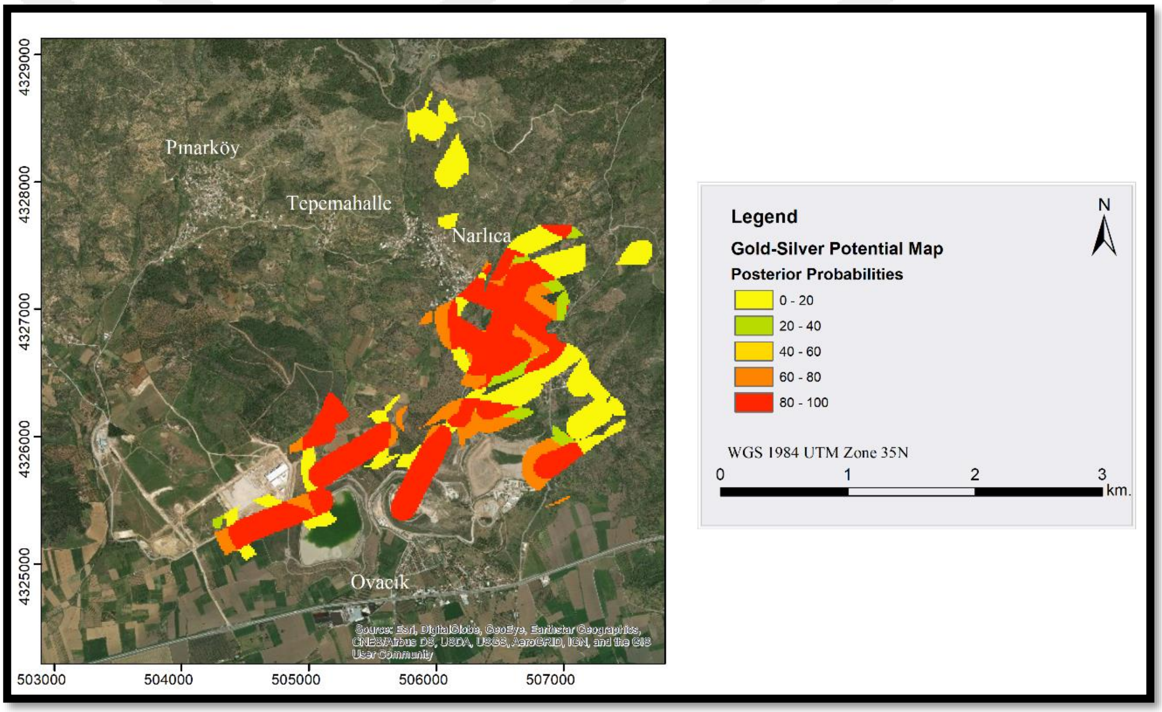

Figure 4.26. *Gold-Silver potential map produced from weights of evidence model*

4.3.5. Result of the fuzzy logic model

The fuzzy logic is a knowledge-driven approach and relies on the knowledge of the geoscience expert in determining the spatial correlation between the predicting mineral and the evidential layers. The fuzzy logic model best suits new areas where no or little mineral exploration works have been done. The mineral potential map produced from the fuzzy logic model can be used as a guide during the drilling operation. The evidential layers used in the fuzzy logic modeling were first weighted according to the studentized contrast values from the result of the weights of evidence model. This approach helped to improve the prediction result of the fuzzy logic model. The result from the fuzzy logic is shown in Figure 4.27. The high potential prediction zones are indicated in red color. These areas are almost the same as the high potential prediction zones produced from the weights of evidence. The moderate prediction zones are shown in orange colors whiles no or low gold predicted zones are indicated in yellow color. The absolute values associated with mineral prediction maps ranges from 0 to 100. Values to closer to 100 represent high and favorable gold locations whiles values closer to 0 give an indication of no potential gold mineralization. These absolute values of the fuzzy logic prediction model are equivalent to the posterior probabilities of the weights of evidence model.

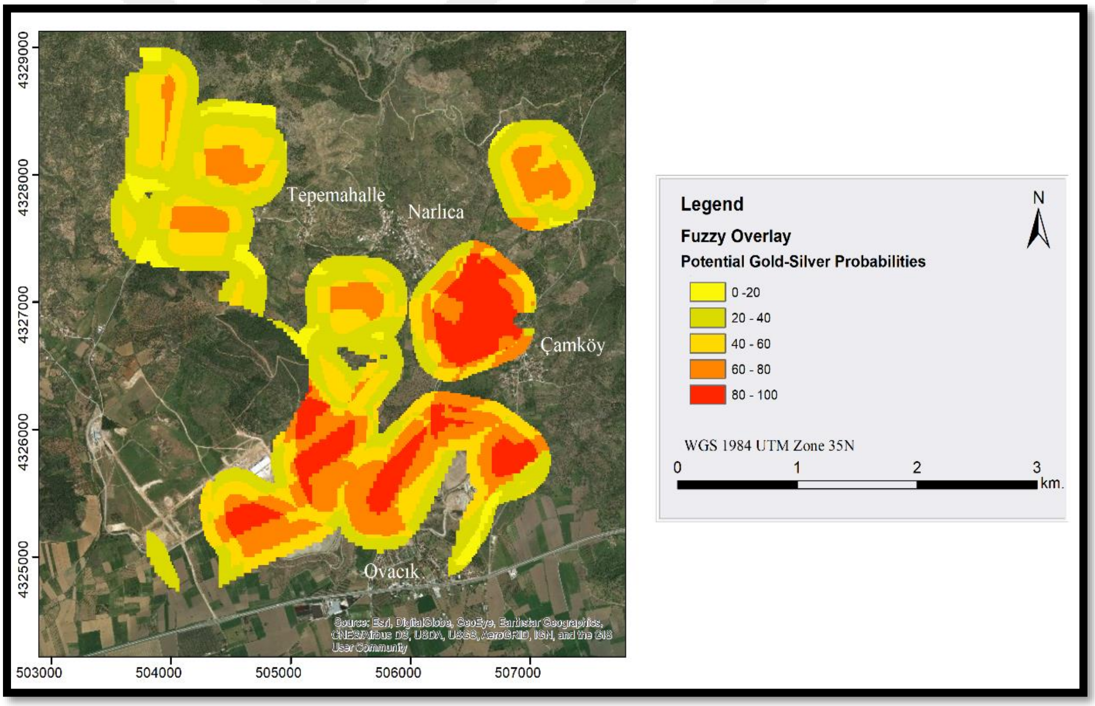

Figure 4.27. *Gold-Silver potential map produced from fuzzy logic model*

4.3.6. Validation result

Seventy known gold points were used to verify the accuracy of the gold potential maps produced from the weights of evidences and fuzzy logic models. All the seventy known gold points fall within the high probability zone (80-100) of the map produced from the weights of evidences model. However, for the map produced from the fuzzy logic model, sixty out of seventy validation points fall within the highly rated gold zones. Ten of seventy validation points, however, fall within the less gold favorable zones. From the validation result, the performance of the weights of evidence is not quite different from the fuzzy logic model even though the fuzzy logic model was based on the knowledge-driven model.

5. CONCLUSION AND RECOMMENDATION

The mining history of Turkey dated back to ancient Roman times and important minerals such as copper, silver, tin, mercury, gold, and coal have been mined in both ancient and recent times. In modern times, more mineral exploration projects have not been undertaken with modern techniques in Turkey and therefore the possibilities of discovering new deposits are high with modern techniques such as remote sensing. Epithermal gold especially has not been fully explored despite Turkey's rich potentials.

The introduction of remote sensing in mineral exploration has brought a lot of relieves to the exploration geologists. Remote sensing techniques can offer both direct and indirect types of glue in locating and mapping minerals. Mineral exploration is an ongoing activity because of non-renewability of minerals. This, therefore, calls for the use of the most efficient and effective methods and data such as remote sensing data and techniques.

Remote Sensing data and techniques have contributed immensely to the success of most mineral exploration works. The availability of Remote Sensing data especially ASTER and Landsat have reduced the burden of mineral exploration works in terms of cost and time because of their wide coverage area. The ability of the Remote Sensing satellite sensors to capture and record the emitted and reflected radiance from the minerals makes them detectable. Most minerals exhibited some detectable absorption features in the visible infrared (VNIR) and the shortwave infrared (SWIR) of the electromagnetic spectrum and hence are detected by either band ratio technique or principal component analysis.

The illite index can be applied on the ASTER image to identify the most probable epithermal gold-silver before carrying out geochemical and geophysical operations such as drilling. In addition, the hydrothermal alteration zones identified by the illite index can be integrated with geochemical and geophysical data to predict the potential locations of gold-silver. The illite index was developed by considering the spectral response of argillic alteration minerals, particularly illite mineral, the geology and landcover of Ovacık, İzmir. Considering the geologic factors when developing the illite index helped to improve the mapping and identifying of argillic alteration zones associated with epithermal gold-silver mineralization. The illite index can be used to identify argillic alteration zones associated with epithermal gold-silver mineralization in areas similar to the geology and landcover of İzmir.

The argillic alteration zones obtained from all the three types of the principal component analyses confirmed the validity and reliability of the illite index in mapping and identifying the hydrothermal alteration zones associated with the gold-silver mineralization in the study area. The illite index is very simple to apply on the ASTER image to map and identify hydrothermal alteration of gold. For effective use of the illite index, the following conditions must be fulfilled; the image pixel must be converted into surface reflectance and the vegetation cover must be masked out before applying the illite index even though it can produce good alteration result without satisfying these conditions.

The principal component analysis was able to map and identify the argillic alteration zones of epithermal gold-silver deposits as the illite index, however, the illite index gave a better argillic alteration result than the principal component analysis. The effect of solar illumination, slope, and topography did not influence the argillic alteration demarcation by the illite index. These defects were canceled out once band ratio is performed. This is one of the reasons why image band ratio technique is still relevant in mapping and identifying features such as hydrothermal alteration zones, vegetation, water bodies, and soil.

Performing the three different forms of principal component analysis gave broad options in comparing and validating the argillic alteration zones produced from the newly developed index, the illite index. The Crosta technique of the principal component analysis offered the best argillic alteration results among the principal component analysis. The Crosta technique gave an alteration result close to the result obtained from the illite index. The Crosta technique also offered the opportunity to form color composite images from its principal component images. From the Crosta technique color composite images, the best combinations for predicting the existence of argillic alteration in the study area were PC1, PC3 and PC4.

The argillic alteration zone produced from the illite index and the principal component analysis would help in discovering the occurrence of possible gold mineralization within the study area. It is worth noting that all the delineated argillic alteration zones cannot lead to the discovery of gold deposits, however, the highly rated zones are the most likely ones that are associated with the epithermal gold deposits in the study area and need further exploration works such drilling. The Ovacık Gold Mine which was used as the reference point in extracting the spectral signature was in the highly rated argillic alteration zones.

The application of Geographic Information Systems and Remote Sensing in mineral exploration have been demonstrated in this study. The Remote Sensing serves as a source of importance evidential layers in the mineral exploration model. Hydrothermal alteration zones associated with mineralization, fault delineation and geophysical data can be obtained from Remote Sensing techniques. The Geographic Information Systems was used to integrate the various geospatial datasets to produce the gold potential map of the study area. The main essence of using Geographic Information Systems in mineral exploration is to provide a common platform for the integration of multiple sources of geospatial data in order to produce optimal mineral prediction models.

The weights of evidence and the fuzzy logic model were the two forms of GIS algorithms used to predict the potential locations of gold deposits within the study area. Both the weights of evidence and the fuzzy logic models allow for the integration of multiple sources of geospatial datasets. This helped improve the prediction accuracy of the argillic alteration result produced by the illite index. In the weights of evidence model, the weights for the evidential layers were estimated based on the spatial associations between the known gold deposit locations and the evidence layers. The utilization of both the data-driven and knowledge driven models in this study ensured the comparison of the two types of mineral potential mapping modeling concepts. The pair of weights (W+ and W-) indicate the type of spatial association correlation between the deposit locations and evidence. Positive weight is an indication of positive correlation whiles negative weight expresses a negative correlation between the known gold deposit locations and the evidence. The advantage of the weights of evidence model is that there are probabilities associated with predicted gold locations. These probabilities were based on the spatial association between the known gold locations and the presence of all the evidential layers. The weights of evidence avoid the bias of the researchers in determining the spatial correlation between the evidential layers and the deposit because it is a data-driven approach rather than knowledge driven approach.

The weights of evidence model cannot be applied in areas where no mineral exploration has taken place. It is therefore not a suitable method to be used during the early stages of mineral exploration. Another disadvantage of the weights of evidence is the assumption of conditional independence among the evidential layers. This assumption of weights of evidence is inconsistency with the basic assumption of mineral exploration which consists of identifying and recognizing correlation or dependence among the predicting variables. Geological processes of generation ore deposit may in a way leads to some degree of correlations among other processes of mineral formation.

The fuzzy logic is a knowledge-driven model and does not necessarily required training sites in predicting the potential locations of the mineral deposits. However, in this study, the evidential layers were reclassified based on the spatial correlation results from the weights of evidence model. This helped avoid the bias in deciding which themes of the evidential layer were more important in the mineral prediction.

The fuzzy logic model delineated a large gold potential area than the weights of evidence. All the areas mapped out by the weights of evidence model were also mapped out by the fuzzy logic model. The fuzzy logic model was used to verify the result of the weights of evidence even though the accuracy of the fuzzy logic model was low. The Ovacık Gold Mine was identified by both the weights of evidence and a fuzzy logic model. Though the absolute values for the posterior probability from the weights of evidence model are lower than absolute values from the fuzzy logic model, the weights of evidence model are relatively the best predictor of potential gold locations in this study.

REFERENCES

Abdeen, M. M., Allison, T. K., Abdelsalam, M. G., and Stern, R. J. (2001). Application of ASTER band-ratio images for geological mapping in arid regions; the Neoproterozoic Allaqi Suture, Egypt. *The Geological Society of America (GSA),*, Abstract.

Aboelkhair, H., Ninomiya, Y., Watanabe, Y., and Sato, I. (2010). Processing and interpretation of ASTER TIR data for mapping of rare-metal-enriched albite granitoids in the Central Eastern Desert of Egypt. *Journal of African Earth Sciences, 58*(1), 141-151.

Abrams, M., Hook, S., and Ramachandran, B. (1999). *ASTER User Handbook, Version 2, NASA/Jet Propulsion Laboratory, Pasadena.*

Agterberg, F., Bonham-Carter, G., and Wright, D. (1990). Statistical pattern integration for mineral exploration. *Computer applications in Resource Estimation Prediction and Assement for Metals and Petroleum*, 1-21.

Agterberg, F. P., and Cheng, Q. (2002). Conditional independence test for weights-of-evidence modeling. *Nat Resour Res, 11*, 249–255.

Akay, E., and Erdoğan, B. (2004). Evolution of Neogene calc-alkaline to alkaline volcanism in the Aliaga–Foca region (Western Anatolia, Turkey). *Journal of Asian Earth Sciences*(24), 367–387.

Ali, O. A. M., Ali, A. Y., & Sumait, B. S. (2015). Comparison between the Effects of Different Types of Membership Functions on Fuzzy Logic Controller Performance *International Journal of Emerging Engineering Research and Technology, 3*(3), 76-83.

Amer, R., Mezayen, A. E., and Hasanein, M. (2016). ASTER spectral analysis for alteration minerals associated with gold mineralization. *Ore Geology Reviews, 75*, 239-251.

Amera, S. A. (2007). *Spectral Remote Sensing of Hydrothermal Alteration associated with Volcanogenic Massive Sulphide Deposits, Gorob-Hope area, Namibia.* (Masters), International Institute For Geo-Information Science And Earth Observation Enschede, The Netherlands.

An, P., Moon, W. M., and Rencz, A. N. (1991). Application of fuzzy theory for integration of geological, geophysical and remotely sensed data. *Can J Explor Geophys, 27*, 1–11.

Arafat, S., Farg, E., Shokr, M., and Al-Kzaz, G. (2013). Internet-Based Spectral Database for Different Land Covers in Egypt. *Advances in Remote Sensing, 02*(02), 85-92.

Arindam, G., Biswajit, G., Kumar, K. V., and Sukanya, C. (2015). Implementation of reflection spectroscopy based new ASTER indices and principal components to delineate chromitite and associated ultramafic–mafic complex in parts of Dharwar Craton, India. *Advances in Space Research, 56*(7), 1453-1468.

Arindam, G., and Kumar, K. V. (2015). Comparative analysis on utilisation of linear spectral unmixing and band ratio methods for processing ASTER data to delineate bauxite over a part of Chotonagpur plateau, Jharkhand, India. *Geocarto International, 31*(4), 367-384.

Arindam, G., and Kumar, V. (2016). New ASTER derived thermal indices to delineate mineralogy of different granitoids of an Archaean Craton and analysis of their potentials with reference to Ninomiya's indices for delineating quartz and mafic minerals of granitoids—An analysis in Dharwar Craton, India. *Ore Geology Reviews, 74*, 76-87.

Aydal, D., Arda, E., and Dumanlilar, Ö. (2007). Application of the Crosta technique for alteration mapping of granitoidic rocks using ETM+ data: case study from eastern Tauride belt (SE Turkey). *International Journal of Remote Sensing, 28*(17), 3895-3913.

Azizi, H., Tarverdi, M. A., and Akbarpour, A. (2010). Extraction of hydrothermal alterations from ASTER SWIR data from east Zanjan, northern Iran. *Advances in Space Research, 46*(1), 99-109.

Baldridge, A. M., Hook, S. J., Grove, C. I., and Rivera, G. (2009). The ASTER spectral library version 2.0. *Remote Sensing of Environment, 113*(4), 711-715.

Baugh, B., and Hamman, G. (2013). An Introduction to SWIR Retrieved from http://www.sensorsmag.com/components/introduction-to-swir.

Belton, V., and Gear, T. (1983). On a shortcoming of Saaty's method of analytic hierarchies. *Omega, 11*(3), 228–230.

Berk, A., Bernstein, L. S., Anderson, G. P., Acharya, P. K., Robertson, D. C., and Chetwynd, J. H. (1998). MODTRAN Cloud and Multiple Scattering Upgrades with Application to AVIRIS S. M. Adler-Golden. *Remote Sensing of Environment*(65), 367–375.

Boloki, M., and Poormirzaee, R. (2010). Using ASTER Image Processing for Hydrothermal Alteration and Key Alteration Minerals Mapping. *Latest Trends on Engineering Mechanics, Structures, Engineering Geology*, 77-82.

Bonham-Carter, G., Agterberg, F., and Wright, D. (1989). *Integration of geological datasets for gold exploration in Nova Scotia.*

Bonham-Carter, G. F. (1994). *Geographic Information Systems for Geoscientists: Modelling with GIS*. Pergamon: Oxford.

Boroushaki, S., and Malczewski, J. (2008). Implementing an extension of the analytical hierarchy process using ordered weighted averaging operators with fuzzy quantifiers in ArcGIS. *Computers and Geosciences, 34*(4), 99–410.

Carranza, E. J. (2009). Improved wildcat modeling of mineral prospectivity. *Resource Geology, 60*, 129–149.

Carranza, E. J. (2008). Geochemical anomaly and mineral prospectivity mappingin GIS. In M. Hale (Ed.), *Handbook of Exploration and Environmental Geochemistry* (3-351). Amsterdam: Elsevier.

Carranza, E. J. M. (2004). Weights of Evidence Modeling of Mineral Potential: A Case Study Using Small Number of Prospects, Abra, Philippines. *Natural Resources Research, 13*(3), 173-187.

Carranza, E. J. M., and Hale, M. (2002). Mineral imaging with Landsat Thematic Mapper data for hydrothermal alteration mapping in heavily vegetated terrane. *International Journal of Remote Sensing, 23*(22), 4827-4852.

Carvalh, O. A. D., and Meneses, P. R. (2000). *Spectral Correlation Mapper (SCM); An Improvement on the Spectral Angle Mapper (SAM).* 1-8.

Carver, S. J. (1991). Integrating multi-criteria evaluation with geographical information systems. *International Journal of Geographical Information Systems, 5*(3), 321–339.

Chandrasekar, N., Mujabar, P. S., and Rajamanickam, G. V. (2011). Investigation of heavy-mineral deposits using multispectral satellite data. *International Journal of Remote Sensing, 32*(23), 8641-8655.

Chavez, P. S., Berlin, G. L., and Sowers, L. B. (1982). Statistical method for selecting Landsat MSS ratios. *Journal of Applied Photographic Engineering, 8*, 23-30.

Chavez, P. S., Guptill, S. C., and Bowell, J. A. (1984). Image processing techniques for thematic mapper data. *Proc. ASPRS-ACSM Tech, paper 2*, 728-742.

Church, R. L., Gerrard, R. A., Gilpin, M., and Stine, P. (2003). Constructing cell-based habitat patches useful in conservation planning. *Annals of the Association of American Geographers, 93*(4), 814–827.

Clark, R. N. (1999). *Remote Sensing for the Earth Sciences Chapter 1: Spectroscopy of Rocks and Minerals, and Principles of Spectroscopy, in Manual of Remote Sensing*. New York: John Wiley and Sons.

Clark, R. N., and Roush, T. L. (1984). Reflectance spectroscopy: Quantitative analysis techniques for remote sensing applications. *Journal of Geophysical Research: Solid Earth, 89*(7), 6329-6340.

Clark, R. N., Swayze, G. A., King, T. V. V., Middlebrook, B., Calvin, W. M., and Gorelick, N. (1990). *The U. S. Geological Survey, Digital Spectral Library and Analysis Software.* Paper presented at the Proceedings of the Second Airborne Visible/Infrared Imaging Spectrometer (AVIRIS) Workshop.

Clark, R. N., Swayze, G. A., Wise, R., Livo, E., Hoefen, T., Kokaly, R., and Sutley, S. J. (2007). USGS digital spectral library splib06a: U.S. Geological Survey, Digital Data Series 231. Retrieved from http://speclab.cr.usgs.gov/spectral.lib06.

Coolbaugh, M. F., Raines, G. L., and Zehner, R. E. (2007). Assessment of exploration bias in data driven predictive models and the estimation of undiscovered resources. *Nat. Resour. Res., 16*, 199–207.

Cornell, R. M., and Schwertmann, U. (2003). T*he Iron Oxides: Structure, Properties, Reactions, Occurrences and Uses*.York City: John Wiley & Sons, Inc.

Cowen, D. (1988). GIS versus CAD versus DBMS: What are the differences? *Photogrammetric Engineering and Remote Sensing, 54*(11), 1551-1555.

Crosta, A. P., Sabine, C., and Taranik, J. V. (1998). Hydrothermal Alteration Mapping at Bodie, California, using AVIRIS Hyperspectral Data. *Remote Sensing of Environment, 65*, 309-319.

Department of Geology; Aligarh Muslim University. (unknown). Interaction of EMR with Earth's Surface. Retrieved from http://www.geol-amu.org/notes/mw4-2-4.htm.

Edwards, A. J. (2015). Radiometric Correction of Satellite Images: When And Why Radiometric Correction is Necessary. Retrieved from http://unesdoc.unesco.org/images/0011/001197/119752e.pdf.

Eldrandaly, K. A. (2013). Exploring multi-criteria decision strategies in GIS with linguistic quantifiers: an extension of the analytical network process using ordered weighted averaging operators. *International Journal of Geographical Information Science, 27*(2), 2455–2482.

Encyclopædia Britannica. (2017). Electromagnetic spectrum. Retrieved from https://www.britannica.com/science/electromagnetic-spectrum.

Ercan, T., Turkecan, A., Akyürek, B., Günay, E., Cevikbaş, A., Ateş, M., Ozkirişçi, E. (1984). The geology of Dikili-Bergama-Çan-darlı area (western Anatolia) and petrology of the magmatic rocks. *Jeoloji Mühendisliği Dergisi*(20), 47-60.

Feick, R. D., and Hall, B. G. (2004). A method for examining the spatial dimension of multi-criteria weight sensitivity. *International Journal of Geographical Information Science, 18*(8), 815-840.

Frimmel, H. E. (2008). Earth's continental crustal gold endowment. *Earth and Planetary Science Letters, 267*(1-2), 45-55.

Gabr, S., Ghulam, A., and Kusky, T. (2010). Detecting areas of high-potential gold mineralization using ASTER data. *Ore Geology Reviews, 38*(1-2), 59-69.

Gebreslasie, M. T., Ahmed, F. B., and van Aardt, J. A. (2009). Image-based reflectance conversion of ASTER and IKONOS imagery as precursor to structural assessment of plantation forests in KwaZulu-Natal, South Africa. *Southern Forests: a Journal of Forest Science, 71*(4), 259-265.

Gemitzi, A., Tsihrintzi, A. V., Voudrias, E., Petalas, C., and Stravodimos, G. (2007). Combining geographic information system, multicriteria evaluation techniques and fuzzy logic in siting MSW landfills. *Environmental Geology, 51*(5), 797–811.

Goodchild, M. F. (2001). Issues in spatially explicit modeling. In D. C. Parker, T. Berger, & S. M. Manson (Eds.), *Agent-Based Models of Land-Use and Land-Cover Change*. Proceedings of an International Workshop, October 4-7, Irvine, California, USA.

Goodchild, M. F., and Janelle, D. G. (2004). *Thinking spatially in the social sciences*. New York: Oxford University Press.

Goodwin, P., and Wright, G. (1998). *Decision analysis for management judgment*. Chichester: Wiley.

Graham, S. (1999). Remote Sensing. Retrieved from https://earthobservatory.nasa.gov/Features/RemoteSensing/printall.php.

Granek, J. (2016). *Application of Machine Learning Algorithms to Mineral Prospectivity Mapping.* (PhD), The University of British Columbia.

Green, E. P., Mumby, P. J., Edwards, A. J., and Clark, C. D. (2000). *Remote Sensing Handbook for Tropical Coastal Management* A. J. Edwards (Ed.) Retrieved from http://unesdoc.unesco.org/images/0011/001197/119752e.pdf.

Greene, R., Devillers, R., Luther, J. E., and Eddy, B. G. (2011). GIS-based multiple-criteria decision analysis. Geography. *Compass, 5*(6), 412–432.

Guha, A., and Vinod, V. K. (2016). New ASTER derived thermal indices to delineate mineralogy of different granitoids of an Archaean Craton and analysis of their potentials with reference to Ninomiya's indices for delineating quartz and mafic minerals of granitoids—An analysis in Dharwar Craton, India. *Ore Geology Reviews, 74*, 76-87.

Guha, A., Rao, A., Ravi, S., Kumar, K. V., and Rao, E. N. D. (2012). Analysis of the potentials of kimberlite rock spectra as spectral end member – a case study using kimberlite rock spectra from the Narayanpet kimberlite field (NKF), Andhrapradesh. *Curr Sci. , 103*, 1096–1104.

Hamza, M. H. (2016). Dasymetric Mapping as a Tool to Assess the Spatial Distribution of Population in Jeddah City (Kingdom of Saudi Arabia). *Current Urban Studies, 4* (3), 329-342.

Harris, D., and Pan, G. (1999). Mineral favorability mapping: a comparison of artificial neural networks, logistic regression, and discriminant analysis. *Natural Resources Research, 8*(2), 93-109.

Harris Geospatial Solutions Inc. (2018). Hyperspectral Analysis: SAM and SFF Tutorial. Retrieved from http://www.harrisgeospatial.com/docs/Whole-Pixel_Hyperspectral_Analysis_Tutorial.html.

Hartley, B. K. (2014). *Evaluation of Weights of Evidence to Predict Gold Occurrences in Northern Minnesota's Archean Greenstone Belts.* (Master of Science), University of Southern California.

Hewson, R. D., Cudahy, T. J., Mizuhiko, S., Ueda, K., and Mauger, A. J. (2005). Seamless geological map generation using ASTER in the Broken Hill-Curnamona province of Australia. *Remote Sensing of Environment, 99*(1-2), 159-172.

Hewson, R. D., T. J. Cudahy, A. C. Burtt, K. Okada, and Mauger., A. J. (2004). Assessment of ASTER imagery for geological mapping within the Broken Hill and Olary Domains. *In: 12-th Australasian Remote Sensing and photogrammetric Conference proceedings. Perth, Western Australia.*

Humboldt State University. (2015). Interaction of EMR with Earth's Surfaces. Retrieved from http://gsp.humboldt.edu/olm_2015/Courses/GSP_216_Online/lesson2-1/surface.html.

Hunt, G. R. (1977). Spectral Signatures of Particulate Minerals in the Visible and near Infrared. *Geophysics, 42*(3), 501-513.

Jankowski, P., Ligmann-Zielinska, A., and Swobodzinski, M. (2008). Choice modeler: A web-based spatial multiple criteria evaluation tool. *Transactions in GIS, 12*(4), 541–561.

Jensen, J. R. (2005). *Introductory Digital Image Processing* (3rd ed.): Prentice Hall.

Joerin, F., Theriault, M., and Musy, A. (2001). Using GIS and outranking multi-criteria analysis for land-use suitability assessment. *International Journal of Geographical Information Science, 15*(2), 153–174.

Jun, L., Songwei, C., Duanyou, L., Bin, W., Shuo, L., Liming, Z., and (2008). Research On False Color Image Composite And Enhancement Methods Based On Ratio Images. *The International Archives of the Photogrammetry, Remote Sensing and Spatial Information Sciences, Vol. XXXVII*(Part B7).

Kalinowski, A., and Oliver, S. (2004). ASTER Mineral Index Processing Manual. Retrieved from http://www.ga.gov.au/webtemp/image_cache/GA7833.pdf.

Karnatak, H. K., Saran, S., Bhatia, K., and Roy, P. S. (2007). Multicriteria spatial decision analysis in web GIS environment. *GeoInformatica, 11*(4), 407–429.

kauth, R. J., and Thomas, G. S. (1976). *The Tasseled cap- a graphic description of the spectral-temporal development of agricultural crops as seen by Landsat.* Paper presented at the Proceedings of the Symposium on Machine processing of Remotely Sensed Data, Purdue University, West Lafayette, Indiana (West Lfayette, Indiana: Laboratory for Applications of Remote Sensing).

Koza Altn Işletmeleri. (2015). *Volume 10 Exploration Projects*. Retrieved from SRK Consulting(U.S), Inc: https://www.akinipek.info/.

Laakso, K., Rivard, B., and Rogge, D. (2016). Enhanced detection of gossans using hyperspectral data: Example from the Cape Smith Belt of northern Quebec, Canada. *ISPRS Journal of Photogrammetry and Remote Sensing*(114), 137-150.

Lagat, J. (2009). *Hydrothermal Alteration Mineralogy In Geothermal Fields With Case Examples From Olkaria Domes Geothermal Field, Kenya.* Paper presented at the Exploration for Geothermal Resources, Naivasha, Kenya.

Ligmann-Zielinska, A., and Jankowski, P. (2008). *A framework for sensitivity analysis in spatial multiple criteria evaluation.* Paper presented at the Geographic Information Science, Proceedings 5th International Conference, GIScience, Park City, UT. Berlin/Heidelberg.

Ligmann-Zielinska, A., and Jankowski, P. (2012). Impact of proximity-adjusted preferences on rank-order stability in geographical multicriteria decision analysis. *Journal of Geographical Systems, 14*(2), 67–187.

Loughlin, W. P. (1991). Principal Component Analysis for Alteration Mapping. *Photogrammetric Engineering and Remote Sensing, 57*(9), 1163-1169.

Malczewski, J. (1999). *GIS and multicriteria decision analysis*. New York: Wiley.

Malczewski, J. (2002). On the use of weighted liner combination method in GIS: Common and best practice approaches. *Transactions in GIS, 4*(1), 5–22.

Malczewski, J. (2006). GIS-based multicriteria decision analysis: A survey of the literature. *International Journal of Geographical Information Science, 20*(7), 703–726.

Malczewski, J., and Rinner, C. (2015). *Multicriteria Decision Analysis in Geographic Information Science, Advances in Geographic Information Science*. New York: Springer.

Marinoni, O. (2004). Implementation of the analytical hierarchy process with VBA in ArcGIS. *Computers and Geosciences, 30*(6), 637–646.

Mars, J. C., and Rowan, L. C. (2010). Spectral assessment of new ASTER SWIR surface reflectance data products for spectroscopic mapping of rocks and minerals. *Remote Sensing of Environment, 114*(9), 2011-2025.

Martin, N. J., B . St Onge, and Waaub, J. P. (2003). An integrated decision aid system for the development of Saint Charles River alluvial plain, Quebec, Canada. *International Journal of Environment and Pollution, 12*(2–3), 264–279.

Mining Turkey. (2011). Mineral Exploration: What, Where and Why in Turkey. *Mining and Earth Sciences Magazine, 1*(7)*,* 1-33.

Mohy, H., El-Magd, I. A., and Basta, F. F. (2016). Newly Improved Band Ratio of ASTER Data for Lithological Mapping of the Fawakhir Area, Central Eastern Desert, Egypt. *Journal of the Indian Society of Remote Sensing, 44*(5), 735-746.

NASA. (2013). The Electromagnetic Spectrum. Retrieved from https://imagine.gsfc.nasa.gov/science/toolbox/emspectrum1.html.

NASA LP DAAC. (2015). ASTER Level 1 Precision Terrain Corrected Registered At-Sensor Radiance V003 [Data set]. NASA EOSDIS Land Processes DAAC.. Retrieved from https://doi.org/10.5067/aster/ast_l1t.003

NLN for Remote Sensing. (1999). Spectral Reflectance of Minerals and Rocks. Retrieved from http://www.nln.geos.ed.ac.uk/courses/english/frs/f2710/f2710003.htm.

Nyerges, T. L., and Jankowski, P. (2011). *Regional and urban GIS: A decision support approach*. New York: Guilford Press.

O'Sullivan, D., and Unwin, D. J. (2010). *Geographic information analysis*. Hoboken: John Wiley and Sons.

Paolini, L., Grings, F., Sobrino, J. A., Jiménez Muñoz, J. C., and Karszenbaum, H. (2006). Radiometric correction effects in Landsat multi-date/multi-sensor change detection studies. *International Journal of Remote Sensing, 27*(4), 685-704.

Parashar, C. (2015). *Mapping of Alteration mineral zones by combining techniques of Remote Sensing and Spectroscopy in the parts of SE- Rajastha.* (Master of Technology in Remote Sensing and GIS), Andhra University.

Parece, T., Campbell, J. B., and McGee, J. (2015). *Remote Sensing Analysis in an ArcMap Environment,* 349.

Patel, N., and Kaushal, B. (2011). Classification of features selected through Optimum Index Factor (OIF) for improving classification accuracy. *Journal of Forestry Research, 22*(1), 99-105.

Phani, R. (2014). An analysis of lineaments and mineral occurrences of Veligallu Schist Belt and surroundings, Eastern Dharwar Craton, India using Remote Sensing and GIS. *Journal of Multidisciplinary Engineering Science and Technology (JMEST), 1* (5), 198-204.

Pontual, S., Merry, N., Gamson, P. (2008). Spectral interpretation - Field manual. GMEX. Spectral Analysis guides for mineral exploration: AusSpec International Pty. Ltd., 189.

Porwal, A., Carranza, E. J. M., and Hale, M. (2003). Knowledge-driven and data-driven fuzzy models for predictive mineral potential mapping. *Natural Resources Research, 12*(1), 1–25.

Pour, A. B., and Hashim, M. (2011). Identification of hydrothermal alteration minerals for exploring of porphyry copper deposit using ASTER data, SE Iran. *Journal of Asian Earth Sciences, 42*(6), 1309-1323.

Prakash, A. (2000). *Thermal Remote Sensing: Concepts, Issues And Applications*. Paper presented at the XIXth ISPRS Congress Amsterdam, The Netherlands.

Qaid, A. M., and Basavarajappa, H. T. (2008). Application of Optimum Index Factor Technique to Landsat-7 Data for Geological Mapping of North East of Hajjah, Yemen. *American-Eurasian Journal of Scientific Research, 3*(1), 84-91.

Quadros, T. F. P. d., Koppe, J. C., Strieder, A. J., and Costa, J. a. F. C. L. (2006). Mineral-Potential Mapping: A Comparison of Weights-of-Evidence and Fuzzy Methods. *Natural Resources Research, 15*, 49-65.

Raines, G., Sawatzky, D., and Bonham-Carter, G. (2010). *Incorporating expert knowledge: New fuzzy logic tools in ArcGIS 10*.

Rajesh, H. M. (2004). Application of remote sensing and GIS in mineral resource mapping-An overview. *Journal of Mineralogical and Petrological Sciences, 99*, 83-103.

Riebeek, H. (2014). Why is that Forest Red and that Cloud Blue? How to Interpret a False-Color Satellite Image. Retrieved from https://earthobservatory.nasa.gov/features/FalseColor/page1.php.

Rinner, C., and Malczewski, J. (2002). Web-enabled spatial decision analysis using ordered weighted averaging (OWA). *Journal of Geographical Systems, 4*(4), 385–403.

Rouse, J. W., Haas, R. H., Schell, J. A., and Deering, D. W. (1973). *Monitoring Vegetation Systems in the Great Plains with ERTS,* Paper presented at the Third Earth Resources Technology Satellite-1 Symposium, Washington DC, NASA SP-351.

Rowan, L. C., and Mars, J. C. (2003). Lithologic mapping in the Mountain Pass, California area using Advanced Spaceborn Thermal Emission and Reflection Radiometer (ASTER) data. *Remote Sensing of Environment, 84*, 250-266.

Rowan, L. C., Schmidt, R. G., and Mars, J. C. (2006). Distribution of hydrothermally altered rocks in the Reko Diq, Pakistan mineralized area based on spectral analysis of ASTER data. *Remote Sensing of Environment, 104*(1), 74-87.

Saadat, S., and Ghoorchi, M. (2009). Primary analysis for enhancing the iron oxide and alteration minerals, using ETM+ data: a case study of Kuh-e-Zar gold deposit, NE Iran. *Iranian Journal of Earth Sciences, 1*, 73-83.

Saaty, T. L. (1996). *Decision Making with Dependence and Feedback:* . Pittsburgh: RWS Publications.

Sadeghi-Niaraki, A., and Kim, K. (2009). Ontology based personalized route planning system using a multi-criteria decision making approach. *Expert Systems with Applications, 36*(2), 2250–2259.

Salem, S. M., Sharkawi, M. E., El-Alfy, Z., Soliman, N. M., and Ahmed, S. E. (2016). Exploration of gold occurrences in alteration zones at Dungash district, Southeastern Desert of Egypt using ASTER data and geochemical analyses. *Journal of African Earth Sciences, 117*, 389-400.

Salem, S. M., Soliman, N. M., Ramadan, T. M., and Greiling, R. O. (2013). Exploration of new gold occurrences in the alteration zones at the Barramiya District, Central Eastern Desert of Egypt using ASTER data and geological studies. *Arabian Journal of Geosciences, 7*(5), 1717-1731.

San, B. T., and Suzen, M. L. (2010). *Evaluation of Different Atmospheric Correction Algorithms for Eo-1 Hyperion Imagery*. Paper presented at the International Archives of the Photogrammetry, Remote Sensing and Spatial Information Science, Kyoto Japan.

Seyitoğlu, G. (1997). The Simav Graben: an example of young E-W trending structures in the Late Cenozoic extensional system of western Turkey. *Turkish Journal of Earth Sciences*(6), 135–141.

Shanks III, and Pat, W. C. (2012). *Hydrothermal alteration in volcanogenic massive sulfide occurrence model: U.S. Geological Survey Scientific Investigations Report 2010–5070 –C*.

Simon, N., Ali, C. A., Mohamed, K. R., and Sharir, K. (2016). Best Band Ratio Combinations for the Lithological Discrimination of the Dayang Bunting and Tuba Islands, Langkawi, Malaysia. *Sains Malaysiana, 45*(5), 659–667.

Singh, S. (2015). Why SWIR Band in Remote Sensing? Retrieved from http://www.insticc.org/portal/NewsDetails/TabId/246/ArtMID/1130/ArticleID/755/Why-SWIR-Band-in-Remote-Sensing.aspx.

Skabar, A. (2003). *Mineral potential mapping using feed-forward neural networks* Paper presented at the Proceedings of the International Joint Conference on Neural Networks, 1814- 1819.

Song, C., Woodcock, C. E., Seto, K. C., Pax-Lenney, M., and Macomber, S. A. (2001). Classification and change detection using Landsat TM data: When and how to correct atmospheric effects? *Remote Sensing of Environment*(75), 230–244.

Sonka M., Hlavac V., Boyle R. (1993) *Image pre-processing. In: Image Processing, Analysis and Machine Vision*. Springer, Boston, MA

Sugumaran, R., and DeGroote, J. (2011). *Spatial decision support systems: Principles and practices*. FLA: CRC Press.

Tangestani, M. H., and Moore, F. (2014). Comparison of Three Principal Component Analysis Techniques to Porphyry Copper Alteration Mapping: A Case Study, Meiduk Area, Kerman, Iran. *Canadian Journal of Remote Sensing, 27*(2), 176-182.

Tkach, R., and Simonovic, S. (1997). A new approach to multicriteria decision making in water resources. *Journal of Geographical Information and Decision Analysis, 1*(1), 25–43.

Tommaso, I. D., and Rubinstein, N. (2007). Hydrothermal alteration mapping using ASTER data in the Infiernillo porphyry deposit, Argentina. *Ore Geology Reviews, 32*(1-2), 275-290.

Traforti, A., Mari, G., Carli, C., Demurtas, M., Massironi, M., and Toro, G. D. (2017). VNIR reflectance spectroscopy of natural carbonate rocks: implication for remote sensing identification of fault damage zones. *Geophysical Research Abstracts, 19*.

USGS. (2016). Atmospheric Transmittance Information. Retrieved from https://landsat.usgs.gov.

Van Herwijnen, M., & Rietveld, P. (1999). Spatial Dimensions in Multicriteria Analysis. In J. C. Thill (Ed.), *Spatial Multicriteria Decision Making and Analysis; A geographic information sciences approach*. Brookfield: Ashgate.

Yajima, T. (2014). *ASTER Data Analysis Applied to Mineral Resource Exploration and Geological Mapping* (Masters), Nagoya University Retrieved from http://ir.nul.nagoyau.ac.jp/jspui/bitstream/2237/20226/1/k10533_%E4%B8%BB%E8%AB%96%E6%96%87.pdf.

Yamaguchi, Y., and Naito, C. (2003). Spectral indices for lithologic discrimination and mapping by using the ASTER SWIR bands. *International Journal of Remote Sensing, 24*(22), 4311-4323.

Yang, Z., Willis, P., and Mueller, R. (2008). *Impact of Band-Ratio Enhanced AWIFS Image on Crop Classification Accuracy*. Paper presented at the Pecora 17 Conference.

Yılmaz, H. (2002). Ovacık Gold Deposit: An Example of Quartz-Adularia-Type Gold Mineralization in Turkey. *Economic Geology, 97*(8), 1829-1839.

Yılmaz, H., Sönmez, F. N., Akay, E., Şener, A. K., and Tufan, S. T. (2013). Low-sulfidation epithermal Au-Ag mineralization in the Sındırgı District, Balıkesir Province, Turkey. *Turkish Journal of Earth Sciences*(22), 485-522.

Yılmaz, Y., Genç, S. C., Karacık, Z., and Altunkaynak, S. (2001). Two contrasting magmatic association of NW Anatolia and tectonic significance. *Journal of Geodynamics* (31), 243–271.

Yousefi, M., and Nykänen, V. (2016). Data-driven logistic-based weighting of geochemical and geological evidence layers in mineral prospectivity mapping. *Journal of Geochemical Exploration*, 94–106.

Zadeh, L. A. (1965). Fuzzy sets. *Information and Control, 8*(3), 338–353.

Zhang, N., and Zhou, K. (2015). Mineral prospectivity mapping with weights of evidence and fuzzy logic methods. *Journal of Intelligent and Fuzzy Systems, 29*, 2639–2651.

Zhu, X., and Dale, A. P. (2001). Java AHP: A web-based decision analysis tool for natural resource and environmental management. *Environmental Modelling and Software, 16*(3), 251–262.

CURRICULUM VITAE

Name and surname : Clement Kwang

Foreign Language : Turkish

Place and Year of Birth : Drobo, Ghana / 1894

E-Posta : kwangclement@hotmail.com

Education and Work Experience

2019, Anadolu University, Institute of Earth and Space Sciences, Department of Remote Sensing and Geographic Information Systems.

2013, Kwame Nkrumah University of Science and Technology, Geomatic Engineering Department.

2009, University of Mines and Technology, Geomatic Engineering Department.

2018-2019, Web GIS Expert, PITON R&D and Software House, Eskisehir, Turkey.

2012-2014, Surveyor, Amalgamated Survey Ltd, Kenyasi, Ghana.

2009-2010, ICT Tutor, Berekum Presby School, Ghana.

Publications

Kwang C., Adjei I. and Osei Jnr E.M (2018) The Contributions of Geographic Information Systems (GIS) to the Creditability and Transparency of the 2016 General Elections in Ghana.Global Journal of Human Social Science: F Political Science Volume XVIII Issue I Version I Year 2018, Online ISSN: 2249-460x & Print ISSN: 0975-587

Kwang C., Osei Jnr E.M and A. S Amoah (2018) Comparing of Landsat 8 and Sentinel 2A using Water Extraction Indexes over Volta River. Journal of Geography and Geology; Vol. 10, No. 1; 2018 ISSN 1916-9779 E-ISSN 1916-9787

Twumasi Y.D., Kwang C. (2017) GIS Aided Prospect Siting of Boreholes for Maximum Yield. International Journal of Scientific Engineering and Science, Volume 1, Issue 9, pp. 4-8, 2017. ISSN (Online): 2456-7361

Kwang C, Twumasi YD, Boakye L, Oppong-Twum JE, Agyei-Frimpong S (2017) Optimal Landfill Sites for Kumasi Metropolis Using Geographic Information Systems and Multi criteria Decision Analysis. Geoinfor Geostat: An Overview 5:4. DOI: 10.4172/2327-4581.1000163

Kwang C, Osei Jnr EM (2017) Accra Flood Modelling through Application of Geographic Information Systems (GIS), Remote Sensing Techniques and Analytical Hierarchy Process. J Remote Sensing & GIS 6: 191. DOI:10.4172/2469-4134.1000191

Twumasi, Y.D., Kwang, C., Boakye, L., Agyei-Frimpong, S., Oppong-Twum, J.E., (2016) Abattoir Waste Contribution to Municipal Waste Generation, International Journal of scientific research and management (IJSRM), ||Volume||4||Issue||11||Pages||4812-4825||2016||, Website: www.ijsrm.in ISSN (e): 2321-3418

Kwang C., Osei Jnr E.M. and Duker, A.A. (2014) Application of Remote Sensing and Geographic Information Systems for Gold Potential Mapping in Birim North District of Eastern Region of Ghana, International Journal of Remote Sensing Applications. DOI:10.14355/ijrsa.2014.0401.05

Awards

2019, PhD, PhD in Remote Sensing & Geographic Information Systems (GIS), Anadolu University

2013, MSc, MSc in Geomatic Engineering, Kwame Nkrumah University of Science and Technology

2009, BSc, BSc in Geomatic Engineering, University of Mines and Technology